INTELLIGENT LOAD MANAGEMENT FOR ON-BOARD AIRCRAFT GENERATOR SYSTEMS

by

GEORGIOS ALEXANDROS AMARANTIDIS KORONAIOS

A thesis submitted to
the University of Birmingham
for the degree of
DOCTOR OF PHILOSOPHY

School of Engineering
University of Birmingham
October 2019

ABSTRACT

This thesis describes research that has been undertaken to develop an Intelligent Load Management system that assists in overheat protection of on-board aircraft generators; both under normal operation and under fault conditions.

There is an ongoing demand to optimise military aircraft performance by decreasing weight, operating costs and gas emissions, whilst increasing overall reliability. Recently, a move towards a more electric aircraft has become increasingly popular to address these demands. Flight critical systems such as: cabin pressure, flight control, surface actuation, landing gear, breaking, etc. which were conventionally controlled by pneumatic or hydraulic systems, are now included in a wider electrical network. This conversion to electrical systems increases the need for constant and uninterrupted provision of power. Generators are limited by the amount of power they can provide. An excess demand of current for a prolonged period of time can lead to overheating, which in turn, can lead catastrophic failure due to insulation degradation. The state of the art overheat protection method is using a thermo-mechanical fuse. In case of overheat the generator trips offline, with only essential systems remaining operable, in order to prevent further damage.

The proposed alternative is to produce an “intelligent fuse” where models, knowledge of the mission profile, and temperature measurements are combined to predict future temperatures and manage the loading of the generators. A lab-based AC generator system was used as the main plant for this research. Based on that generator, a

lumped parameter thermo-electric model was derived. It was further used as a simulation tool for faults and as a surrogate for a generator when multiple generators exist in the same system. This approach provided a high fit (<97%) in scenarios that had been advised by BAE Systems for all relevant temperatures.

A large part of the predictive methods used, revolved around using linear models. Both white box and black box approaches were assessed; with autoregressive exogenous models (ARX) providing the best performance for estimating the temperatures of sensitive parts of the generator using the information of measured currents.

In order to accommodate for faults during the mission, adaptive models were created. They considered variations of measured currents and measured temperatures to more accurately estimate future temperatures. These models either took the form of ARX or neural networks. Each provided their distinct advantages; with neural networks achieving more accurate prediction with high prediction horizons, whilst ARX being more robust throughout. This made ARX the preferred candidate for this application.

To ensure appropriate load management, both open loop and closed loop techniques were explored. Both neural networks open loop and closed control loops provided suitable solutions, with the control loops providing the least amount of performance compromise when no load management was necessary.

These ideas were extended to multi-generator systems. They were tested in simulation scenarios and in a hardware in the loop scenario, where the relative efficiency gain of having ILM in the system was subsequently assessed. ILM is also validated and tested on a BAE System aircraft generator in the Brough test facilities. Tests were run both under normal conditions and after a fault was introduced to the machine. The adaptive models provided an overall fit of at least 90% for the relevant temperatures under all conditions.

I would like to dedicate this thesis to my loving parents . . .

ACKNOWLEGEMENTS

I would like to thank both EPSRC and BAE Systems for funding this research. I would also like to extend gratitude to Gordon Woodhouse and Ian Harrington, my industrial supervisors; as well as to Stuart Fox, whose help has been instrumental whilst working with BAE Systems.

Thanks to my academic supervisors, Roger Dixon and Peter Hubbard. Their support has been vital and has gone above and beyond my expectations and I hope I do your efforts service! I would also like to thank my examiners for taking the time to read and critique this work in order to scientifically validate these findings.

Thanks to my friends and family; both to those who ’got it ‘and to those who still don’t really understand; thank you all the same and I am glad you have been here. I would like to thank my partner, Heather, for her love and support.

Lastly, I would like to thank my friends and colleagues, Nabilah, Precious and Jack for offering academic, personal support and a sense of comradery! Our chats and exchange of stories have helped getting me here. Thank you!

TABLE OF CONTENTS

LIST OF FIGURES

LIST OF TABLES

LIST OF ABBREVIATIONS

ANN	Artificial neural network
ARMAX	Autoregressive moving average exogenous
ARX	Autoregressive exogenous
CFD	Computational fluid dynamics
CSCF	Constant speed constant frequency
CSD	Constant speed drive
DAQ	Data acquisition
ECS	Environmental control systems
FEM	Finite element modelling
G^{-1}LM	Inverse model load management
IDG	Integrated drive generator
ILM	Intelligent Load Management
KGLM	Controller based load management
MEA	More Electric Aircraft
MIMO	Multi- input Multi Output
MISO	Multi-input single output
MLP	Multilayer perception
MPC	Model predictive control
NARX	Nonlinear Autoregressive exogenous
NNARX	Neural Network autoregressive exogenous

NNLM	Neural network load management
PHM	Prognosis and health management
ReLU	Rectified linear unit
SISO	Single input Single Output
VF	Variable frequency
VSCF	Variable speed constant frequency

CHAPTER 1

INTRODUCTION

This thesis addresses the method of "Intelligent Load Management" (ILM) as a means of overheat protection of the on-board aircraft generator systems.

Intelligent Load Management is a novel, model-based, fault tolerant approach that suggests appropriate electrical load allocation to specific generators, to maximise the load driven whilst protecting the generators from overheating. Compared to traditional methods, ILM reduces the risk of overheat in scenarios where faults occur and ensures a higher up-time of the systems.

1.1 Background information

As it is often common, technological advancements are facilitated by war; so was the more electric aircraft born during WWII. The main direction of aeronautical design had been to decrease the weight of aircraft, as they were mostly operated completely mechanically. Meanwhile, electric system technologies were also emerging.

Introducing electrical systems, enabled enhanced fault tolerance and condition monitoring; whilst decreasing maintenance costs and increasing overall reliability of the systems.

With the involvement of NASA several studies were carried out that backed up this trend [41].

There is also an environmental/ legislation-based push with the Flightpath 2050 program calling for: 75% decrease in carbon emissions per passenger kilometer; nitrogen oxide reduction by 90%; and 60% the noise of the aircraft. The need for more ecofriendly aircraft is a strong motivator towards a more electric aircraft.

Although technologies have greatly evolved since the mid-40s, the crux of the design has been the decrease and -hopefully- the elimination of mechanical systems on aircraft; whilst having a primary electrical system.

These recent developments are exemplified in recent avionic trends with Boeing 787 Dreamliner and the Airbus A350 XWB. These aircraft employ novel design and manufacturing technologies alongside new materials and other improved practices.

1.2 Problem Statement

There is an ongoing demand to optimise aircraft performance by decreasing weight, operating costs and gas emissions, whilst increasing overall reliability. In the past two decades a move towards the more electric aircraft (MEA) has become increasingly popular in order to address these demands, this is especially important in military applications. Flight critical systems such as: cabin pressure, flight control, surface actuation, landing gear, breaking, etc. that were conventionally controlled by pneumatic or hydraulic systems, are now included in a wider electrical network. This conversion to electrical systems makes the need for constant and uninterrupted provision of current increasingly important.

Generators are limited by the amount of power they can provide. An excess demand of current for a prolonged period of time can lead to overheating, which can cause catastrophic failure due to insulation degradation. The state of the art approach to prevent overheating is the use of a temperature fuse. In case of an overheat the generator is isolated to prevent further damage. Only essential systems are kept online, which means the mission has to be aborted and the aircraft returned to base for hands-on maintenance.

By using the envisaged ILM system, overheat does not result to an immediate incapacitation of the generators, rather to a more graceful degradation of the system, where loads are taken offline to ensure relative health and usability of the generator system.

To achieve the full benefits of ILM, a combination of quantifiable engineering metrics are used in conjunction with softer aspects, such as ease of implementation by the users. The system created and described herein is not meant to autonomously do the load allocation but suggest such allocation to the user and await for confirmation.

1.3 Intelligent Load Management Overview

The goal of ILM is to provide an alternative to the thermal fuse for generator overheat protection. This is done by using temperature predictions to estimate how much load each generator can drive safely. In the case where that safety limit is exceeded and the generator would overheat, load is shed from the generator. In a multi generator system, the shed load from one generator is attempted to be driven by the others.

These concepts can be summarised diagrammatically, as seen in Fig 1.1, which provides a simplified view of the load management system for a single generator system.

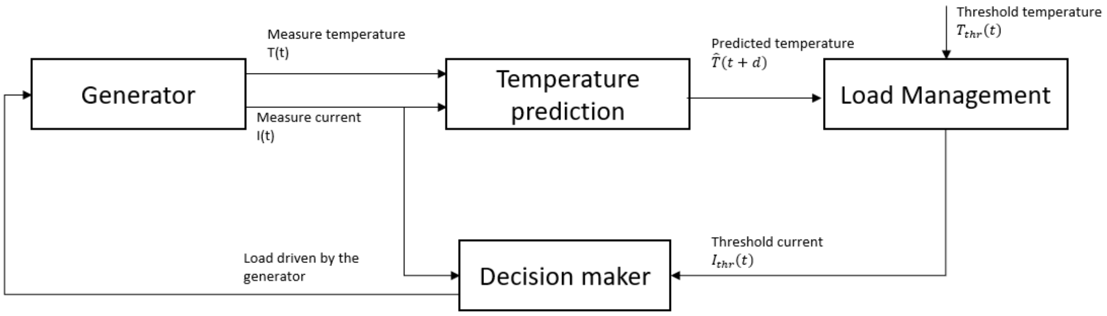

Fig. 1.1 Simplified representation of ILM on a single generator.

In summary, measurements are made on the generator for currents and temperatures. These measurements are used for estimating the temperature fluctuation in the future. These predictions, in conjunction with the threshold temperature $T_{thr}(t)$, i.e. the maximum temperature the generator can reach safely, are used to estimate the threshold current for that generator $I_{thr}(t)$. The load is subsequently adjusted to ensure the threshold current is not exceeded.

This idea can be extended to any number of generators that operate in the same system with multiple temperatures of interest for each generator using matrix notation. In which case, $\boldsymbol{T}(t)$ would contain temperature information in one dimension, the generator number on the second and time on the third. In that case, the decision maker also decides which generator the load is allocated to, in order to ensure there is no unnecessary loss in efficiency. The same idea applies for the current quantities in $\boldsymbol{I}(t)$.

1.4 Novelty Contributions

The main novelty that this thesis provides to the body of knowledge is the introduction and proof of concept of a fault tolerant intelligent load management system for aircraft generator systems. Subsequent novelties correspond to the Chapters of the thesis and are as follows:

Creating an "implementation focused" lumped parameter thermal model for a generator system, discussed in Chapter 3. This model integrates thermal and electrical characteristics of the generator. It mirrors the generator at hand and allows for simulation based testing.

Designing linear models for describing the generator behaviour under normal operating conditions; Chapter 4. Linear models are created for their use in controller design in the decision maker module. Black box autoregressive exogenous (ARX) models are used to cover cases where component values of the generator cannot be extracted.

Creating adaptive models (both linear and nonlinear) for introducing a fault tolerant behaviour to the system. This would enable the continuous operation of the system when under normal conditions as well as after it has been subjected to a fault; Chapter 5.

Tailoring specific load management algorithms, using Control laws and Machine learning techniques, that ensure the generator remains under acceptable thermal conditions; Chapter 6.

Demonstrating the efficacy of the Load Management system on a lab-based generator (not on-board aircraft) and on a BAE Systems on-board aircraft generator; Chapter 7.

1.5 Aims and Objectives

The overarching aim of the thesis is to create an Intelligent Load Management algorithm that can predict future temperatures of generators and hence calculate allowed maximum load, whilst running in real time. Different methods are investigated, and distinct approaches are proposed for specific architectures.

The objectives are outlined below:

- the design and validation of simulation models that are to be used for testing purposes instead of the real generators;
- the design and validation of prognostic models that are able to predict the future temperatures of the system based on given inputs;
- the design and validation of a load management algorithm that takes into account the present and future states of the generators and allocates the loads to specific generators in order to ensure maximum functionality while not overheating;
- to agree on test plans and execute them together with BAE Systems for testing on aircraft generators, hence demonstrate the process on such generators.

1.6 Thesis Overview

This thesis outlines the principal results and findings of the objectives of the previous section alongside the processes followed to achieve them.

Chapter 2 encompasses the review of relevant literature in order to identify the current state of the art in the field of load management on aircraft generators and methods followed. Other appropriate methods and techniques from neighbouring fields are also considered. Furthermore gaps in the current literature and practice are identified.

Chapter 3 introduces the system of interest, in this case a lab- based generator. This takes the form of both a physical system, with its instrumentation, as well as a validated simulation model used for testing purposes. In the modelling process a lumped parameter approach is used drawing attention to the interaction between electrical and thermal characteristics of the system.

Chapter 4 details the steps taken to acquire a linear model from the system of interest. This linear model is used as a predictive tool for the real time load management. Approaches of a linearised physics based model, and black box modelling, namely Autoregressive eXogenous (ARX) and state space are compared regarding accuracy of fit to real data and complexity. The chosen models (ARX) are also validated against acquired data.

Chapter 5 discusses the creation of adaptive models and their use in a fault tolerant system. In this chapter suitability of specific models in different cases is also explored. Faults are introduced and the behaviour of classic adaptive ARX and Neural Network ARX (NNARX) are compared when predicting the behaviour of the system after a fault occurs. This comparison is based on prediction accuracy, response time and complexity.

Chapter 6 outlines the algorithms and approaches for load management under the limitations identified in Chapter 5. Open and closed loop methodologies are discussed; namely inverse modelling and controller-based techniques. These methods are compared against each other using specific quantifiable metrics assessing accuracy of correction, loss of efficiency and potential risk of damage to avionic equipment.

Chapter 7 demonstrates the applicability of ILM on different generators. The initial generator is first considered as a validation process through hardware in the loop testing. Furthermore, an aircraft generator is also considered for a demonstration of possible extensions of this project to machines of different types.

Chapter 8 documents the conclusions and main findings of the thesis, alongside with recommendations for the implementation of the developed technologies.

A diagrammatic depiction of the thesis layout and interconnection of topics covered is presented below in Figure 1.2.

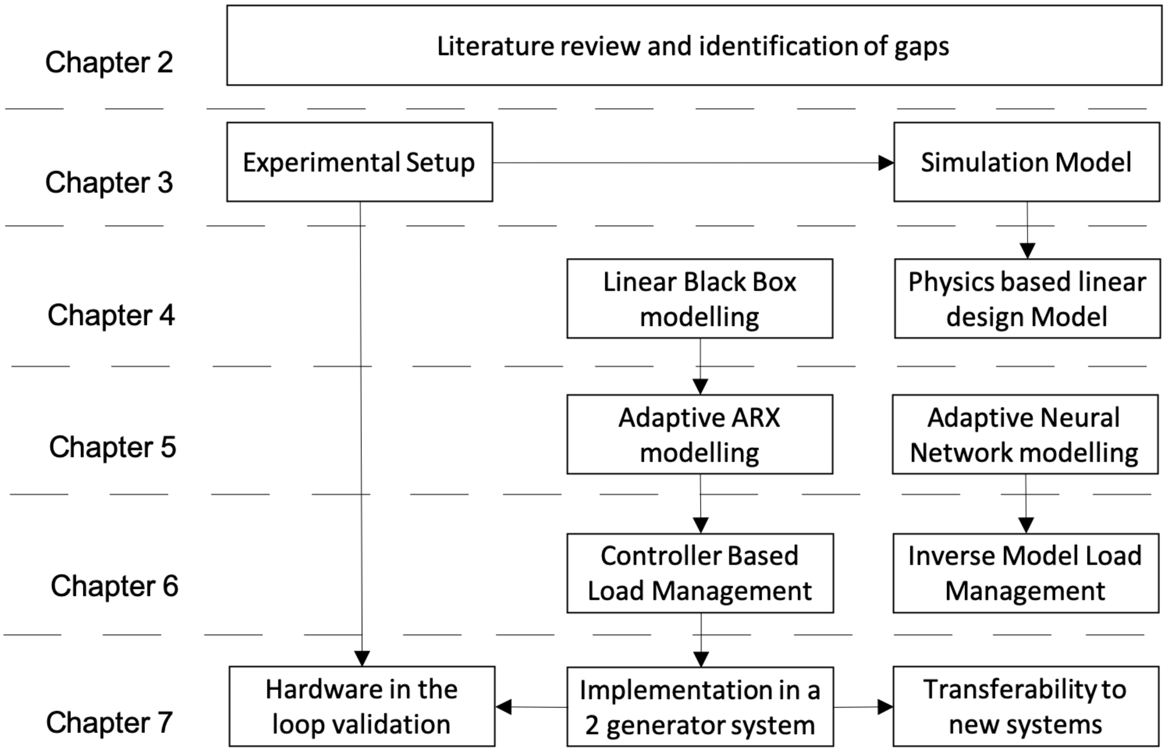

Fig. 1.2 Schematic representation of the thesis structure.

CHAPTER 2

LITERATURE REVIEW

2.1 Introduction

The purpose of the load management system being developed is to be used as a prognostic aid that assists in preventing failure of the generator system due to overheat. This review discusses studies in the areas of: aircraft power systems; prognostic health management; thermal modelling; prediction; and load management. The literature review is structured as follows. The first section reviews the idea of the more electric aircraft and its overall purpose in the industry. Following this, the development of aircraft power systems is reviewed while considering different types of power generation employed in different aircraft. Current approaches to aircraft load management are then reviewed and their limitations are discussed.

For development of the intelligent load management, modeling of the temperature of the generator, as well as prediction of future temperatures is necessary. Therefore, research on these topics is reviewed and discussed.

2.2 More Electric Aircraft

In the past few decades, the idea of the more electric aircraft has become increasingly popular. Non propulsive, flight critical systems such as: cabin pressure; flight control; surface actuation; landing gear; breaking; etc. that were previously controlled by pneumatic or hydraulic systems are now included in a wider electrical network [80, 83, 78, 105, 104]. These power subsystems are all sourced from the aircraft main engine by different methods. The engine provides mechanical power via a shaft; which is distributed to fuel, hydraulic and lubrication pumps; furthermore, it also provides mechanical input to the generators.[2, 48, 60, 77]. Pneumatic power is obtained "by bleeding" the compressor. This provides power to several subsystems including: the engine’s starter subsystem, and wing anti-icing and Environmental Control Systems (ECS). Meanwhile, according to Moir and Seabridge "power subsystems are distributed throughout the aircraft for driving actuation systems such as flight control actuators, landing gear brakes, utility actuators, avionics, lighting, galleys, commercial loads and weapon systems" [2, 60, 77].

The adoption of MEA has several objectives, such as

- Firstly, hydraulic systems are susceptible to leakage and contamination problems. Removing them can improve the aircraft reliability, whilst reducing complexity, weight, installation and running cost [25, 73, 77, 103].
- Employment of electrical starting for the aero-engine through the generator scheme eliminates a variety of mechanical equipment and reduces engine starting power

[22, 33, 61].

- Advanced Magnetic Bearing (AMB) can be incorporated in generators for the power units and can hence assist in having reduced amount of lubrication and mechanical equipment around the engine [2, 41, 48, 61].
- The implementation of fan shaft generator, that can enable emergency power extraction under "windmill conditions". This dismisses the need for the conventional single-shot ram air turbine, and hence increases the systems' overall safety, in case the engine sustains faults [2, 77].

Fig. 2.1 Aircraft systems affected by the more electric aircraft initiative.

2.3 Aircraft Power Systems

The electrical systems on board aircraft have been developed drastically within the last century.

In the 40s and 50s, systems used 28VDC generators, with each being powered by each engine. DC batteries were also fitted and an inverter provided 115VAC to the flight instruments [61, 1]. Later the V-bomber increased the power requirements with an increase in electrical systems [74, 107]. They were fitted with 115VAC generators powered by each engine. Parallel operation was employed to provide the advantages of no break power, which increased the demand for control and protection circuitry. The F-4 phantom introduced high power AC systems, where 115VAC 400Hz generators were employed [107, 61]. In order to avoid issues due to the engine speed variation, a constant speed drive (CSD) was required [30, 28]. Due to its complex nature, the CSD was accompanied with reliability issues, particularly in military applications where the engine throttle settings were changed very frequently throughout the duration of a mission. The F-18 fighter took advantage of the newly emerged variable speed/ constant frequency (VSCF) technology; the VSCF systems removed the undesirable CSD and the variable frequency was transformed to constant by the means of solid state technology [61, 81]. Meanwhile, the US military was developing systems running from 270VDC generators [44, 23]. Part of these generators' power was converted to 115VAC 400Hz or 28VDC in order to run specific equipment or loads. This is claimed to be more efficient than the conventional approach due to the reduced amount of power conversion, which in turn reduces the weight of the aircraft. Figure 2.2 shows a schematic representation of the historical evolution of on-board generator technologies.

Several technologies have been developed for AC on-board generators. Constant frequency (CF) are the most commonly used due to their ease of integration with the rest of the systems. However, a constant speed drive is necessary in order to provide them with a constant speed input. This makes them costly and impractical to use. VSCF [32] generators may be implemented in two different ways: either with a DC Link Converter or with a cycloconverter [2]. The DC link is the preferred option for most military environments due to its simplicity and reliability [61]. The cycloconverter converts the variable AC power to fixed AC amplitude and frequency. Cycloconverters are more efficient when the lagging power factor decreases. Last but not least, the Variable Frequency approach, also named ’frequency wild’, has been popularised. This technology does not attempt to minimise the effects of engine speed ratio to power output. As a result, the frequency varies from 380 to720 Hz. This fluctuation of frequency can have an impact on sensitive aircraft loads, such as AC electric motors. Hence there is a trade-off between simple power supply systems and the performance of other aircraft systems.

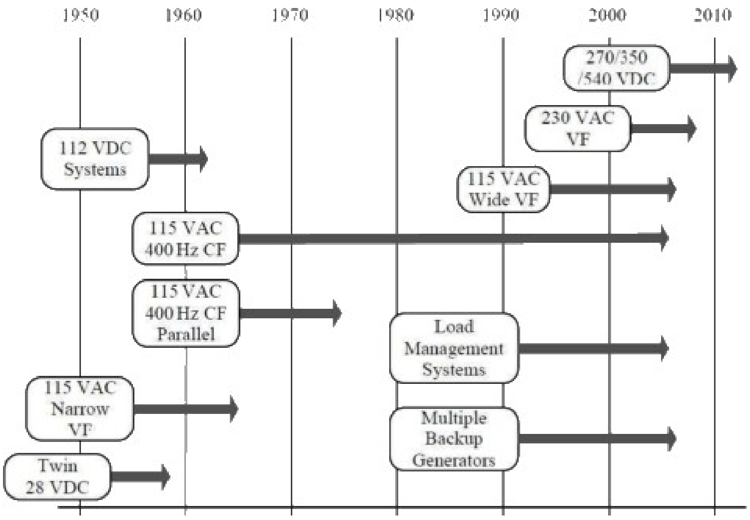

Fig. 2.2 Evolution of on-board generators [61].

The electrical power system for a twin-engine aircraft is provided in Fig. 2.3 [61]. A main AC generator fitted upon the engine provides 115VAC 3φ constant frequency power to the left and right busbars. The auxiliary power unit also provides 115VAC 3φ constant frequency which is used during ground servicing operations. If the generator sustains a fault, the auxiliary subsystem can also provide power during flight.

The generator used for the initial steps of this research is a constant frequency machine, the reasoning behind this is purely logistical though (as it was the device provided). The developed system is further validated and tested with a variable speed constant frequency system. The overall aim is for Intelligent load management to be applicable to a wide range of generators, hence why their characteristics are further explored.

2.3.1 AC Constant Frequency Systems

The most commonly encountered generators on board aircraft are three-stage wound-field synchronous [33, 47]. The reasoning behind this, is their inherent safety; as they can be de-energised and hence removed (if necessary) via being directly controlled.

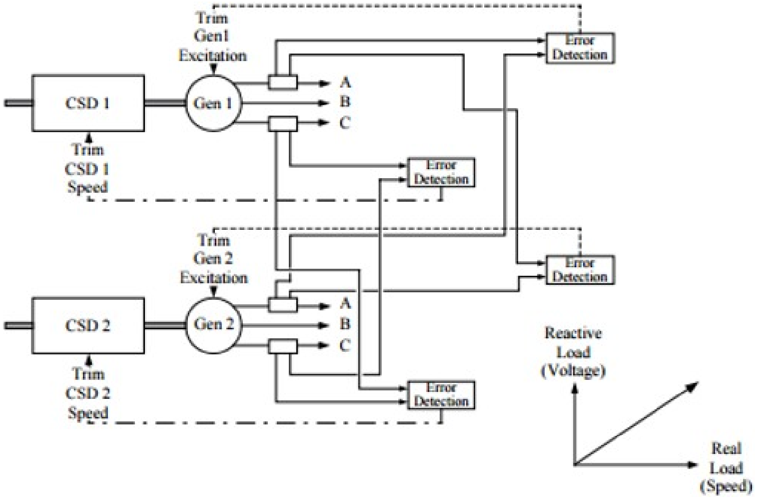

Fig. 2.3 Twin engine aircraft power network [61].

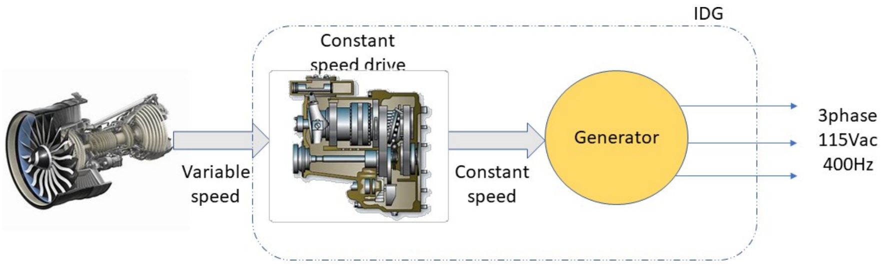

Fig. 2.4 Integrated drive generator with a constant speed drive

Constant Frequency, Integrated Drive Generator

The Integrated Drive Generator (IDG) is the most common generator technology in civilian application [79]. The aircraft engine is used as a power source for electrical generation system; therefore, the variable speed of the engine needs to be accommodated for. This is performed by including a CSD which acts as an automatic gearbox which, in turn, maintains the input speed to the generator at a constant level, in order to ensure constant frequency output. The drawback of such a system is that it is expensive to purchase and maintain due to the CSD. Figure 2.4 demonstrates in a block diagram an IDG with a CSG, which takes the variable speed input form the aircraft engine and produces a constant frequency voltage.

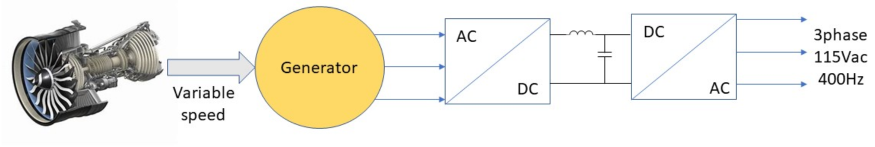

Fig. 2.5 Variable speed input to constant frequency using a DC link.

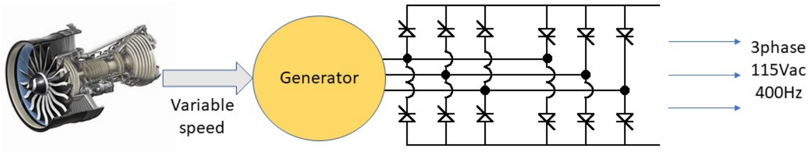

Fig. 2.6 Power generation using the cycloconverter approach.

2.3.2 Variable Speed Constant Frequency

Contrary to the IDG approach, where the input to the generator is regulated, in this approach the variable frequency output is electronically converted. This provides a weight improvement as it circumvents the need for a heavy constant speed drive. The two prevalent methods are the DC link and the cycloconverter. In the DC link the power is initially converted to DC before converted back to 115VAC 400Hz using a rectifier and an inverter [31].

Another method for generating constant frequency voltage involves matrix or cycloconverters, which can be placed between an AC generator and their corresponding loads. In the cycloconverter approach, 6 phases are generated at high frequencies. This approach takes advantage in of solid-state devices that are employed for switching between these phases. The cycloconverter approach (as demonstrated in Fig 2.6), although it appears to be complex, has been implemented successfully in military applications in the US, such as the F-18, F-117 and V-22 ultra-high altitude reconnaissance aircraft [63, 64].

2.3.3 Variable Frequency

As a matter of power generation, Variable Frequency (VF), often referred to as “frequency wild”, is the cheapest and most reliable. There is no attempt to nullify the effect of the difference in engine speed to power output. Although the voltage is regulated to 115VAC the frequency varies between 380- 720Hz, as shown in Fig. 2.7.

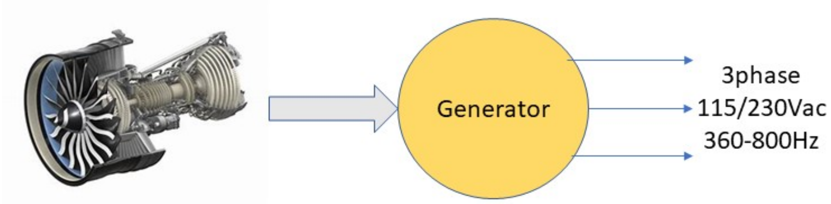

Fig. 2.7 Variable speed generator providing a variable frequency output.

Since there is no accompanying equipment (such as a CSD), the weight, cost and complexity of the generator system is decreased [106]. The drawback with the variable frequency is the sensitive aircraft loads, such as the electric motors, can suffer. On some applications the VF can be accommodated, but in others a controller might need to be implemented. Oftentimes, the manufacturers increase the requirements of the suppliers to provide equipment that can withstand the change in frequency.

VSCF systems provide greater configurability than their CSCF frequency counterparts. Generators with integrated drives, are placed close to the engine so that they can use constant speed drives, whilst the converters of the VSCF are not limited logistically. These systems can be designed to be placed closer to the electrical loads they drive if that enables a preferred aircraft weight distribution. Despite their advantages, though, VSCF are mostly exclusively seen in military applications due to the reliability level of the power electronic converters [105].

2.3.4 28VDC

In 28VDC avionic systems, the generators are regulated to 28VDC. This ensures that no complications arise due to potential transients and fluctuations. The DC generators are self-exciting and the conversion to DC power is performed by using a commutator.

28VDC is mostly found in older generation aircraft [15]. Although low voltage DC systems, had been successful in the past, they can no longer be solely used, as they struggle to meet the higher amount of electric power demand stemming from the increased power requirements of the equipment. That said, some examples of 28VDC are still present in smaller civilian aircraft such as the ATR-600, Dornier 328 and Falcon 2000. Some military aircraft also use 28VDC starter generators such as CN235, IJT-36 and C295.

2.3.5 270VDC

The use of 270VDC is based on the same principle of increasing the voltage from 28VDC to 115VAC. This was pioneered by the US military with F-22 Raptor, A-12 as well as the helicopter RAH-66 Comanche. The reduction in the size of the current carrying conductors can assist in decreasing power dissipation, voltage drop and net weight of the aircraft.

There are some drawbacks associated with this increase in voltage. Firstly, the supply of components that can be driven by 270VDC is expensive, since this a new technology. A lot of subsystems still require 28VDC and 115VAC; therefore, using 270VDC increases the need for robust electrical insulation techniques. Some of these developments have been performed to increase the popularity of electrical systems in military applications and to replace the conventional secondary power and hydraulic power systems.

The electrical distribution of the Lockheed Martin F-22 is shown below; converters are used to supply the loads requiring 28VDC and 115VAC. F-35 shares this design, although it is a single engine aircraft. Switched reluctance generators are also used with double channels for 80kW as a means of redundancy [48, 105].

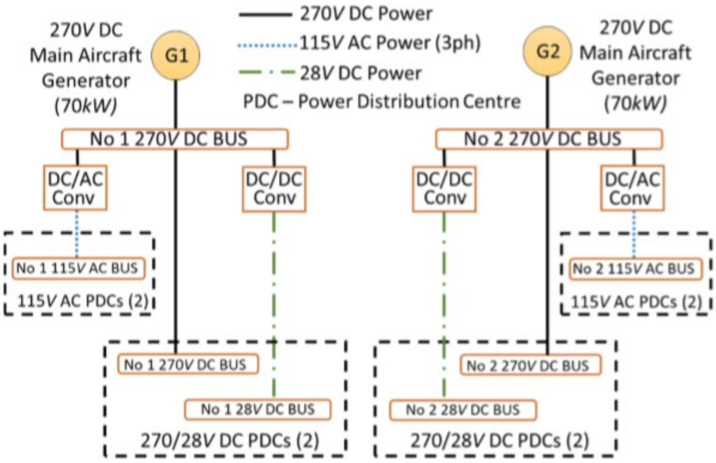

Fig. 2.8 Electrical distribution system of the F-22 Raptor [62].

2.4 Aircraft Load Management

2.4.1 Terminology

In the literature, there exists a varied and nuanced terminology for the methods and functions controlling electrical systems. Firstly, energy management refers to approaches or systems that control energy flow. It is most commonly encountered when describing systems that encompass batteries and other storage devices, or systems that have a battery as their primary source of electrical power. Meanwhile, power management is used as a term when the systems of interest have no relevant storage devices, hence there is an inference of ensuring that the power generated is equal to the power consumed. The term electrical load management (ELM) is often encountered in avionic applications in the context of controlling loading of specific generators, but not the generators themselves. The term source management, on the other hand, refers to systems where multiple power sources are available and controllable. These power sources are controlled to provide an improvement in system efficiency [84]. These terms are not uniquely used when referring to aircraft technologies, but they are also commonly encountered in smart grid technologies [46, 51].

The term "intelligent" has been used to describe the decision-making aspect of the application. It must not be confused with Siemens’s "Intelligent load management", which is a temperature control system for buildings.

Shokooh et al. [86] describes "intelligent load shedding" as a means of ensuring frequency stability of generators replacing the conventional breaker interlock scheme. Intelligent load shedding only takes into account a single generator, whereas ILM can take into account a larger generator power system, with the aim of ensuring no overheat failures, whist optimising the load that remains on-line.

2.4.2 Current Methods of Aircraft Load Management

Whenever the aircraft features multiple available energy sources (i.e., a fuel cell, different sets of batteries, several generators, a photovoltaic panel or a regenerative windmilling system), decisions concerning the amount of power delivered to the different electronic subsystems and which of those sources will deliver energy to which subsystem have to be optimised for each specific mission. This task can become impossible for a remote human controller or pilot to fulfill.

An improper electrical power management could lead into an inefficient flight, wasted energy or worse, failure to complete a mission. The proposed solution is based on a power management system that takes into account all the variables of the plane (including its efficiency and flight limits) and uses fuzzy logic to take decisions related with the power consumption, which are not only better for the optimisation of the mission, but also closer to how a human would behave in the same situation. As a result, the system can relieve the workload of the human controller or pilot and also evaluate the feasibility of the mission.

Schlabe [84] discusses the state of the art of load management on aircraft which is detecting overload and disconnecting suspect loads based on a priority list, as per Lyman's invention [57]. Sodoski [89] considers the user interface approach to Lyman's hierarchical approach. According to the patent, there needs to be an electrical load manager centre that communicates to the crew members the power supplied to loads, and as an extension making that power individually controllable.

The idea of intelligent power distribution has been adopted in several instances in the aeronautic field. Glahn et al. [37] use this idea for a localised application; in the kitchenette of civil aircraft. This is done by identifying a maximum power consumption of the appliances, if that maximum is reached, the power allocated to one or more units is reduced in the background.

Barzegar et al. [11] take advantage of the interconnectivity between main and secondary busbars. They formulate the optimisation problem as a mixed integer and quadratic programming problem. It is attempted to allocate load appropriately, even under the cases where certain generators are unable to provide power to their primary busbars.

All these approaches are employing sensible techniques for ensuring the maximisation of power to the relevant aircraft subsystems, but due to the lack of prognostic aspect, there is a risk of -further- damage to the generators and loads. All these ideas are developed having civilian applications in mind, where there is a larger leeway due to the number of generators on-board and the possibility of redundancy. Most load management techniques fail to consider conditions of failures (with the exception of [11]), in which the authors consider connection failures between generators and busbars. Load management is most likely to be necessary after the occurrence of a fault, and therefore these conditions are extremely important. Most load management techniques currently, employ aggressive compensation of load. There is an accompanying risk of damage being caused due to unpredicted transient response of loads due to a sharp change to the power provided to them. There is an extra reliance on the manufacturers of such subsystems to be able to work alongside the load management techniques that are employed in each case. There also lies a drawback of using power as a guiding measurement for a hierarchical load management. Excess power can be drawn due to a short going undetected and undiagnosed; hence excess action might be taken to accommodate for this, whereas a more targeted approach could have resulted to lesser load shedding.

2.5 Prognosis and Health Management

A large focus of the research provided in this body of work is the introduction of fault tolerant prognostic methods in the field of electrical generators on-board aircraft. In this section literature related to prognosis and health management (PHM) on aircraft systems is discussed.

Kalgren et al. [49] provide definitions of essential terminology in the field of health management. They define health management as an "approach utilising measurements, models, and software to perform incipient fault detection, condition assessment, and failure progression prediction". This enables possible improvements on fault detection, graceful degradation, and maintenance planning. Prognostic health management can also enable improved system reliability and availability, which is especially important for mission critical equipment; it reduces logistics delay time and repair actions as well as further reduces costs during the whole product lifecycle.

PHM implementation in the U.S. is also mandated by the Department of Defence in an attempt to decrease sustainment and operation costs [93]. Apart from reduced costs, it is also recognised that PHM systems enhance mission reliability, increase safety and reduce aircraft downtime due to maintenance [40]. This philosophy is becoming increasingly evident mainly in aircraft engine systems. Orsagh et al. [72] discuss PHM in the context of avionic system power supplies, specifically switch-mode power supplies. They consider faults occurring at component level, i.e. at the switching transistors, filtering capacitors or rectifying diodes. Batzel and Swanson [12] focus on the rotor circuit, as it has been shown [13, 59] that PHM can greatly assist with fault detection. Seeded fault experiments are used to verify that the initial stages of rotor faults are observable under a variety of generator load conditions. In [12] "a tracking filter is used to gauge the deterioration and predict generator remaining useful life". Using this data, one can decrease the system costs by avoiding unexpected failures.

A framework for post prognostic decision making is provided by Iyer [43], where it enables the "user to make optimal decisions based on the expression of rigorous trade-offs between different prognostic and external information sources". Different decision alternatives are assessed under operational boundary conditions using user-specific and interactive collaboration.

Smeulers [88] uses the premise that the RUL of a component "depends directly on its health parameters and its usage levels". Therefore, increased data on the actual health of a device further increases accurate predictions. Ageing models for the component can be updated and adapted using said data. This adaptation ensures an increased model temporal accuracy. As a result, the age of the component has a direct correlation to the volume of data gathered and hence to the accuracy of the prediction.

2.6 Physics Based White Box Thermal Modelling

The most prevalent schools of thought for thermal modelling and analysis of electrical machines are: analytical lumped parameters and numerical methods [14]. In this section, their preferred applications and drawbacks are presented and discussed.

Boglietti et al. [14] mention that for machines of small to medium size, thermal analysis has not been a focal point of research. Their focus is to use thermal models for improving the design of machines, "as the losses are critically dependent on the temperature, and vice versa".

An issue that commonly arises in thermal modeling is the cross disciplinary rift between electrical engineers that design the generators and mechanical engineers performing thermal analysis.

2.6.1 Lumped Parameters

Lumped parameter analysis of electrical machines involves the organisation of components based on their geometry; similar geometric components are modeled as a single node. These models have low computational requirements and their accuracy often depends upon the choice of parameters. The accompanying drawback, though, is the fact that the developer needs to invest effort into constructing a model that accurately depicts the main heat transfer paths [58]. The heat transfer occurs using thermodynamic principles of convection and conduction [16, 90]. However, perhaps because many researchers on this area are electrical engineers, lumped parameter heat transfer network is often modeled using equivalent electrical components and the analysis consists of calculation heat flow through conduction, convection and radiation 'conductances' for different parts of the generator.

2.6.2 Numerical Methods

The advantage that numerical analysis provides is that any device geometry can be modelled. However, there is an increased demand for computational power. The two main types of numerical methods used are "Finite Element Analysis" (FEA) and "Computational Fluid Dynamics" (CFD). CFD is able to predict coolant flow around complex regions, such as around the end windings [65, 90]. Finite elements can only be used to describe heat transfer due to conduction; for convection empirical techniques, similar to the lumped parameter methods, are used.

There are software packages that such as "FLUX" that provide a framework for both electromagnetic and thermal analysis, but they are focused on design optimisation.

FEA solutions often require background knowledge in heat transfer as well. Finite elements, though, can be used very effectively for calculating equivalent thermal conductivity between components; such conductivity can then be used in network analysis, as shown by Powell [68].

2.7 System Identification

System identification is a modeling technique that employed a statistical approach to building mathematical models of dynamic systems from measured data. System identification techniques have their basis in statistical methods, therefore it can be argued that the foundations of system identification were laid by Gauss and Fisher. The term system identification was first used by Zadeh in 1962 [109], where it was defined as follows: "Identification is the determination, on the basis on input and output, of a system within in a specified class of systems, to which the system under test is equivalent". Further development can be attributed to Åström and Bohlin [7], Eykhoff [34] and Box [17]. For engineers, the most interesting thing is the actual model, particularly the transfer functions. The parameter vectors are just a means of acquiring the transfer functions. With Ljung’s research [56] system identification became a "design problem". By further understanding the effects of experimental conditions can have, one can treat the model topologies, structures, and model quality criteria as design variables towards used for tradeoffs for the model being identified [36, 54].

The procedure of system identification is defined as follows:

1. The task at hand and the purpose of the model need to be described.
2. Examination of the initial data to understand the effects that are desirable to capture.
3. Identification of which effects are inherent to the system, and whether tests conducted are repeatable.
4. Based on the understanding from the previous steps, experimental procedure focused on data acquisition is designed.
5. Based on the data gathered experimentally and understanding of the system, a model structure is identified. The aforementioned structure can vary in topology and complexity.
6. Estimation and verification of the models takes place using different datasets.

System identification is used in a variety of fields ranging from engineering [67] to economics [53] and healthcare [27]. That said, the author was unable to find works that use system identification to model heat flow and losses in generators. Graham [38] briefly touches on this in his thesis but does not explore it in depth. His models, especially for windings, show poor fitting for transient conditions with errors up to 20^{o}C.

Young et al. [108] have developed Computer-Aided Program for Time Series Analysis and Identification of Noisy Systems (CAPTAIN) toolbox. This provides algorithms for identification, estimation and non-stationary timeseries analysis. This is facilitated by the use of time varying parameter models, which allows for dynamic regression techniques to be employed [97]. Taylor [95] has demonstrated the effectiveness of this toolbox having it used for environmental timeseries analysis and in hyper fast switching of Peltier cooling systems [96].

Ishark, Tajjudin and Ismail [42, 94] from UiTM have used System identification techniques for modeling Electro-hydraulic actuators and designing controllers for such systems. They discuss different model orders and they compare their goodness of fit to the data, as well as their response to PID controllers designed. That said, they do not provide comparison between different model structures or between the black box model and the physics model of the actuator.

Garlick [35] uses system identification and ARX models in a model-based monitoring system for bearing temperature modeling in wind turbines. Among other points, the importance of identifying appropriate model size for the system at hand is discussed and the false inference of complexity implying better model fit is outlined. They also make an important note on appropriate data sets to achieve effective modeling through system identification.

Often system identification is paired with Neural Networks. Santoso [82] uses NARX (Nonlinear Autoregressive eXogenous) models and timeseries analysis to estimate remaining useful life of industrial systems due to bearing damage. He outlines different structures of NARX such as Parallel and Series-Parallel; furthermore, he uses multi-step ahead prediction and compares the accuracy of these predictions.

Neural network based NARX has also been used to model the behaviour of an automotive air conditioning system [69]. In their article, Ng et al. compare different types of ANN structures, namely Multi-Layer Perception (MLP) and radial basis network for modeling the transient cabin temperate. A lot of emphasis is placed on the experimental setup used for the tests. For their application MLP preforms better than the radial basis network. Furthermore they touch on the comparison of using NARX against using a physics based lumped parameter model [39] as a basis for a control system. Employing (or referencing) simpler structures of system identification (potentially ARX/ARMAX) and comparing their performance to NARX could provide an insight on the necessary complexity of the modeled system.

From the research outlined above, system identification appears to be a suitable approach for estimating generator temperatures, as they are timeseries data that intuitively fit in an Autoregressive exogenous model, i.e. the temperature values depend on past temperature values and “some external input”, in this case the losses (and current). Other model structures that fit these characteristics (ARMAX) are also considered in the thesis.

In generators of higher complexity, NARX are explored as they provide an easier implementation of a large number of exogenous inputs in a Series- Parallel manner.

2.8 Adaptive Black Box Modeling

Cai et al. [18] mention the need for adaptive techniques in non-stationary environments. They employ a variable forgetting factor in the design of receivers in wireless communications. Through simulation it is demonstrated that in a non-stationary environment their adaptive methods outperform existing approaches.

When controlling plants of increased complexity adaptive modeling is often used. Commonly, systems with online varying parameters [75] employ the use of Fuzzy systems. In [20] adaptive iterative learning controllers are used for controlling repeatable non-linear system with initial state errors. In other works, the idea of varying the structure and number of parameters has been considered [76].

In more application-oriented works, Triven and Ratnakumari [99] compare model predictive controllers (MPC) to adaptive MPC for temperature control of a continuous stirred tank reactor. They suggest the use of adaptive MPC to address the shortcomings of MPC when faced with prediction degradation. Adaptive MPC addresses this deterioration by adapting the model prediction by considering operating conditions.

Barraza-Barraza in [9] and [10], employs adaptive system identification techniques to estimate the remaining useful life of aluminum plates. She outlines several limitations of the state of the art techniques, such as the requirement of a plethora of historical data for ANN training, create probability distributions and define transition matrices. These limitations and need for data are applicable in the field of heat transfer and simulation. Often algorithms require information under both normal and faulty conditions [19], which are sometimes hard to obtain. The requirement for an increased amount of data is even more prevalent in non-linear applications [87] and [50]. It has been shown that the order of an autoregressive system may vary between normal and faulty conditions [8], which makes the aforementioned issues even more important. Barraza-Barraza mentions that the data requirement issue can be tackled by employing timeseries techniques for providing short time predictions. She proposes adaptive ARX models for assessing remaining useful life without preexisting historical data. She also mentions that the behaviour of the system changes as it degrades; hence adaptation is necessary, which in this case is done via recursive least squares (RLS) methods. She lastly compares different structures of the system as well as different adaptation techniques, showing that the RLS approaches outperform ordinary least squares (OLS). Both nonlinear autoregressive models and linear ARX showed considerable merits when the faults occurred at different rates. All models showed issues when dealing with measurement noise with different tradeoffs. This research is the main driver behind the use of adaptive ARX models for estimating generator temperature after subjected to faults. The main difference is that in this thesis the application is a real time system. Therefore, the same model structure is kept between healthy and faulty generators, as estimating new optimal structure would be too computationally demanding. In order to compensate for this, a forgetting factor approach is employed, so that there is an increased weight on recent data when parameters are estimated.

2.9 Remarks on "Intelligent Power Management for Un- manned Air Vehicles" [38]

This body of work takes heavy inspiration from [38] as well as shares the experimental rig, as (initially) being members of the same academic team. Therefore it is diligent to provide a top-level clarification on the improvements that this work provides to the current body of knowledge developed by Graham. He provided a basis for the thermal modeling (using equivalent electrical components). Furthermore, he touched on static system identification techniques but concluded that they were insufficient for the task at hand. Lastly, there was an initial approach to a load management algorithm using a series of "if" statements.

The improvements mostly take place in the aspect of modeling, prediction and load management algorithms. In this work the author aims to clearly distinguish between electrical and thermal components in a thermo-electrical model of a generator. Furthermore, different model topologies are explored showing the merits of using system identification for this application, in terms of complexity, reconfigurability and implementation. Moreover, adaptive models are used for fault tolerant prediction, which increases the system efficiency by reducing unnecessary load shedding. The load management algorithm developed in this work is more dynamic exploring the reconfiguration and shedding aspect to more depth.

The implementation process is kept in mind even when the algorithmic design is not simple, a -almost- plug and play approach is attempted for its implementation by the user.

Lastly, the design process is transferred from the lab-based generator rig to aircraft generators to provide a proof of concept.

2.10 Conclusions

In this literature review the field of electrical load management on aircraft is explored. It has been shown that current state of the art provides an "ex-post" (after the fact) solution to faults and overheating with very limited prognostics. Furthermore, with the current approach fault tolerance is not an option and still there is risk of damaging the generators. The review has shown that most commonly a lumped parameter approach is used for modeling heat flow through generator components, while the most vulnerable parts to overheat are the stator iron and windings [58]. Thermal management is not commonly considered in the larger generator health management field, even though overheat may pose a substantial risk to the operation of generators. Exploring different modeling techniques, it has been shown in neighboring fields that black box approaches can improve system complexity issues in real time applications. Adaptive systems can also provide more accurate modeling and predictions. Using timeseries analysis methods and adaptive modeling one can reduce the amount of necessary data for an accurate model.

CHAPTER 3

EXPERIMENTAL SETUP AND SIMULATION MODEL

3.1 Introduction

In this chapter two main topics are being discussed. Firstly, the generator used in the experimental setup, alongside with accompanying instrumentation and sensors; as well as the creation of a physics-based model for the generator at hand.

The model of the generator is to be used as a surrogate for testing purposes, including fault analysis alongside algorithm design.

This chapter is structured as follows: the generator used in the experimental set-up followed by the apparatus used for data acquisition are introduced, then the methods of processing the collected data are explained. A nonlinear model of a generator that is used to describe the temperature of the vulnerable generator components is devised and validated using the lab-based generator.

To ensure model fidelity, a parameter sensitivity analysis is performed on the components of the generator that are of interest.

The validation process consists of three main tests that aim to assess the performance of the model under different conditions, namely, steady state response at different loading conditions, response during a changing load, and response during a realistic mission (as per Table 3.1 and Fig. 3.1).

As faults are to be modelled using this model, example faults are provided and discussed at the end of this chapter.

Table 3.1 k- values corresponding to specific stages of flight and their load conditions.

k-value	Stage of flight	5 minutes	continuous
1	Loading and Preparation	40%	27.3%
2	Start and Warm- up	83.3%	66.7%
3	Taxi	100%	83.3%
4	Take-Off and Climb	83.3%	76.7%
5	Cruise	83.3%	70.0%
6	Cruise/ Combat	86.7%	73.3%
7	Landing	100%	76.7%

3.1.1 Generator Load Profile

The research focuses on military applications with a mostly known routine, the loads driven by the generator are described in military specifications MIL-STD-704F and MIL-E-701. The load is described as a percentage of net load over the operational period, where this percentage depends on the stage of flight at hand. Each stage of flight has two parts, the startup (first 5 minutes) and the continuous usage. All stages of flight have a minimum duration of 15 minutes with no upper limit. The 7 stages of flight and their corresponding load profiles (k-values) are presented in Table 3.1.

These stages of flight can be used sequentially to create a full flight profile; an example would be as follows (Fig. 3.1).

3.2 Experimental Setup

The test rig is comprised by three main parts: the electrical generator Fig. 3.2, the load bank Fig. 3.3 and the electrical cabinet Fig. 3.4. The generator used in this test rig is not an aircraft generator; access to such a generator was provided at a later date. Having stated that, validated models and algorithms can provide proof of concept regardless of the type of generator used. The generator used is a commercial synchronous generator (GENCO RF201A) - for exact specifications refer to Table 3.2 below- with the internal airflow being provided by a fan. The mechanical input is provided by a three-phase induction motor that is controlled by a Eurotherm 620 series drive. For the generator to produce rated voltage, the mechanical input is at 1500rpm. The load bank, in turn, is able to draw from 1A to 7A per phase, with the ability of creating unbalanced load and having different power factors.

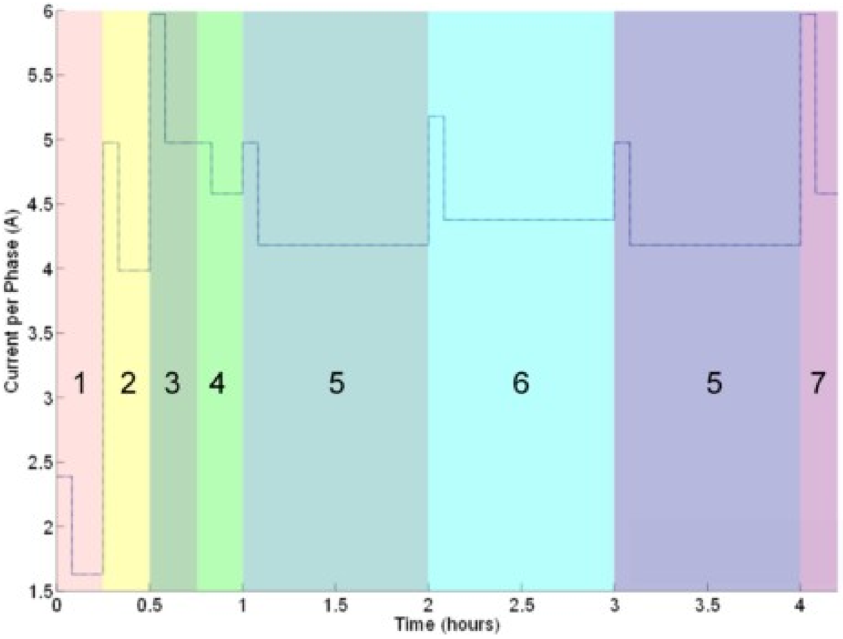

Fig. 3.1 Load per phase for the corresponding stages of flight.

Table 3.2 Generator Rig Specifications.

Type	GENCO RF201A; synchronous including damper winding
Power	5 [KVA]
Voltage	415/240 [V]
Current	7[A]
Number of phases	3
Frequency	50 [Hz]
Shaft Speed	1500[rpm]
Excitation	Brush-less rotation rectifier with aux winding for exciter power
Rating	00P
Insulation class	H
Enclosure type	IP22

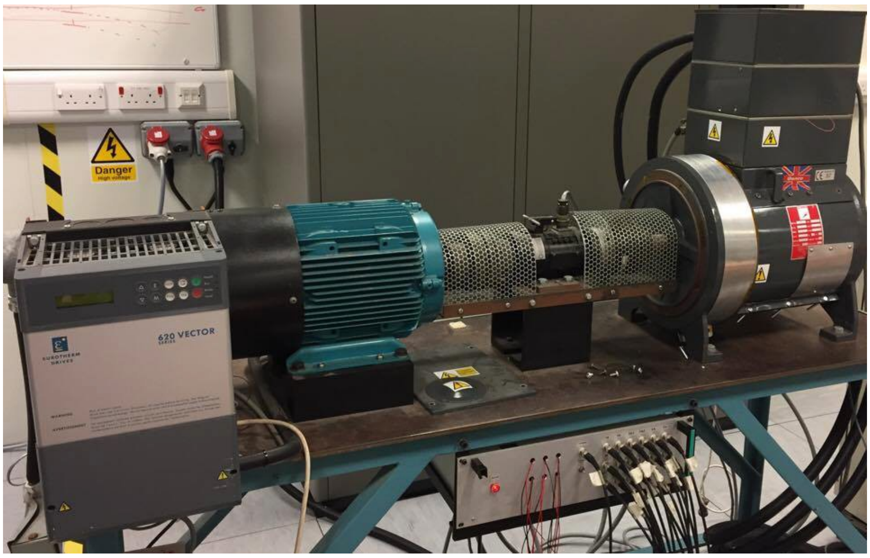

Fig. 3.2 Generator GENCO RF201A (right), Eurotherm drive (left).

Fig. 3.3 Load Bank.

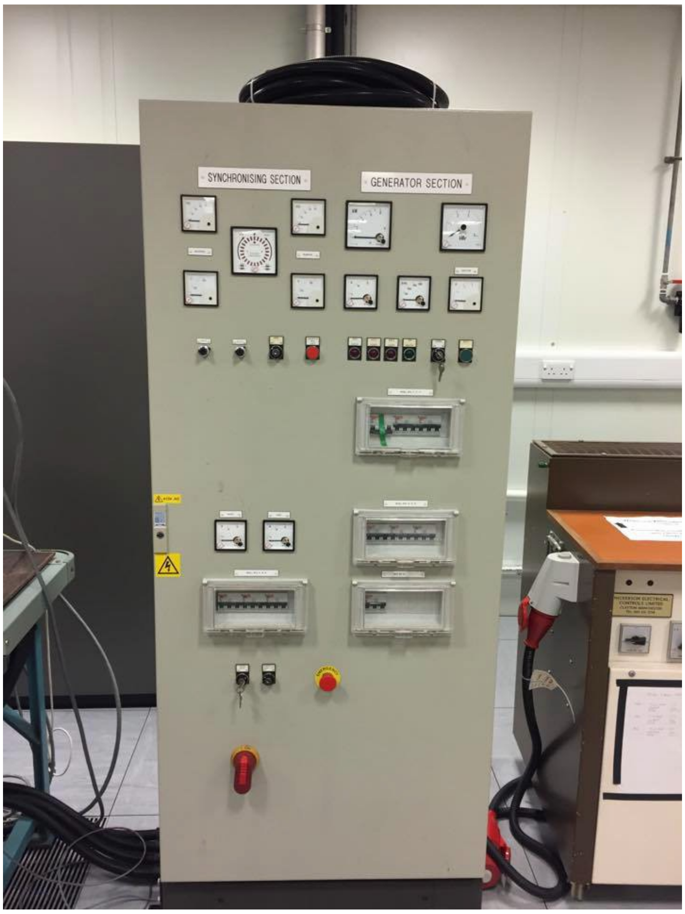

Fig. 3.4 Electrical cabinet.

Table 3.3 List of sensors and their range.

Variable	Signal Label	Range
Stator Phase U Current	IU1	±230A
Stator Phase U Current	IU2	±15A
Stator Phase V Current	IV1	±230A
Stator Phase V Current	IV2	±15A
Stator Phase W Current	IW1	±230A
Stator Phase W Current	IW2	±15A
Stator Phase U- Neutral Voltage	VU	±500V
Stator Phase V- Neutral Voltage	VV	±500V
Stator Phase W- Neutral Voltage	VW	±500V
Exciter Winding Current	Iex	±5A
Exciter Winding Voltage	Vex	±125V
Auxiliary Winding Current	IAux	±2.5A
Auxiliary Winding Voltage	VAux	±500A
Stator Phase U Temperature	TSwU	-50 to 300^{o}C
Stator Phase V Temperature	TSwV	-50 to 300^{o}C
Stator Phase W Temperature	TSwW	-50 to 300^{o}C
Stator Iron Temperature	TSi	-50 to 300^{o}C
Inlet Temperature	TI	-50 to 300^{o}C
Outlet Temperature	TO	-50 to 300^{o}C
Mid Air Pocket Temperature	TMp	-50 to 300^{o}C

The generator has enough similarities to on-board aircraft ones that it can be used for modelling purposes. In order to switch to an on-board aircraft generator some parameters need to be changed but the overall model remains the same. The rig contains a plethora of temperature, current and voltage sensors (outlined in Table 3.3) that are used for data acquisition.

The data most attention is paid to are: the Stator Phase Winding Temperatures, Stator Iron Temperature, Excitation Current and Stator Phase Currents. This information has been shown in [4] to be more important since the Stator Iron and Windings are more likely to exceed the maximum threshold temperatures. The excitation current and load current are directly linked to the copper losses of the aforementioned components and are used as inputs to the models.

3.2.1 Voltage and Current Sensors

Voltage and Current Transformers have been placed to measure in real time the voltages and currents outlined above. The transducers are galvanically isolated; hence there can be a reference to ground for the measurements. The transducers are placed close to the generator and the isolated output signals are routed to an instrumentation terminal, placed under the generator, where the signals are recorded. These signals are put through a filter for them to be transformed to voltages that can be read by the data acquisition card. Figs. 3.5 and 3.6 show the layout of the sensors. The sensors have been calibrated over their operating range. Their calibration takes the form of a first order transfer characteristic (3.1). For both sets of sensors, this is defined in (3.1).

$$L_{(I,V)} = M_{(I,V)}C_1 + C_2 \tag{3.1}$$

where $L_{(I,V)}$ is the line current and voltage respectively, $M_{(I,V)}$ the output current and voltage from the measurement box. C_1 and $C_2$are predefined constants describing the gradient and offset of the linear fit. The C_1 and C_2values for the measured quantities are provided in Table 3.4.

3.2.2 Temperature Sensors

For measuring the temperature at different parts of the generator, platinum resistance thermometers were installed. In total there are 7 thermometers located at the stator windings (3), stator iron (1) and air pockets (3); these locations are shown in the Fig 3.7 below. All thermometers used are identical and have a resistance of 100Ω at 0°C. The resistance in the temperature range of 0°C to 850°C can be calculated from a standard equation (3.2).

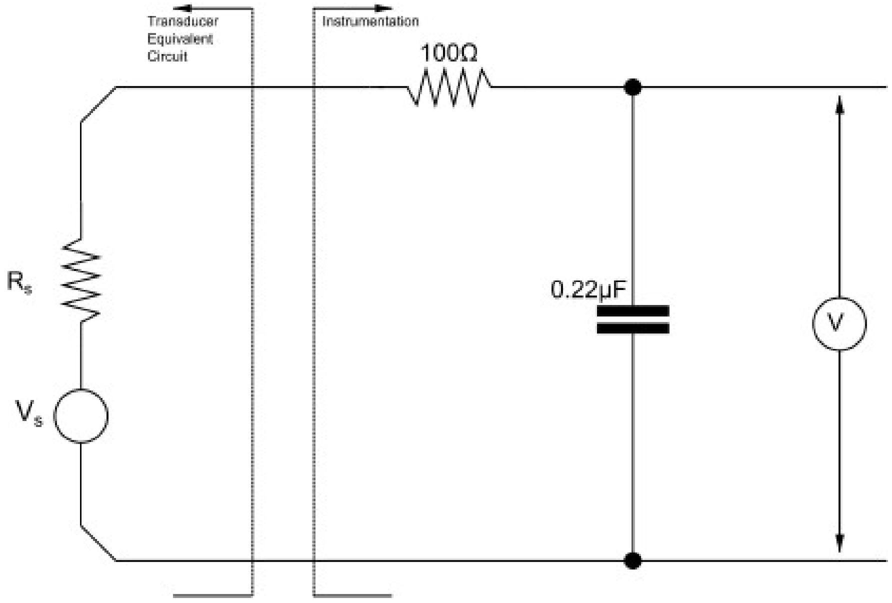

Fig. 3.5 Layout of the Current and Voltage Sensors.

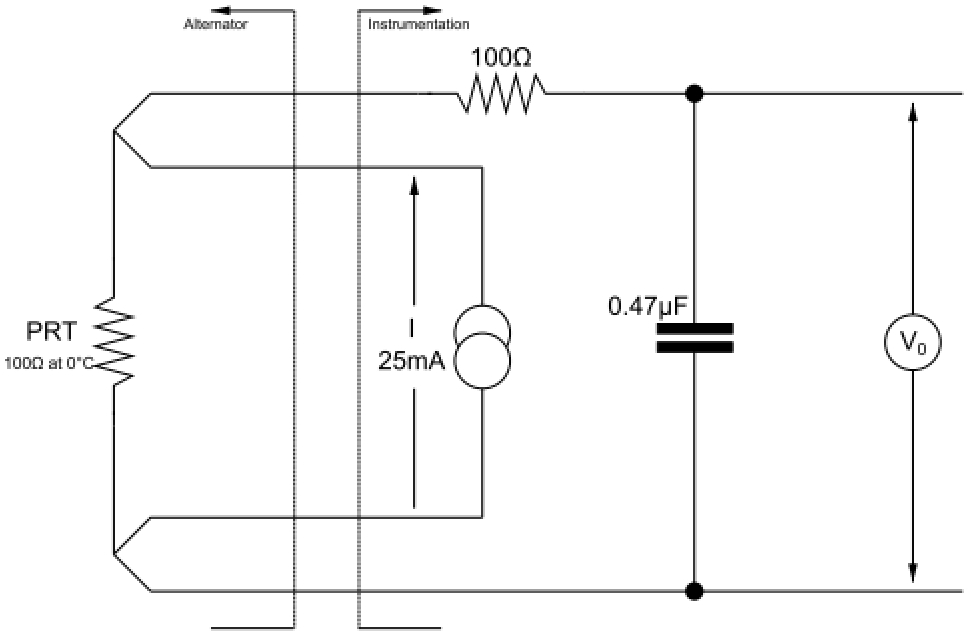

Fig. 3.6 Layout of the Temperature Sensors.

Table 3.4 Gradients and Gains for Sensor Calibration.

Variable	C1	C2
Stator Phase U Current	39.1	0.169
Stator Phase U Current	3.34	-0.0378
Stator Phase V Current	39.1	-0.171
Stator Phase V Current	3.34	-0.113
Stator Phase W Current	39.1	0.191
Stator Phase W Current	3.34	-0.0575
Stator Phase U- Neutral Voltage	66.6	0.491
Stator Phase V- Neutral Voltage	66.6	0.540
Stator Phase W- Neutral Voltage	66.6	0.571
Exciter Winding Current	1.02	0.00224
Exciter Winding Voltage	20.0	0.0697
Auxiliary Winding Current	0.5	0.00484
Auxiliary Winding Voltage	66.6	0.896

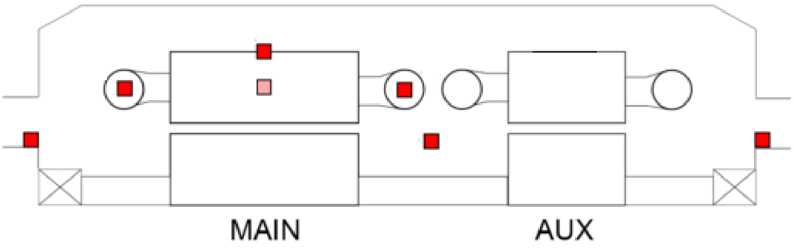

Fig. 3.7 Cross-sectional view of the generator highlighting the location of the thermometers.

$$R_T = R_0(1 + AT + BT^2) \tag{3.2}$$

where R_T is the resistance at temperature T, R_0 is the resistance at 0°C (100Ω), A and B are predefined constants.

$$A = 3.9083 \times 10^{-3}\ {}^oC^{-1}, \tag{3.3}$$

$$B = -5.775 \times 10^{-7}\ {}^oC^{-2} \tag{3.4}$$

The thermometers used are four wire type. As seen in Fig. 3.6, the thermometers are driven by a constant current, hence, the voltage drop is proportional to the resistance which is in turn a function of the resistance of the windings. Each thermometer has a set resistance to temperature relationship. As all DAQ signals are voltages, they need to be calibrated accordingly. To calibrate the voltage input, the PRT was replaced with a resistor. This allowed the potential difference to be transformed to resistance, which was then transformed to measured temperature using (3.2).

3.2.3 Data Acquisition (DAQ)

All data streams mentioned in Table 3.3 are made available as a voltage reading. All data are recorded using a National Instruments (NI) DAQ card and NI LabVIEW. The

DAQ card is a NI PCI-6229, its full specifications are provided in Table 3.5 .

Table 3.5 PCI-6229 Specifications.

Type	NI PCI - 6229
Analogue Inputs	32, 16-Bit, 250 kS/s
Analogue Outputs	4, 16-Bit, 833 kS/s
Digital I/O	48 digital I/O, 32-bit counters, digital triggering
Correlated DIO	32 clocked lines, 1MHz

3.2.4 Data Post Processing

After all data have been collected, they are processed in order to ensure the ease of their further usage in MATLAB. The armature and excitation currents, as well as the winding and stator iron temperatures have been identified to be the most important data. The stator iron and the windings are the areas of the generator most likely to suffer an overheat, whilst the aforementioned currents are the main contributor to this increase in temperature (further discussed in this chapter). The exact values of the currents are calculated by converting the measured voltage to the corresponding quantity, using the information provided above (3.2 – 3.4). The voltage related to phase current measurements is converted from a peak value to RMS. The calculated values are then filtered, every 200 samples the maximum value is found, and all 200 samples are replaced by that value. This ensures the values do not fluctuate and the maximum is not lost (Fig 3.8). In the same manner, the temperatures are calculated by using (3.2) and solving for T and choosing the appropriate root.

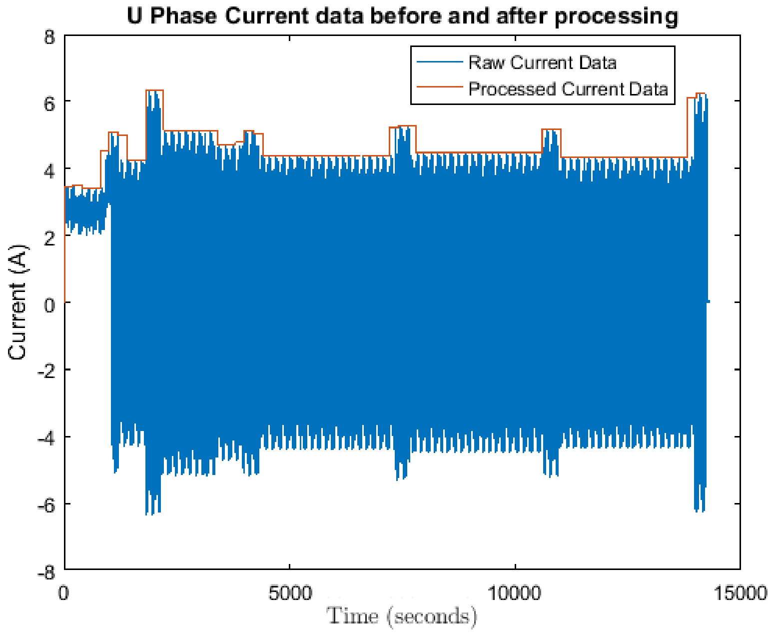

Fig. 3.8 U Phase Current raw data compared to processed data.

3.2.5 Tests

In this section the tests conducted on the generator are outlined. These tests are conducted in order to collect data and hence ensure that all the models are accurate both in terms of steady states and transient behaviour. The tests can be split into three main categories: the constant load tests, responsible for ensuring the correct modelling of steady state conditions; the varied load tests, for transient behaviour; and the realistic mission profile tests, whose focus is on the specific conditions that are more common during a mission.

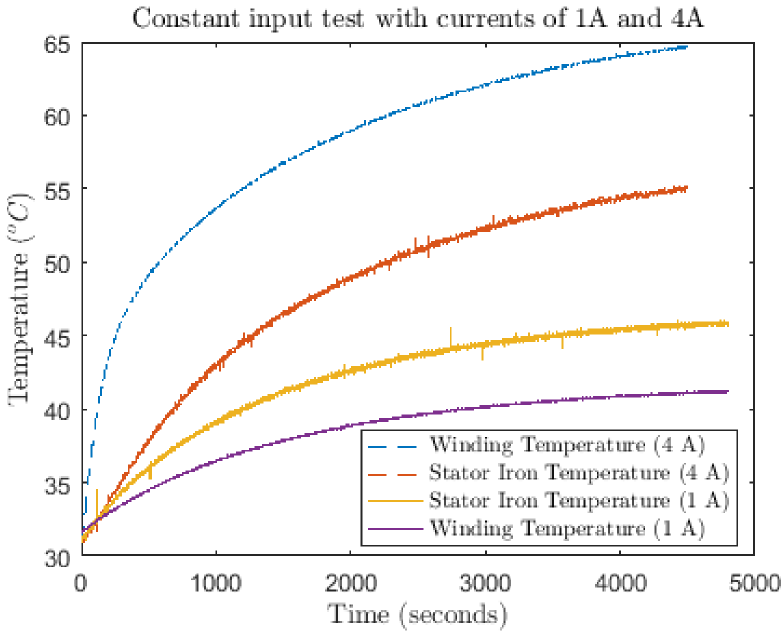

Fig. 3.9 Temperatures of Stator Windings and Stator Iron when driving 4A (60% full load) and 1A (15% full load).

Constant Load

The temperature of the windings and stator iron when driving a constant load are shown in Fig 3.9. Constant load tests provide information on steady state temperatures as well as the heating up/ cooling down transient process.

It can be observed that for the time of the test the generator components are unable to reach a steady state temperature, this is because of the ambient temperature of the room increasing due to the heating up of the generator and the load bank. This assumption is based on the temperature increase being similar during both tests. This information is important, as it suggests that the ambient temperature needs to be taken into account during the modelling process. Furthermore, the temperature of the windings is more sensitive to the increase of current when compared to the stator iron. This is expected due to the difference of mass and material.

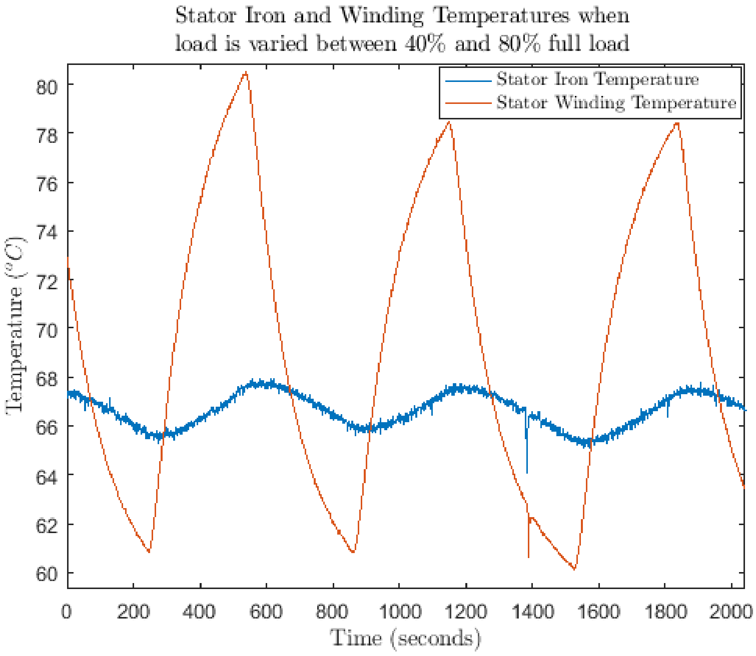

Fig. 3.10 Temperatures of Stator Windings and Stator Iron when driving 40% to 80% of full load.

Varied Load

Varied load tests give further insight into the transient behavior of the system. In this case the load is shifted between 40% and 80% of full load. Figure 3.10 shows the temperature fluctuation as a result of the load change.

Realistic Mission Profile

The purpose of the “Realistic Mission Profile” test is to ensure the model is able to provide high fidelity for the scenarios that may be faced in a mission. By considering the information provided in section 3.1.1 the corresponding load profile is created. The load is varied and currents and temperatures are measured and processed (as described in 3.2.3 and 3.2.4). Figures 3.11 and 3.12 show the increase in temperature as a result of the changing current demand.

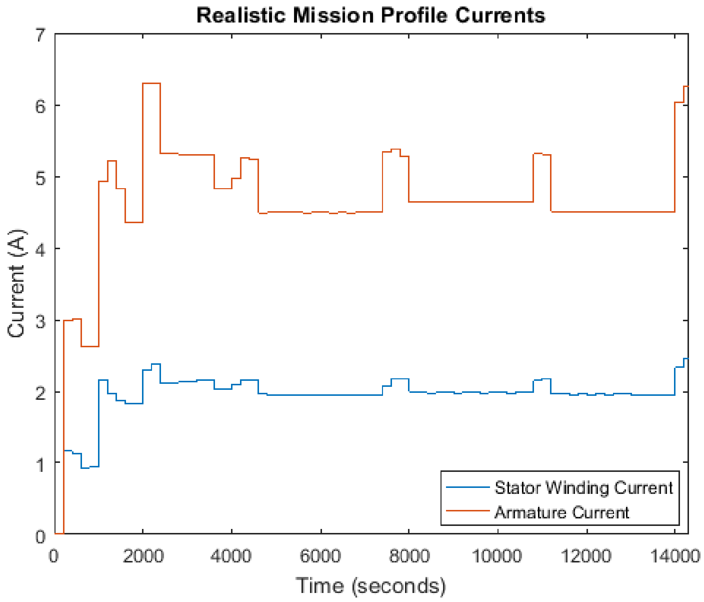

Fig. 3.11 Excitation and armature current of an example mission.

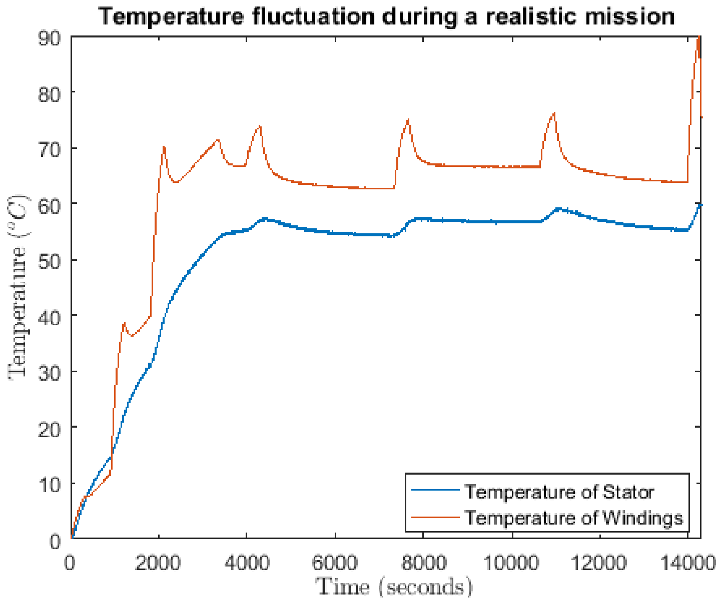

Fig. 3.12 Temperature fluctuation of stator windings and iron.

3.3 White Box Modelling of On-board Aircraft Generators

The purpose of this model is to be used instead of the generator for testing and validation. Having a white box model allows easy alteration of parameters in order to simulate different conditions and faults without risking permanent damage to the experimental set-up. For the model to be of sufficient accuracy, it is split into three main subsystems, outlined in Fig. 3.13: the electrical model, the calculation of the losses, and the thermal model that calculates the temperature of different parts of the machine. The mechanical input provided by the engine and other instrumentation present between the generator and the engine (for instance a CSD) are not in the scope of this research.

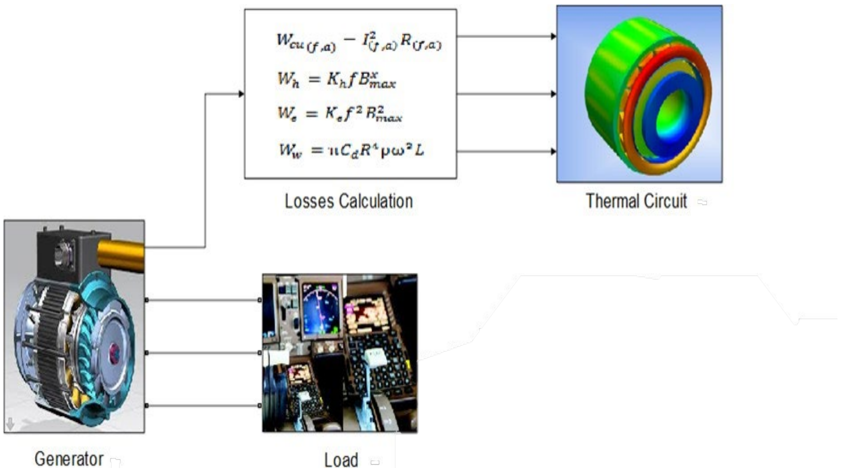

Fig. 3.13 Schematic representation of the parts of the white box model.

3.3.1 Electrical Modelling

28VDC Model

Dub [29] describes in detail the structure of a 28VDC on-board generator and the equations it follows. The magnetic poles excite a stationary magnetic field in which there is a rotating armature coil connected to the commutator segments. Due to the way the field coils are connected to the armature, most DC generators are designed with a parallel excitation (e.g. Fig 3.14).

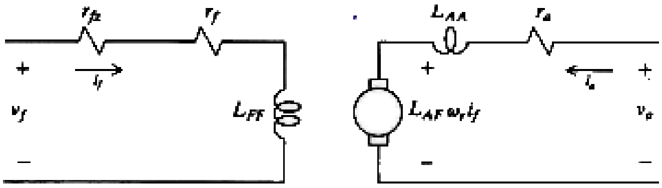

Fig. 3.14 Simple DC generator circuit [52].

In this case the excitation current is converted to excitation voltage by using a lookup table. In the problem at hand however, the access to the excitation current is needed at all times since it constitutes a component of the losses.

Krause [52] describes the DC generator (and/or motor) with the following equations (3.5 – 3.8), describing the mechanical and electrical aspects.

$$E = K_e \omega \tag{3.5}$$

$$K_e = L_{af} I_f \tag{3.6}$$

$$T_e = K_t I_a \tag{3.7}$$

$$J\frac{d\omega}{dt} = T_e - T_i - B\omega - T_f \tag{3.8}$$

where E is the EMF, K_e is the voltage constant, ω is the mechanical speed, L_{af} is the field/armature mutual inductance and I_f is the field current, T_e is the electromechanical torque, K_t is the torque constant (often $K_t = K_e$), I_a is the armature current, J is the inertia, B_m is the viscous friction coefficient and T_f is the Coulomb friction torque (often ignored).

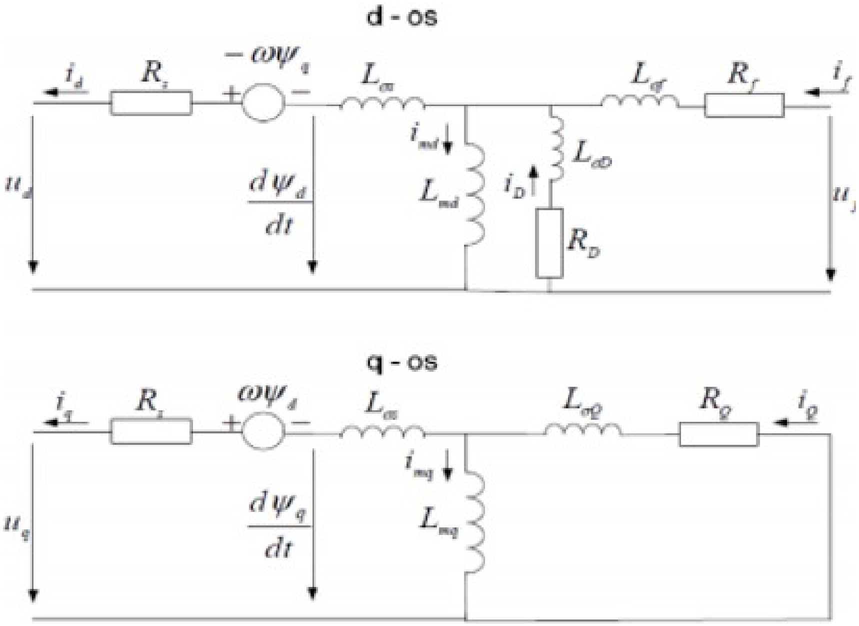

Fig. 3.15 Schematic representation of the standard model in the (d-q) axis.

115VAC Model

The generator is modelled using the standard model which is explained schematically in Fig. 3.15 in the direct- quadrature (d-q) frame of reference, as explained in [102]. Equations (3.9 -3.14) describe its behaviour. As mentioned previously, although the generator in the laboratory-based rig is not an on-board aircraft one, the approach to modelling is the same.

$$T'_{do}\frac{dE'_q}{dt} = -E'_q - (X'_d - X'_d)[I_d - \frac{X'_d - X''_d}{(X'_d - X_{ls})^2}\,(\psi_{1d} + (X'_d - X_{ls})I_d + E'_q)] \tag{3.9}$$

$$T''_{do}\frac{d\psi_{d1}}{dt} = -\psi_{d1} + E'_q - (X'_d - X_{ls})I_d \tag{3.10}$$

$$T'_{do}\frac{dE'_d}{dt} = -E'_d - (X'_q - X'_q)[I_q - \frac{X'_q - X''_q}{\left(X'_q - X_{ls}\right)^2}\left(\psi_{2q} + (X'_q - X_{ls})I_q + E'_d\right)] \tag{3.11}$$

$$T''_{do}\frac{d\psi_{q1}}{dt} = -\psi_{q1} + E'_d - \left(X'_q - X_{ls}\right)I_q \tag{3.12}$$

$$\frac{d\delta}{dt} = \omega - \omega_s \tag{3.13}$$

$$\begin{aligned}\frac{2Hd\omega}{\omega_s dt} &= T_m - \frac{X''_d - X_{ls}}{X'_d - X_{ls}}I_q\left(E'_q + \psi_{1d}\right) - \frac{X''_q - X_{ls}}{X'_q - X_{ls}}I_d\left(E'_d + \psi_{2q}\right)\\ &\quad - \left(X''_q - X''_d\right)I_d I_q - T_{fw}\end{aligned} \tag{3.14}$$

Where $E'_{(d,q)}$ is the transient voltage in the d/q axis respectively, E_{fd} is the field voltage, H is the inertia constant, $I_{d,q}$ is the current in the d/q axis, $T'_{do,dq}$ is the sub-transient constant of the d/q axis, T_M is the mechanical torque, T_{fw} is the additional damping torque (proportional to the speed), $X'_{d,q}$ is the reactance in the d/q axis, X_{ls} is the leakage reactance, δ is the rotor angle, $\psi_{1d,2q}$ are the flux linkage d/q axis damper windings, ω is the rotor speed and ω_S is the synchronous rotor speed. Equations (3.9, 3.10) describe the direct axis dynamics, (3.11, 3.12) describe the quadrature axis dynamics, and (3.13, 3.14) describe the swing equation [4]. Figure 3.16 shows the top-level schematic of the generator circuit; it comprises of the excitation system (AC1A), a governor responsible for providing constant power to the generator and the generator itself. It should be noted that a small parasitic load is added in order to avoid numerical oscillations.

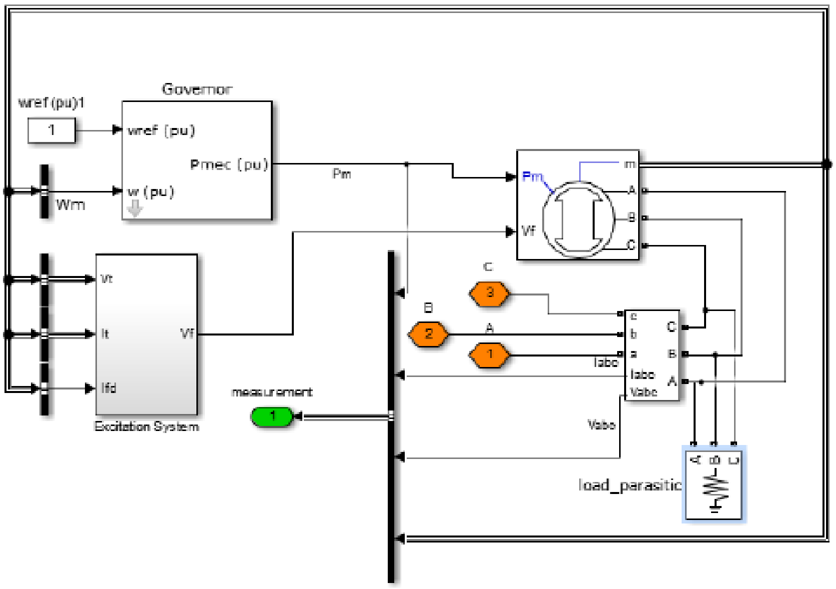

Fig. 3.16 Layout of the generator circuit

3.3.2 Calculation of Losses

The main manifestation of losses in the system is heat. Therefore, calculating such losses providing information on the amount of heat that is input to the system. The losses considered in these models are:

- The Copper Losses (W_{Cu}), which are in turn split in two parts, the excitation field and the armature losses (3.15).
- Hysteresis Losses (3.16). Hysteresis losses are caused due to reversal of magnetisation of the iron core caused when it passes a pole pair. Hysteresis depends upon the iron grade and volume, frequency of the machine, number of poles and flux density.
- Eddy Current Losses (3.17). Eddy current losses are caused due to the rotation of the armature core in the magnetic field. This induces an EMF in the core, which in turn, causes a current flow in the core.

- Windage Losses (3.18). "Windage loss in a generator is the power absorbed by the fluid surrounding the rotor as a result of the relative motion between the rotor and the stator". Windage often increases the temperature of the generator as the energy absorbed manifests as heat [101].

$$W_{cu_{(f,a)}} = I_{(f,a)}^2 R_{(f,a)} \qquad \text{(W)} \qquad (3.15)$$

$$W_h = K_h B_{max}^x \qquad \text{(W/kg)} \qquad (3.16)$$

$$W_e = K_e B_{max}^2 \qquad \text{(W/kg)} \qquad (3.17)$$

$$W_w = \pi C_d L \rho R 4 \omega \qquad \text{(W)} \qquad (3.18)$$

where $I_{f,a}$ and $R_{f,a}$ refers to the field and armature currents and resistances respectively, K_h and K_e are the hysteresis and eddy current coefficients, f is the frequency, B_{max} the maximum magnetic field, L is the length of the cylinder, R is the radius, ρ the density, ω is the angular velocity and C_d is the skin friction coefficient which is defined in [101] as:

$$C_d^{-0.5} = 2.04 + 1.768 \ln(\, R_e C_d^{0.5}) \qquad (3.19)$$

where $R_e$refers to the Reynolds number which in turn depends on the properties of the fluid. It should be noted that the resistance above is modelled as a function of the temperature (3.20),

$$R(T) = R_0[1 + \alpha(T - T_0)] \qquad (3.20)$$

where $R(T)$ is the resistance at the measured temperature $T,$ T_0 , is room temperature, R_0 is the resistance at T_0 and α is the temperature coefficient (which for copper is α_{Cu} = 0.00393/K).

3.3.3 Thermal Circuit

The methods employed for thermal modeling of systems broadly fall into two major categories: lumped parameter analysis and numerical methods [14, 38]. The most common numerical methods used are Finite Element Modelling [70] (FEM) and Computational Fluid Dynamics (CFD) [14, 85]. FEM is a dominant technique in heat conduction problems, where the structure of the body is complex. Splitting the structure into a large number of nodes allows accurate estimation of the temperature of the components as well as the transients. This solution would be implemented as follows: define the geometry, define the differential equations describing the system dynamics, describe the relationship between elements and then solve for the nodal temperatures. This method, although accurate, has two major downsides: it adds extra layers of complexity and requires an increased amount of processing power. CFD monitors the flow of coolant around the structure; hence the heat at different parts of the generator can be calculated. CFD has the same disadvantages as FEM; unnecessary complexity and processing power. These methods were discarded due to being suboptimal for the real time task at hand.

Lumped parameter approach is based on dividing the generator into several parts based on their geometry e.g. stator, rotor, windings, etc. There are two prevalent approaches to lumped parameter thermal modelling: thermal circuit [26, 38, 58] (using thermal components) and electrical equivalent circuit [58]. In the thermal circuit, the lumped parameters are modelled as thermal point masses [4, 92], the heat transfer between such components due to convection and conduction are considered [4, 21, 58]. The inputs to the lumped parameter thermal circuit are the heat emitted from the machine components, i.e. the losses [26, 58]. The equivalent electrical circuit provides a similar approach, the inputs to the circuit are currents, the thermal masses are substituted with capacitors and the heat transfer is modelled as current flowing through resistors/conductors [38, 58]. The equivalent circuit provides the ability to split the lumped parameters into smaller parts with ease, whereas with the thermal circuit such a process is more difficult. That said, such a task is not necessary for the application at hand. Moreover, a thermal circuit is easier to explain to the industry specialists implementing the system and hence has been chosen for this application.

The lumped parameter thermal circuit has been created using Simscape thermal components. The lumped parameters considered were: the frame, stator iron, stator windings, rotor, shaft, bearing plates and flange, as can be observed in Fig. 3.17.

The lumped parameters are considered to be thermal point masses that are proportional to the specific heat capacity of the material and the mass.

$$Q = \frac{dT(t)}{dt} Cm \tag{3.21}$$

where Q is the heat energy stored (J), T is the temperature (K), C is the specific heat capacity (Jkg^{-1}K^{-1}) and m is the mass (kg). It is assumed that the generator is comprised of an iron stator, rotor, and shaft, aluminium frame, and copper windings.

The heat transfer between components can occur in two ways: by convection and conduction, which are described below in (3.22) and (3.23) respectively [21, 58]

$$Q = \Delta T k A \tag{3.22}$$

$$Q = \frac{A}{d} k \Delta T \tag{3.23}$$

where T refers to the temperature (K), A to the area (cm^2), k to the heat transfer coefficient (Wm^{-1}K^{-1}).

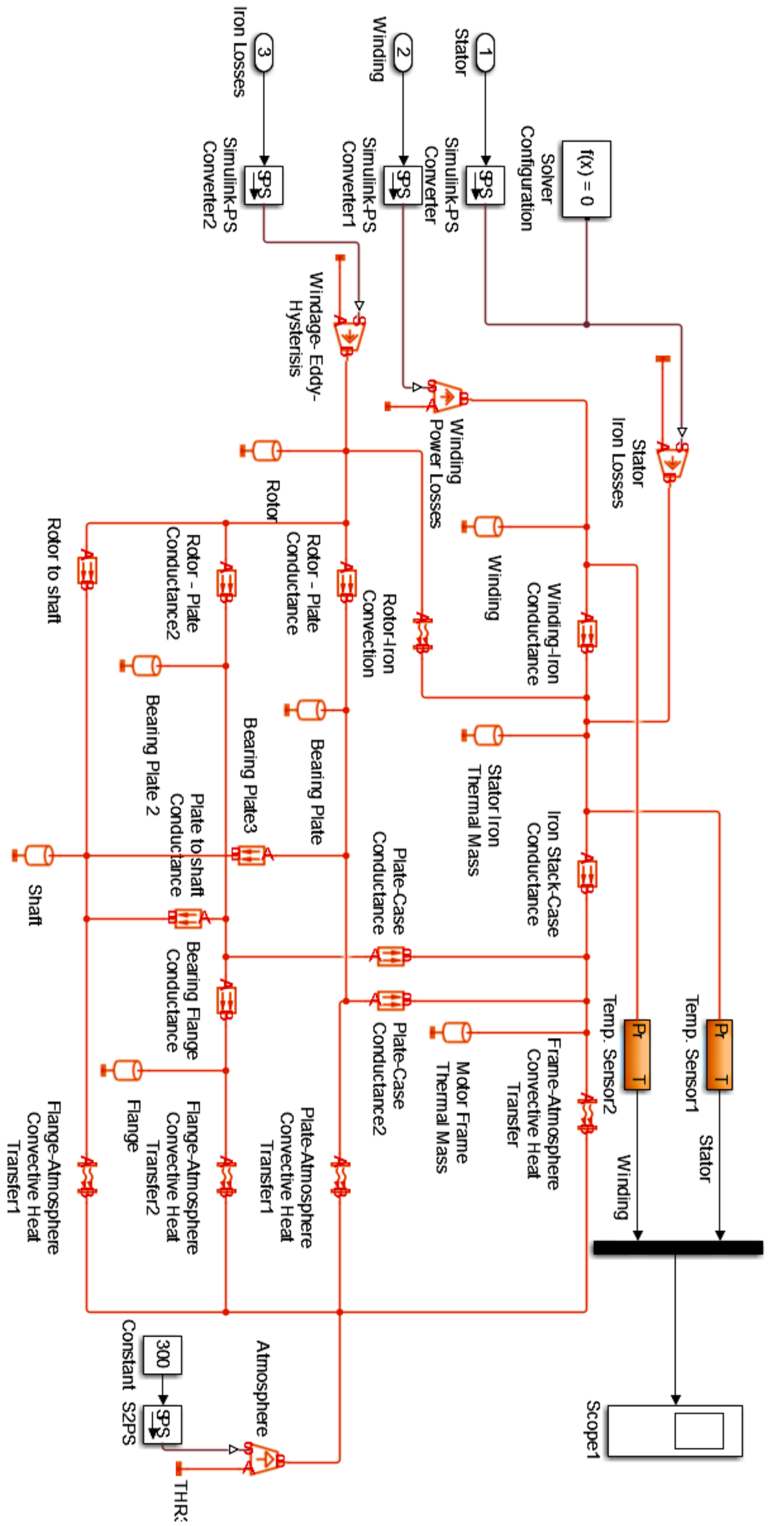

Fig. 3.17 Lumped parameter thermal network in Simscape / Simulink.

Table 3.6 Physical characteristics of the generator.

Variable	Value
Length of the Frame	0.347m
Length of the Stator Iron	0.053m
Length of the Stator Windings	0.053m
Length of the Stator Rotor	0.053m
Length of the Air Gap	0.053m
Length of the Shaft	0.239m
Radius of the Frame	0.159m
Radius of the Shaft	0.023m
Outer Radius of the Stator Iron	0.136m
Outer Radius of the Stator Teeth	0.111m
Outer Radius of the Stator Air Gap	0.099m
Outer Radius of the Rotor	0.098m
Inner Radius of the Stator Iron	0.11m
Inner Radius of the Stator Teeth	0.099m
Inner Radius of the Stator Air Gap	0.098m
Inner Radius of the Rotor	0.023m
Thermal conductivity of copper	401W/Km
Thermal conductivity of iron	80.2W/Km
Thermal conductivity of aluminium	250W/Km
Specific heat capacity of copper	385J/kg/K
Specific heat capacity of iron	447J/kg/K
Specific heat capacity of aluminium	903J/kg/K
Density of copper	8960 kg/m^3
Density of iron	7874 kg/m^3
Density of aluminium	2700 kg/m^3
Generator gross mass	57kg
Stator mass	27kg[1]
Windings mass	4kg[1]
Rotor mass	5kg[1]
Bearing plate mass	3kg[1]
Frame mass	7kg[1]
Shaft mass	6kg[1]
Flange mass	2kg[1]

Table 3.6 provides information of the dimensions of the lumped parameters of the rig as well as information on their physical properties. This information is used for creating the lumped parameter thermal circuit.

---

[1] Masses of lumped parameters are estimated using rough approximations of density and volume relationships, they constitute only a starting point for the estimations.

3.4 Parameter Sensitivity Analysis

The highest degree of uncertainty in the model arises from the calculation of the masses of the lumped parameters, as they are not provided by the manufacturer and the generator cannot be disassembled and components weighed individually. To ensure model fidelity, these quantities are varied around their initial estimate in order to: a) identify the most sensitive parameters, and b) to minimise the model error. When plotting R_T^2 for the stator iron and windings against proportional perturbation, a parabolic result is expected with the maximum existing inside the chosen range.

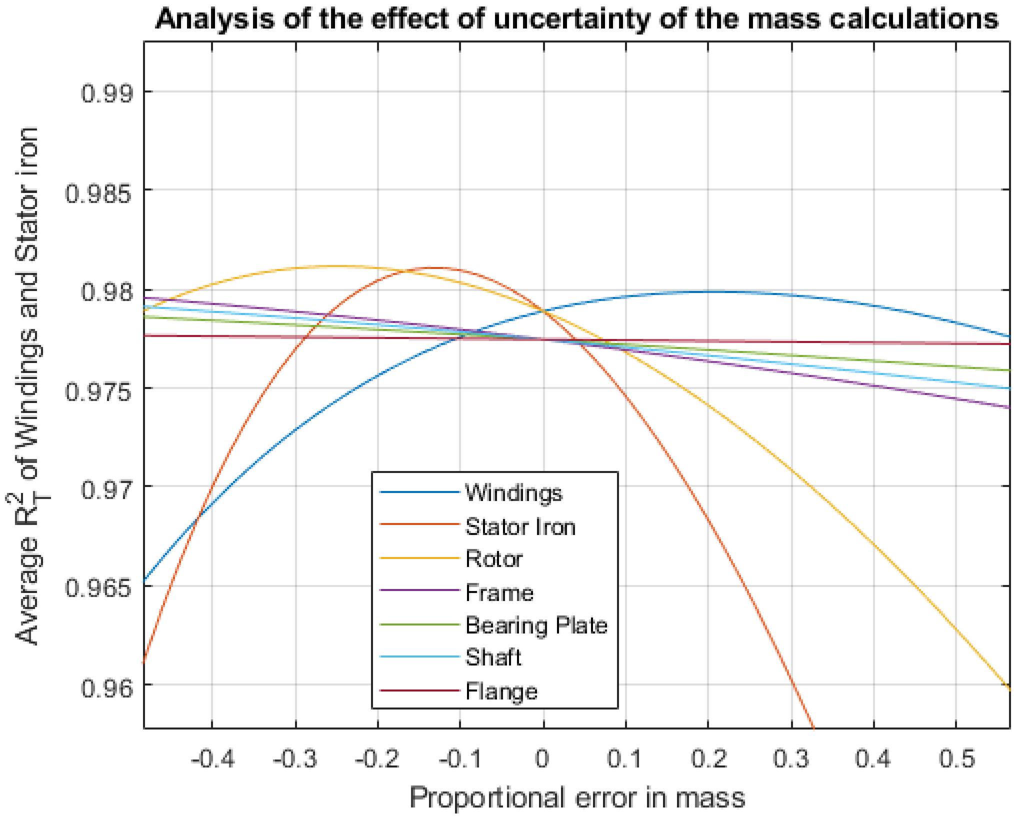

Fig. 3.18 Parameter sensitivity analysis performed on the mass of the lumped parameters.

From Fig. 3.18, it has been identified that the largest change of average stator iron and windings R_T^2 is due to changes in the mass of the stator ($\mathrm{m_{si}}$), windings ($\mathrm{m_{sw}}$) and rotor ($\mathrm{m_r}$), therefore, after all other parameters are set to their local maxima, they are perturbated together to provide a maximum taking into account all three components.

Table 3.7 Change of initial thermal mass estimations.

m_{sw}	m_{si}	m_r	$R^2_{T\,sw}$	$R^2_{T\,si}$	$R^2_{T\,av}$
0.5	0.5	0.5	0.8452	0.8667	0.856
0.5	0.5	0.4	0.8474	0.8713	0.8593
1	1	1	0.8889	0.8349	0.8619
0.5	0.5	0.3	0.8496	0.8757	0.8627
…	…	…	…	…	…
0.9	0.3	0.4	0.9599	0.9664	0.9632
0.2	0.3	0.3	0.9533	0.9732	0.9633
0.5	0.1	0	0.9292	0.9973	0.9633
0.3	0.4	0.7	0.9614	0.9652	0.9633
0.3	0.4	0.6	0.9478	0.9788	0.9633
…	…	…	…	…	…
0.6	-0.1	0.6	0.9744	0.997	0.9857
0.6	0.1	0.5	0.9744	0.997	0.9857
0.7	0.2	1	0.9743	0.9971	0.9857

The masses are adjusted accordingly to optimise the average coefficient of determination. Using the information from Figs. 3.18, 3.19 and 3.20, alongside Table 3.7, the values of the thermal masses were adjusted, as depicted in Table 3.8.

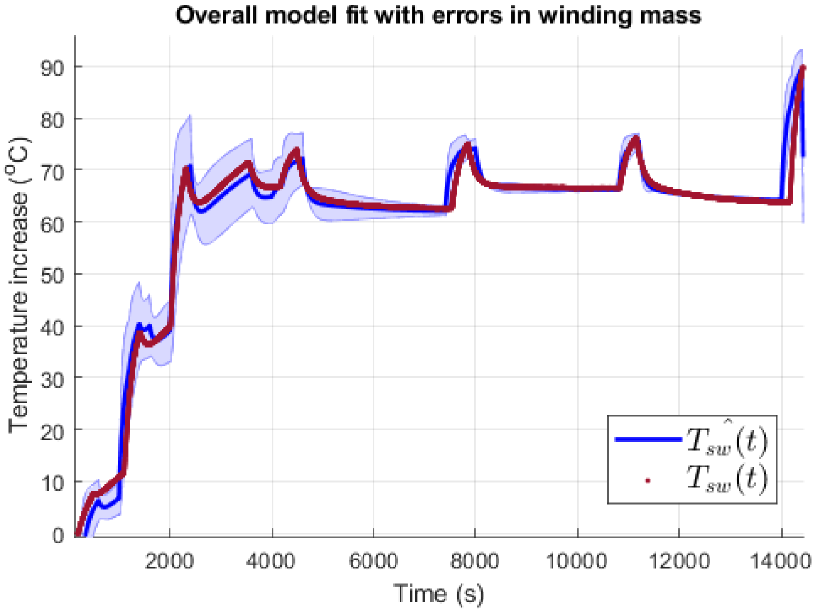

Fig. 3.19 Errors in fit as a function of mass uncertainty for temperature of the windings.

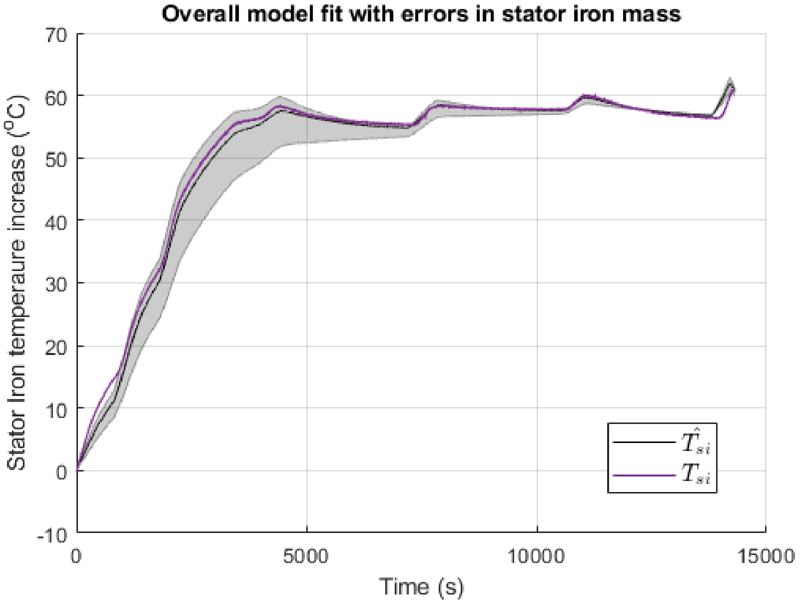

Fig. 3.20 Errors in fit as a function of mass uncertainty for temperature of the stator.

Figures 3.19 and 3.20 demonstrate the temperature fluctuation under different values of the thermal masses of stator windings and stator iron respectively. The uncertainty of the model is higher during the initial transient, where the generator temperature is moved from its initial equilibrium at room temperature. It is also demonstrated that this error converges as the generator reaches another (steady) state of thermal equilibrium.

Table 3.8 Optimised thermal masses.

Variable	Value
Stator mass	24.3 kg
Winding mass	6.8 kg
Rotor mass	7.5 kg
Bearing Plate mass	3 kg
Frame mass	7.5 kg
Shaft mass	6 kg
Flange mass	2 kg

Given the updated parameters, the steady state tests, varied load tests and “realistic mission profile” tests were run, and their coefficient of determination was calculated, so that the suitability and efficacy of the model can be assessed.

3.5 Model Validation

To validate the model, data from the generator rig were used. Three types of tests were run to establish the accuracy of the white box model: a steady state test; a varied load test; and a “realistic mission profile” test. The steady state test uses a step input of a 15% of full load and 60% of full load. The varied load test uses fluctuations between 40% of full load and 80% of full load in a “square wave” fashion, where a full period is 10 minutes (5 minutes 40% followed by 5 minutes 80%). The realistic mission profile was used to assess the accuracy of the mass estimation of the lumped parameters as well. The realistic mission test is assessed in two ways: firstly the behaviour as a whole, and each phase of flight is also assessed separately (Fig. 3.29).

Fig. 3.21 and 3.22 depict the response of a constant 1A and 4A current (15% and 60% of full load) is driven, the temperatures of the stator iron and windings are measured; they are in turn compared to the temperatures provided by the white box model. This is shown in Figs. 3.21 - 3.24. In both cases, the steady state temperature is accurately estimated, as is, for the most part, the initial transient; except for the stator winding temperature at the 4A test, which has an error of 1.9°C. The varied load test, where the load is altered from 40% to 80% of full load is also explored. Figures 3.25 and 3.26 show the comparison of the estimated temperature and the measured temperature for these loading conditions.

Figures 3.27 and 3.28 demonstrate the fit of the estimated temperatures using the white box model for the “realistic mission test”. Figure 3.29 explores the behaviour of the stator winding for each phase of flight separately. This is not repeated for the stator iron, as the behaviour as a whole does not show large perturbations from its steady state. As it can be observed, the temperature estimation of the stator iron is more accurate. This can be explained due to the uniformity of the material as well as its higher specific heat capacity.

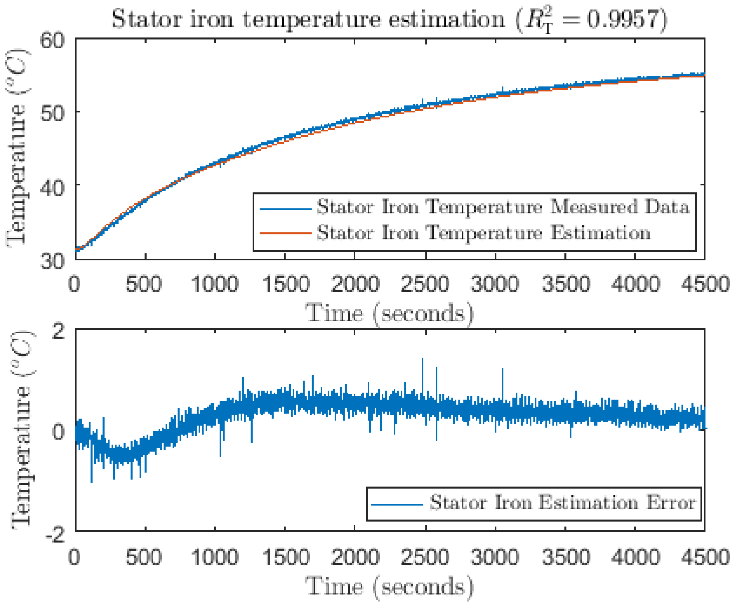

Fig. 3.21 Comparison between measured and estimated data for stator iron temperature whilst driving a constant load of 4A.

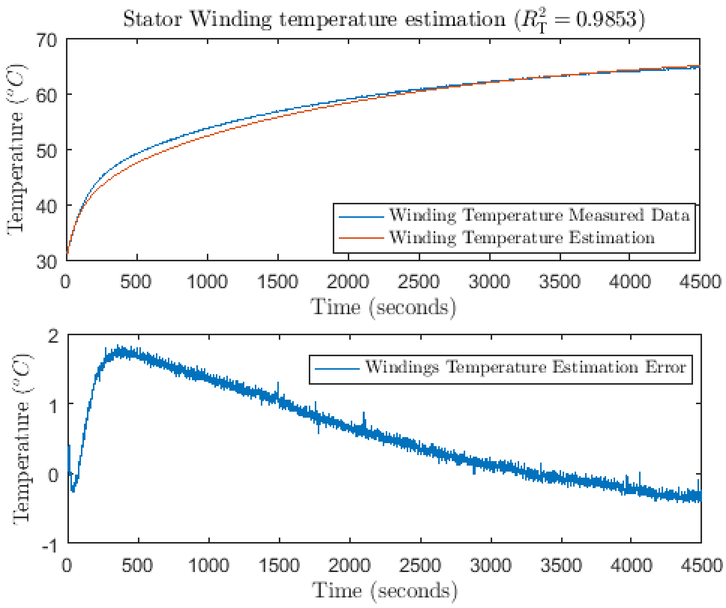

Fig. 3.22 Comparison between measured and estimated data for winding temperature whilst driving a constant load of 4A.

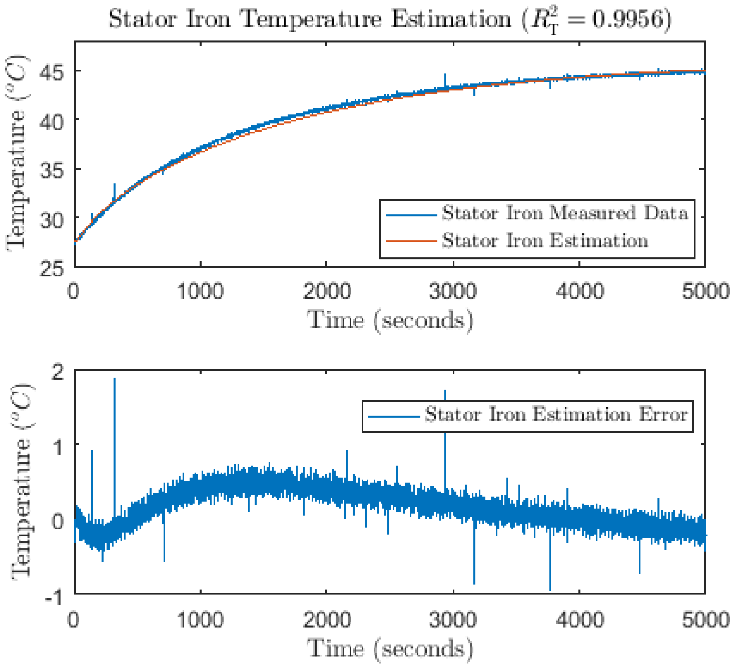

Fig. 3.23 Comparison between measured and estimated data for stator iron temperature whilst driving a constant load of 1A.

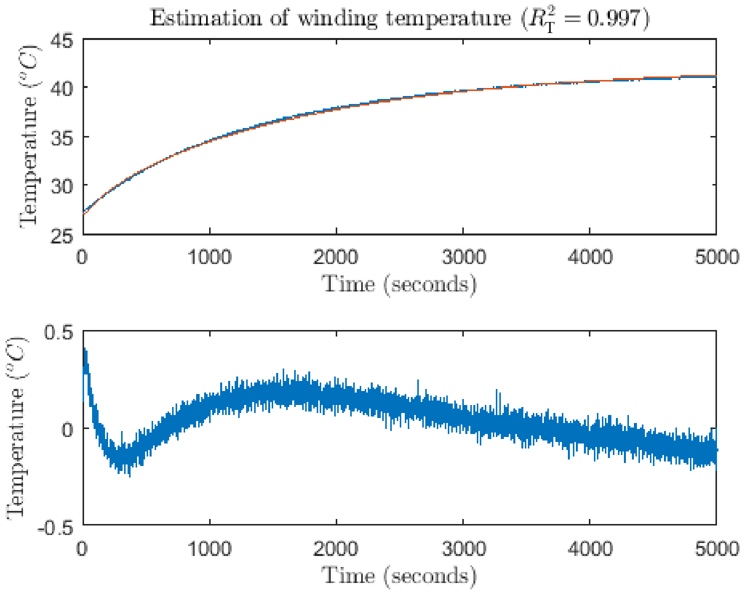

Fig. 3.24 Comparison between measured and estimated data for winding temperature whilst driving a constant load of 1A.

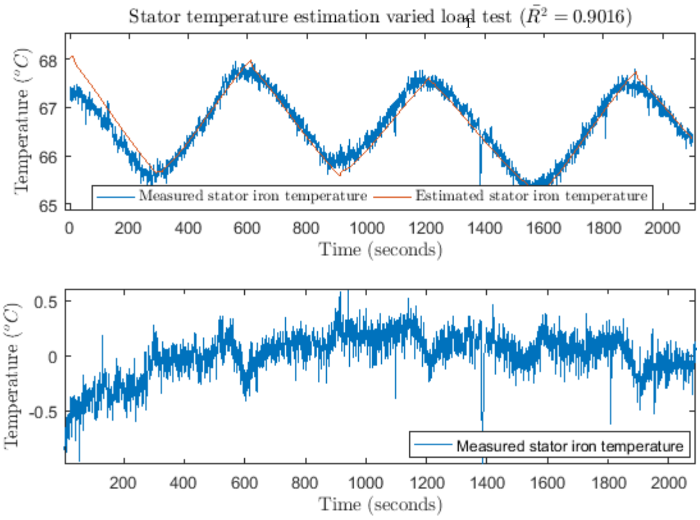

Fig. 3.25 Comparison between measured and estimated data for stator iron temperature for a varied load.

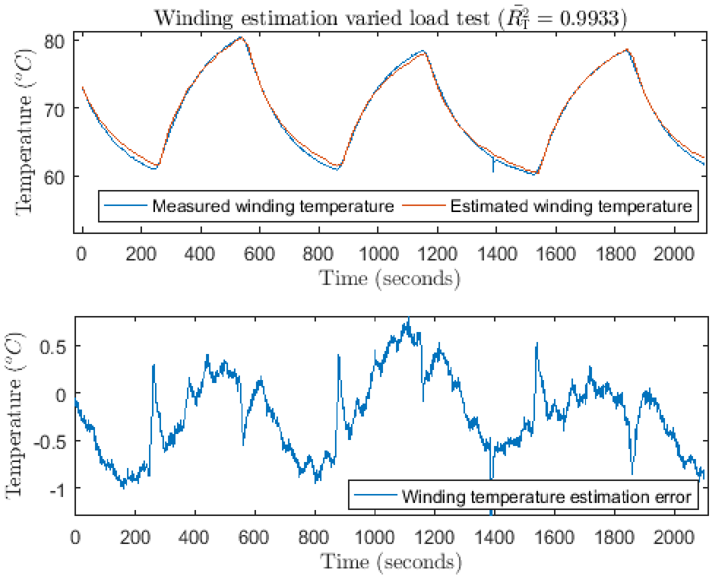

Fig. 3.26 Comparison between measured and estimated data for winding temperature for a varied load.

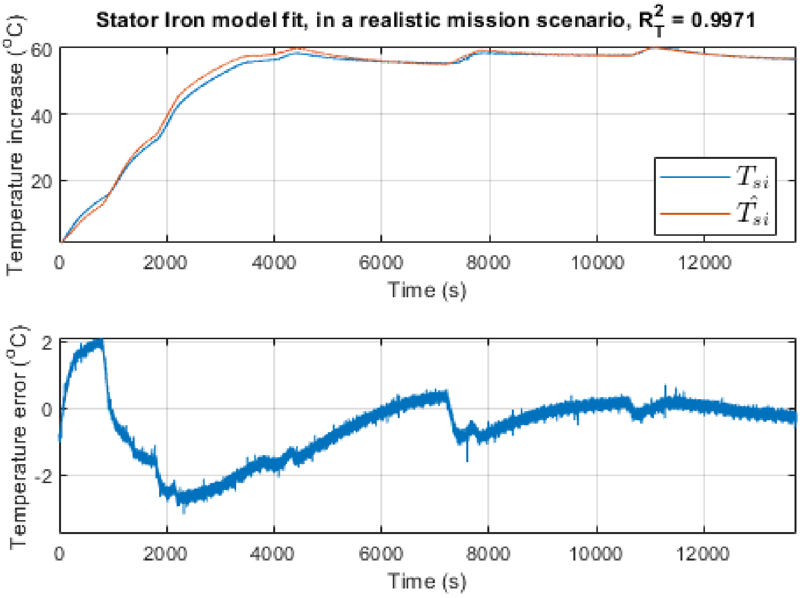

Fig. 3.27 Comparison between measured and estimated data for stator temperature for a realistic mission test.

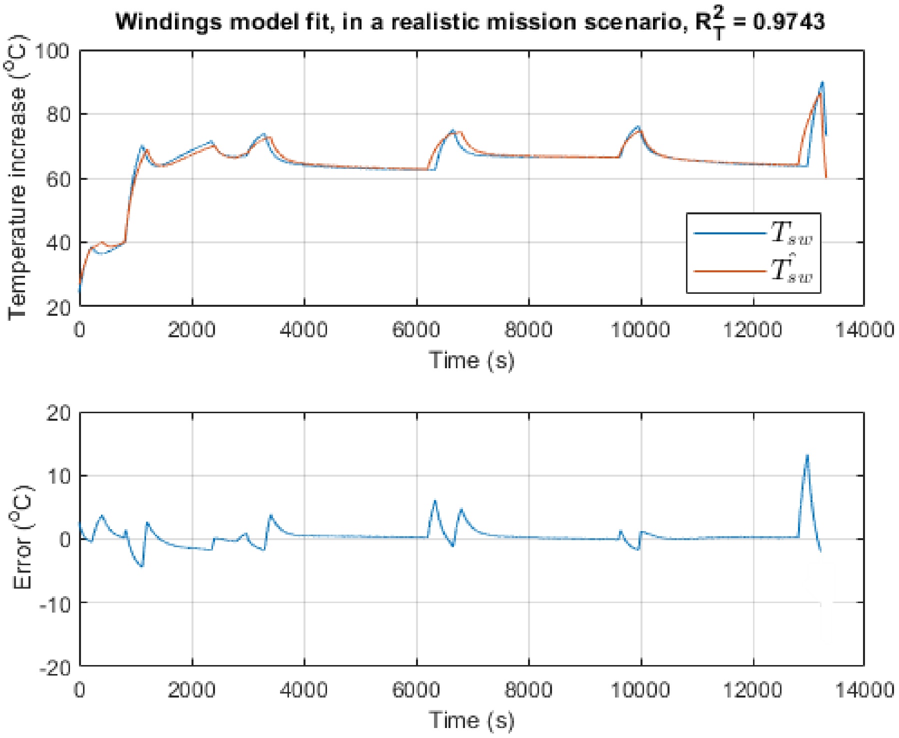

Fig. 3.28 Comparison between measured and estimated data for windings temperature for a realistic mission test.

It can be observed that the main source of error in the estimation of the windings' temperature is their response to transient conditions, therefore R_T^2 is calculated for each phase of flight independently, as it is shown in Fig. 3.29. This process is more important for the windings than for the stator, as the behaviour of the stator is resistant to changes in current as it can be observed when comparing Fig 3.25 with Fig. 3.26 and Fig. 3.27 with Fig. 3.28.

From Figs. 3.21 – 3.29 it can be observed that the model is tuned for accurately modelling temperatures around the operating conditions, at the expense of its behaviour around the low end of the temperatures. Even when the error appears to be large (e.g. Fig. 3.28, ~13000s) that is mainly due to temporal error, rather than an error in the maximum temperature. The maximum error in temperature around the operating region remains around 2°C.

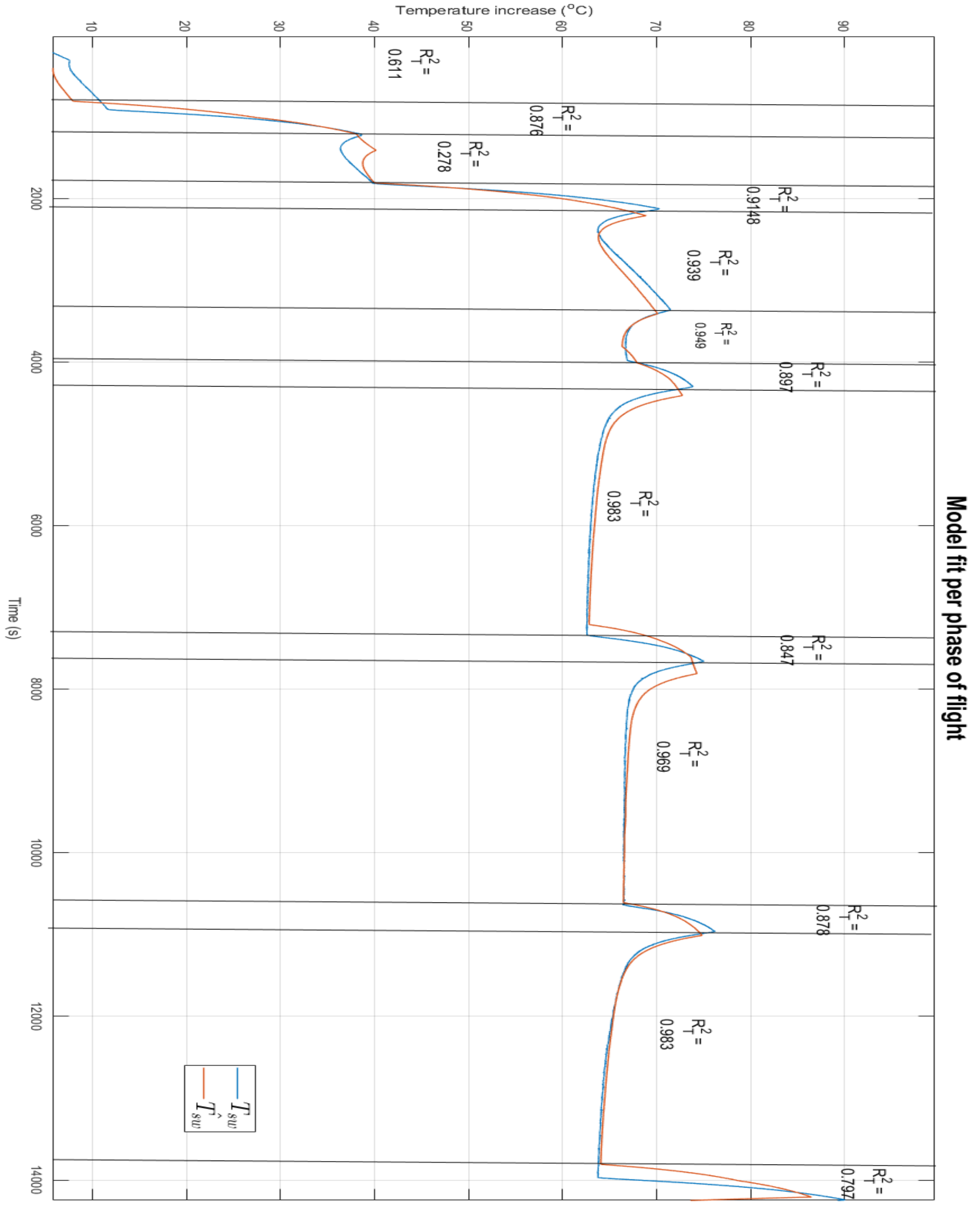

Fig. 3.29 Segmented model fit per phase of flight.

As it can be observed in Fig. 3.29 the behaviour of the model at the steady state parts is satisfactory with R_T^2> 0.95 consistently. The transients have a worse fit; they appear to have a larger settling time, the main justification for this is what appears to be an asynchronicity between the two responses. The most likely reason is the load of the generator not being changed “instantly” during the real test, as such process was done physically. This is most pronounced at 7000s, where R_T^2= 0.847, the acquired data starts its change later and finishes sooner. Nonetheless their error in maximum temperature per phase of flight is less than 4°C. The results of Fig. 3.28 are slightly misleading in that respect, as the error is a function of time and as the results are slightly asynchronous such an error is accentuated. When changes in flight phase are modelled, i.e. the load changes, there is a delay introduced in the real system as this change occurs manually. This nuance is not mirrored in the model, which assumes instantaneous changes at exact predefined times. Lastly, the initial phases of flight perform poorly in comparison, this is less of a concern though, as the focus of the model is the behaviour at high temperatures, where overheating failures may occur.

3.6 Fault Modelling

As alluded to in the introduction of this chapter, this model is also used as a means for understanding the behaviour of the generator after it has been subjected to a fault. The purpose of this section is to provide some examples of faults and how they manifest in the temperature response. The temperature response of the “faulty generators” are depicted in Figs. 3.30 and 3.31 for stator iron and windings respectively. The faults explored in this section are as follows: coolant blockage, increased rotor friction, and degradation of thermal insulation of the windings.

The coolant blockage (of 20%) has been modelled by reducing the heat transfer via convection to the ambient by 20%. Increased rotor friction can be due to mechanical damage and manifests as an increase in windage losses of 20%. Lastly, winding insulation degradation can be due to previous overheat or just routine wear and tear and lack of maintenance, it is modelled as an increase in thermal conductivity of the windings of 30%.

In the windings, the increased friction has the smallest overall effect with an increase in temperature of 3°C consistently across most phases of flight. The initial phases of flight are less affected. Similarly, the coolant blockage has a similar initial behavior, with the added effect of an increased gradient response in the latter phases of flight. This gradient is due to the ambient absorbing less heat. Lastly, the winding insulation degradation affects the initial phases of flight as well, due to the net cooling of the windings being substantially reduced.

Conversely, in the stator iron, the insulation of the windings has almost no effect to the temperature performance. Meanwhile, the coolant blockage has the largest effect resulting to an increased temperature gradient overall as the stator struggles to lose heat to its surroundings by convection. The windage increase affects the rotor similarly to the windings, as the same amount of heat is essentially transferred to both.

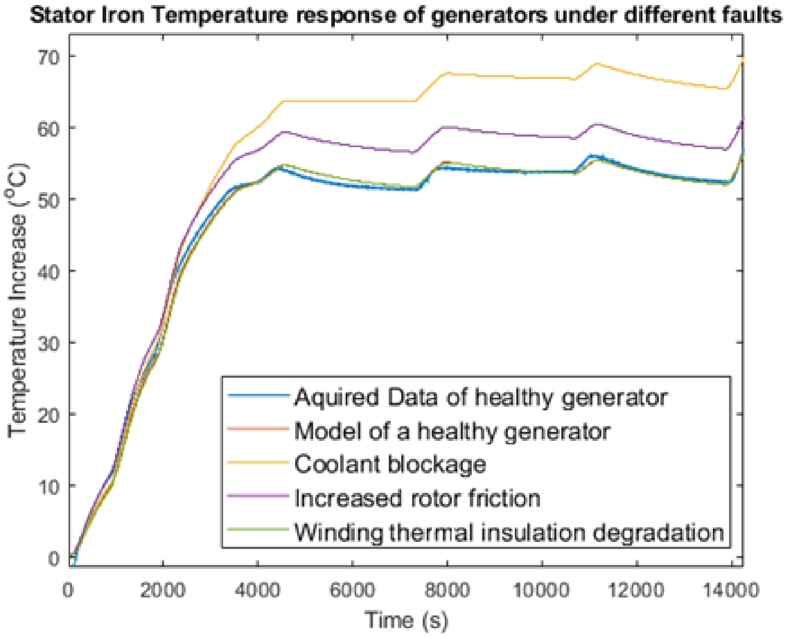

Fig. 3.30 Models of faults of coolant blockage, increased rotor friction and degradation of the thermal insulation of the windings compared to a healthy generator for stator iron temperatures.

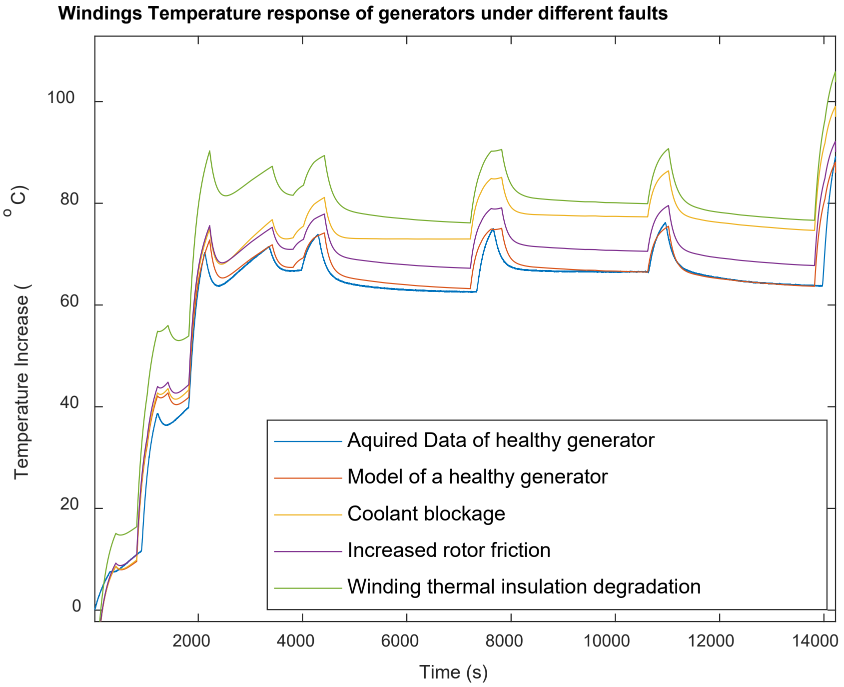

Fig. 3.31 Models of faults of coolant blockage, increased rotor friction and degradation of the thermal insulation of the windings compared to a healthy generator for the winding temperatures.

3.7 Conclusion

Based on the generator rig, a nonlinear white box model that takes into account both electrical and thermal effects, has been created with the purpose of being used as a simulation model for means of testing and validation of other models and algorithms, such as the ones in Chapters 4 and 5.

The simulation model itself has also been validated using data gathered from the generator rig in a variety of cases, namely: steady state tests for specific loading conditions; varied load tests (40% – 80% of full load); and “realistic mission” tests, the structure of which has been defined by BAE Systems. A parameter sensitivity analysis of the thermal masses of the generator was also conducted to assist with the validation process.

The behavior of the system has been explored under faulty conditions with a variety of faults, some of which are used in later chapters to further test the algorithm efficacy.

Overall, the white box model has shown a very close fit over the relevant regions and hence it can be used as a surrogate of the generator for testing purposes.

CHAPTER 4

LINEAR MODELLING

4.1 Introduction

This chapter discusses the creation of linear models used for controller design and prediction algorithms. A white box approach where the models from Chapter 3 are linearised and simplified is compared to a black box system identification approach. This chapter aims to compare the physics based linear model with the preferred black box model; they are compared based on their coefficient of determination. The physics based linearised models are in differential equation form, where the heat flow through each component is modelled.

The black box models in this Chapter are of two main forms, either as autoregressive exogenous (as described in eq. (4.1)) or state space form (4.2-4.3):

$$\hat{\boldsymbol{T}}(t) = \boldsymbol{GI}(t) \tag{4.1}$$

Where $\hat{\boldsymbol{T}}$ is a matrix containing the predicted temperatures of interest at time t; I is a matrix containing information of the armature current and excitation current; and $\boldsymbol{G}$ is a matrix containing transfer functions relating currents to temperatures.

$$\dot{\boldsymbol{x}}(t) = \boldsymbol{A}(\theta)\boldsymbol{x}(t) + \boldsymbol{B}(\theta)\boldsymbol{u}(t) \overset{\mathcal{L}}{\Rightarrow} \boldsymbol{x}(s) = [s\boldsymbol{I} - \boldsymbol{A}(\theta)]^{-1}\boldsymbol{B}(\theta)\boldsymbol{u}(s) \tag{4.2}$$

$$\widehat{\boldsymbol{y}}(t) = \boldsymbol{C}\boldsymbol{x}(t) \overset{\mathcal{L}}{\Rightarrow} \widehat{\boldsymbol{y}}(s) = \boldsymbol{C}\boldsymbol{x}(s) \tag{4.3}$$

where $\boldsymbol{x}(.)$ is the state vector, $\widehat{\boldsymbol{y}}(.)$ is the estimated output vector, $\boldsymbol{u}(.)$ is the input vector, $\boldsymbol{A}(.)$ is the state matrix of size n × n, $\boldsymbol{B}(.)$ is the input matrix of size n × p, $\boldsymbol{C}(.)$ is the output matrix of size p × n, and s is the Laplace operator; it is assumed there is no feed through in this case. The state space model is estimated in continuous domain first and then transformed to the Z domain using the bilinear transform.

The models discussed in this chapter are validated using data from the experimental rig and same tests introduced in Ch. 3. The system identification models are compared with each other, and the preferred option is then compared to the linear physics-based model. They are assessed based on to goodness of fit to acquired data as well as model complexity.

4.2 Linearised White Box Model

By using the model developed in Ch. 3 as a basis, a linear model can be created by making certain assumptions about the behaviour of the system and the information available. The main assumption is the ability to measure the excitation and armature currents. The existence of such information makes the electrical side of the model obsolete, since its purpose was to calculate these currents. The data gathered can instead be used directly as inputs to the model.

Since the technology considered here is constant speed/ constant frequency machines, the frequency and speed dependent losses (eddy current, hysteresis and windage) can be assumed constant for normal operation range. Hence, they can be treated as constant parameters to the system. The copper losses are linearised over their region of operation shown in Figs. 4.1, 4.2. Furthermore, the temperature-resistance relationship is disregarded as part of this simplification. In order to have an aggressive estimation of the temperature, so that no overheat scenario is missed, the maximum resistance of both the windings and the back iron is used.

An approximate linear relationship between the load current and the excitation current can be established for the currents around the most common operating region (4.4). This can be observed in Fig. 4.3, where the coefficient of determination between the measured excitation current and its linear estimation is R_T^2 = 0.8257.

$$I_f(t) = 0.2744 I_s(t) + 0.79 \tag{4.4}$$

The model presented in Chapter 3 can be condensed in the following differential equations (4.5 - 4.12)

$$\dot{T}_{sw} = \frac{T_{sw} A_{sw2si} K_{sw2si}}{d_{sw2si} m_{sw} c_{sw}} - \frac{T_{si} A_{sw2si} K_{sw2si}}{d_{sw2si} m_{sw} c_{sw}} + \frac{I_f^2 R_f}{m_{sw} c_{sw}} \tag{4.5}$$

$$\dot{T}_{si} = -\frac{T_{sw} A_{sw2si} K_{sw2si}}{d_{sw2si} m_{si} c_{si}} + \frac{T_{si} A_{sw2si} K_{sw2si}}{d_{sw2si} m_{si} c_{si}} - \frac{T_r k_{r2si} A_{r2si}}{m_{si} c_{si}} + \frac{I_a^2 R_a}{m_{si} c_{si}} \tag{4.6}$$

$$\begin{aligned}\dot{T}_r = &-\frac{T_{si} k_{r2si} A_{r2si}}{m_r c_r} - \frac{T_{sh} A_{r2sh} K_{r2sh}}{d_{r2sh} m_r c_r} - \frac{T_{bp2} A_{r2bp2} K_{r2bp2}}{d_{r2bp2} m_r c_r} - \frac{T_{bp1} A_{r2bp1} K_{r2bp1}}{d_{r2bp1} m_r c_r} \\ &+ \frac{T_r}{m_r c_r} \left(\frac{A_{r2bp1} K_{rbp1}}{d_{r2bp1}} + \frac{A_{r2bp2} K_{r2bp2}}{d_{r2bp2}} + \frac{A_{r2sh} K_{r2sh}}{d_{r2sh}} + K_{r2si} A_{r2si} \right) \\ &+ \frac{\Sigma L}{m_r c_r}\end{aligned} \tag{4.7}$$

$$\begin{aligned}\dot{T}_{sh} = &-\frac{T_r A_{r2sh} K_{r2sh}}{d_{r2sh} m_{sh} c_{sh}} - \frac{T_{bp2} A_{sh2bp2} K_{sh2bp2}}{d_{sh2bp2} m_{sh} c_{sh}} - \frac{T_{bp1} A_{sh2bp1} K_{sh2bp1}}{d_{sh2bp1} m_{sh} c_{sh}} \\ &+ \frac{T_{sh}}{m_{sh} c_{sh}} \left(\frac{A_{r2bp1} K_{r2bp1}}{d_{r2bp1}} + \frac{A_{r2sh} K_{r2sh}}{d_{r2sh}} + \frac{A_{sh2bp2} K_{sh2bp2}}{d_{sh2bp2}} \right. \\ &\left. + A_{sh2amb} k_{sh2amb} \right)\end{aligned} \tag{4.8}$$

$$\begin{aligned}\dot{T}_{bp2} = &-\frac{T_r A_{r2bp2} K_{r2bp2}}{d_{r2bp2} m_{bp2} c_{bp2}} - \frac{T_{sh} A_{sh2bp2} K_{sh2bp2}}{d_{sh2bp2} m_{bp2} c_{bp2}} - \frac{T_{fr} A_{bp22fr} K_{bp22fr}}{d_{bp22fr} m_{bp2} c_{bp2}} \\ &- \frac{T_{fl} A_{bp22fl} K_{bp22fl}}{d_{bp22fl} m_{bp2} c_{bp2}} \\ &+ \frac{T_{vp2}}{m_{bp2} c_{bp2}} \left(\frac{A_{r2bp2} K_{r2bp2}}{d_{r2bp2}} + \frac{A_{sh2bp2} K_{sh2bp2}}{d_{sh2bp2}} + \frac{A_{bp22fl} K_{bp22fl}}{d_{bp22fl}} \right. \\ &\left. + \frac{A_{bp22fr} K_{bp22fr}}{d_{bp22fr}} \right)\end{aligned} \tag{4.9}$$

$$\begin{aligned}\dot{T}_{fl} - \frac{T_{bp2} A_{bp2fl} K_{bp2fl}}{d_{bp2fl} m_{fl} c_{fl}} + \frac{T_{fl}}{m_{fl} c_{fl}} \left(\frac{A_{bp2fl} K_{bp2fl}}{d_{bp2fl}} + A_{fl2amb} k_{fl2amb} \right) \\ - \frac{T_{amb} T_{fl2amb} k_{fl2amb}}{m_{fl} c_{fl}}\end{aligned} \tag{4.10}$$

$$\begin{aligned}\dot{T}_{bp1} = &-\frac{T_r A_{r2bp1} K_{r2bp1}}{d_{r2bp1} m_{bp1} c_{bp1}} - \frac{T_{sh} A_{sh2bp1} K_{sh2bp1}}{d_{sh2bp1} m_{bp1} c_{bp1}} - \frac{T_{fr} A_{bp12fr} K_{bp12fr}}{d_{bp2fr} m_{bp1} c_{bp1}} \\ &+ \frac{T_{bp1}}{m_{bp1} c_{bp1}} \left(\frac{A_{r2bp1} K_{r2bp1}}{d_{r2bp1}} + \frac{A_{sh2bp1} K_{sh2bp1}}{d_{sh2bp1}} + k_{bp12amb} A_{bp12amb} \right. \\ &\left. + \frac{A_{bp12fr} K_{bp12fr}}{d_{bp12fr}} \right) - \frac{T_{amb} k_{bp12amb} A_{bp12amb}}{c_{bp1} m_{bp1}}\end{aligned} \tag{4.11}$$

$$\begin{aligned}\dot{T}_{fr} = &-\frac{T_{si} A_{si2fr} K_{si2fr}}{d_{si2fr} m_{fr} c_{fr}} - \frac{T_{bp1} A_{bp12fr} K_{bp12fr}}{d_{bp12fr} m_{fr} c_{fr}} - \frac{T_{bp2} A_{bp22fr} K_{bp22fr}}{d_{bp22fr} m_{fr} c_{fr}} \\ &+ \frac{T_{fr}}{m_{fr} c_{fr}} \left(\frac{A_{si2fr} K_{si2fr}}{d_{si2fr}} + \frac{A_{bp12fr} K_{bp12fr}}{d_{bp12fr}} + \frac{A_{bp22fr} K_{bp22fr}}{d_{bp22fr}} \right. \\ &\left. + A_{fr2amb} k_{fr2amb} \right) - \frac{T_{amb} A_{fr2amb} k_{fr2amb}}{m_{fr} c_{fr}}\end{aligned} \tag{4.12}$$

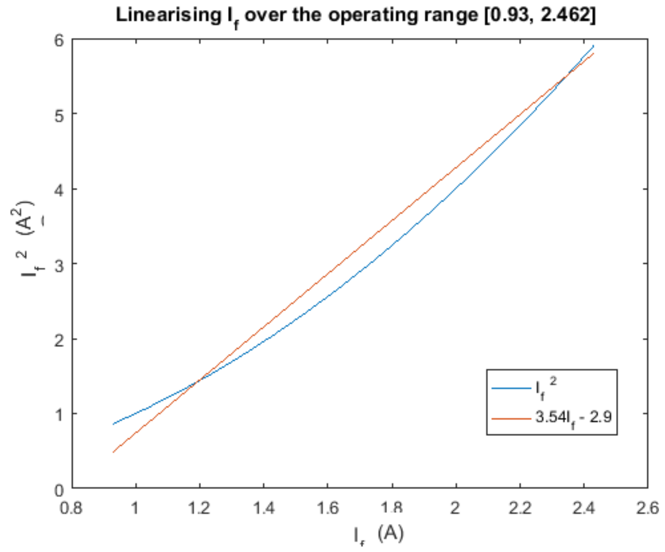

Fig. 4.1 Linearisation of Stator Winding Losses, R_T^2 = 0.9843.

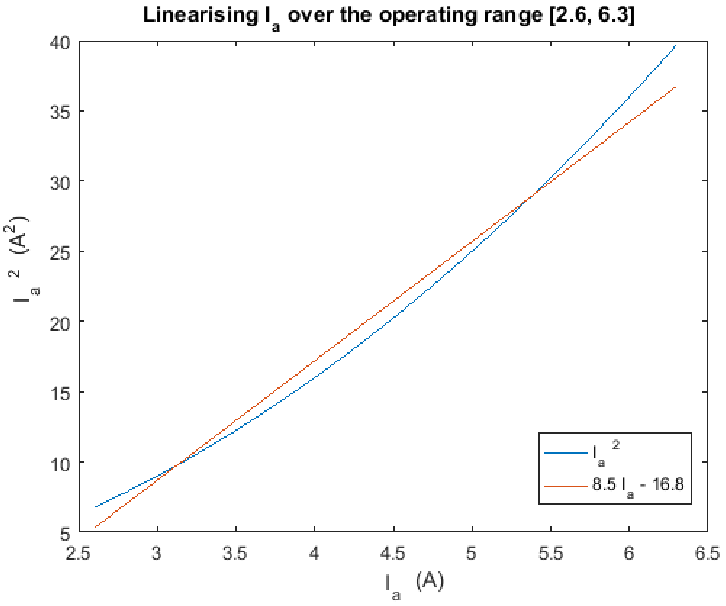

Fig. 4.2 Linearisation of Stator Iron Losses, R_T^2 = 0.9865.

where A is the contact area between two surfaces, d is the width, K is the thermal conductivity constant and k is the heat transfer coefficient. Subscripts denote between which lumped parameters the heat transfer takes place: sw denotes the windings, si the stator iron, r the rotor, sh the shaft, fl the flange, $bp1$ and $bp2$ the bearing plates, fr the frame and amb the ambient; for example A_{sw2si} denotes the area of contact between the windings and the iron etc.

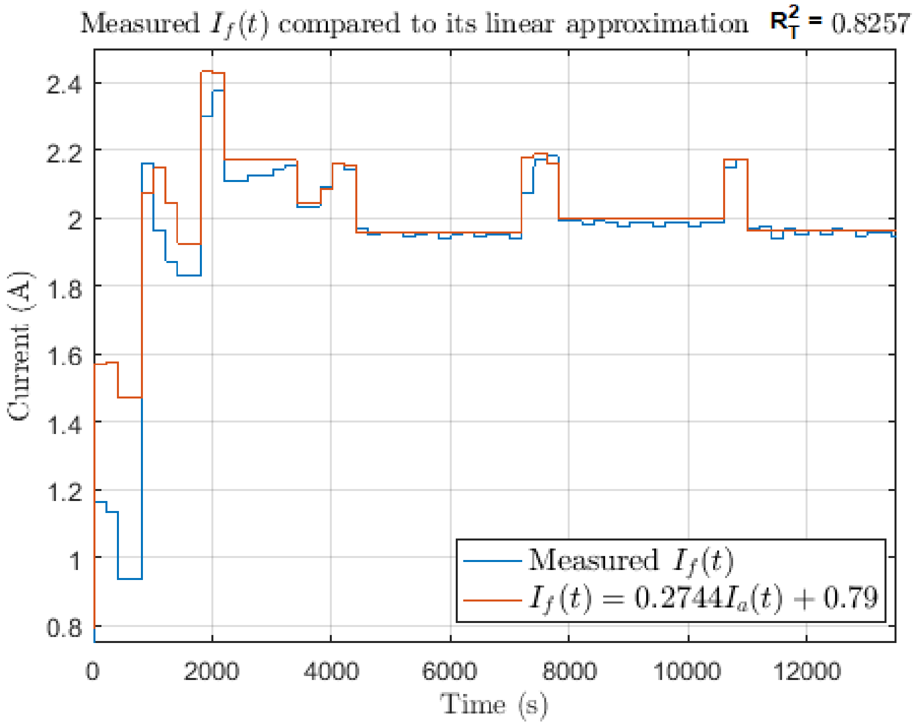

Fig. 4.3 Comparing the measured Excitation current, I_f (t) and its linearly estimated counterpart.

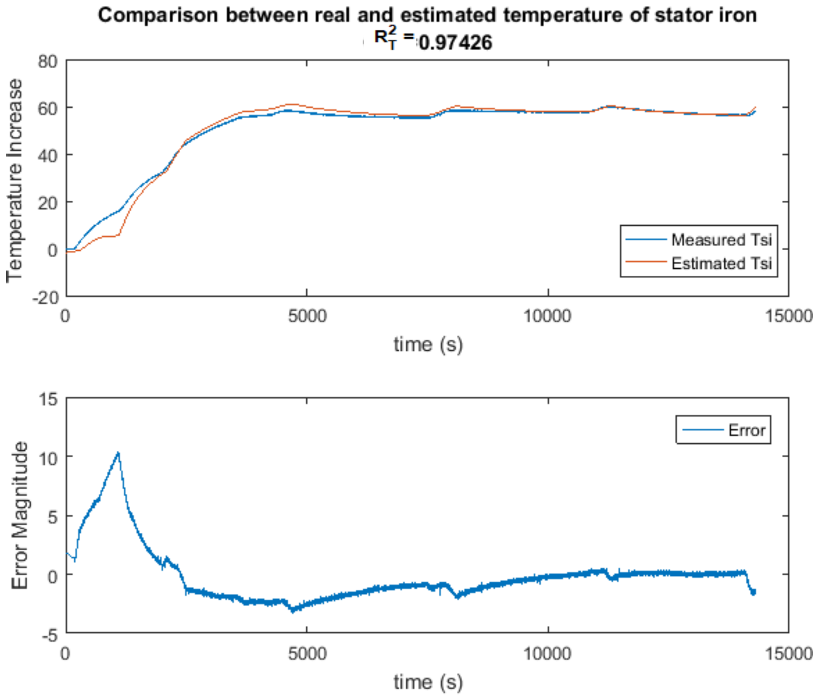

Fig. 4.4 Comparison of the linearised model to the measured temperature data of the stator iron.

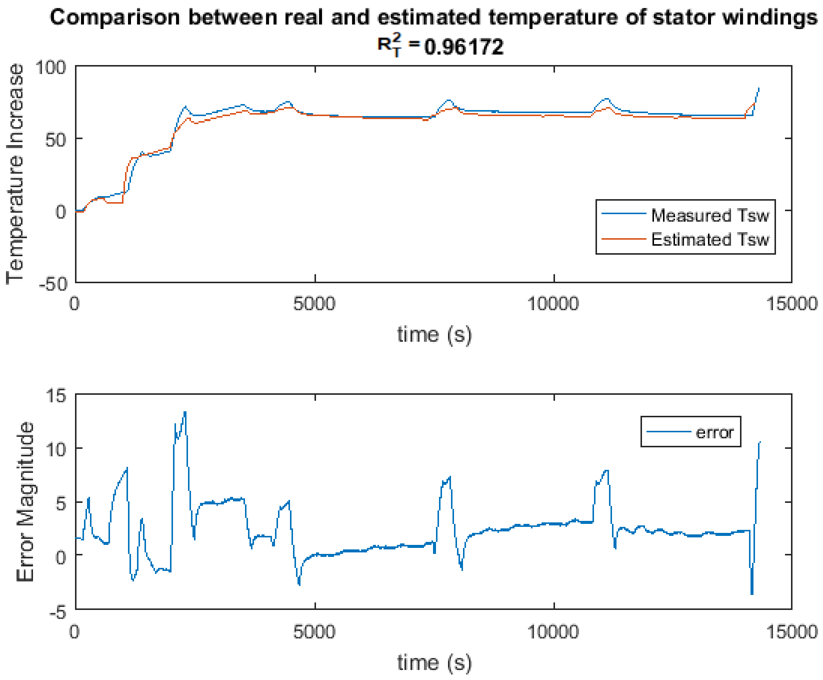

Fig. 4.5 Comparison of the linearised model to the measured temperature data of the windings.

Figures 4.4 and 4.5 show the response of the linearised system. Their responses are compared to the measured data from the generator rig (presented in Chapter 3).

Table. 4.1 Goodness of fit of the linearised white box model.

Signal	R_T^2	Maximum Error (°C)
Nonlinear Stator Iron	0.99	5.1
Linearised Stator Iron	0.974	10.1
Nonlinear Stator Windings	0.979	10.0
Linearised Stator Windings	0.962	14.0

4.3 System Identification, Linear Black Box Modelling

A shortcoming of physics-based models is their reliance on accurate model parameter acquisition. The information needed to create a white box physics-based model is hard to collect and in-depth knowledge of the machine structure and properties is necessary. This implies several tests need to be run to establish all the relevant information. When collaborating with industry partners, such time-consuming tests might be hard to conduct and hence a white box model can be difficult to implement. Furthermore, assuming these tests are done when the machine is first obtained, degradation of the generators due to usage is not taken into account, hence some of the measured parameters are subject to uncertainty. A black box approach eases the implementation process, since there is no need for knowledge of the physics of the system and the tests needed are much easier to run by non-specialist staff. The black box method depicted in this body of work is system identification.

System identification parameter estimation is achieved using linear regression as follows. Assume the difference equation (4.13), where: $u(t)$ is the measured input, $y(t)$ is the measured output, e is the error between the predicted output value ($\hat{y}(t)$) and the measured output value $y(t)$, and $\boldsymbol{\theta} = (a_1, a_2 \dots a_n, b_1 \dots b_m)^T$ is an independent parameter vector used to parametrise the model. The elements of $\boldsymbol{\theta}$ can be denoted as $A(z)$ and $B(z)$ signifying the a and b elements respectively (4.14, 4.15).

$$A(z)y(t) = B(z)u(t) + e(t) \tag{4.13}$$

$$A(z) = 1 + \sum_{k=1}^{\infty} a_k z^{-k} \tag{4.14}$$

$$B(z) = \sum_{k=1}^{\infty} b_k z^{-k} \tag{4.15}$$

Let the prediction response error be defined as the difference of measured output values to predicted output values (4.16).

$$e(t) = y(t) - \hat{y}(t|\boldsymbol{\theta}) \tag{4.16}$$

By substituting (4.16) into (4.13), it follows that the predictor can then be expressed as (4.17).

$$A(z)y(t) = B(z)u(t) + y(t) - \hat{y}(t|\boldsymbol{\theta}) \;\Leftrightarrow \hat{y}(t|\boldsymbol{\theta}) = B(z) + [1 - A(z)]y(t) \tag{4.17}$$

The output and input vectors can be expressed in a single data vector $\boldsymbol{\phi}(t) = [-y(t-1), y(t-2), \dots, y(t-n_a), u(t-1), u(t-2), \dots u(t-n_b)]^T$, hence the previous definition of (4.17) can be rewritten as the product of the parameter vector ($\boldsymbol{\theta}$) and data vector $\boldsymbol{\phi}(t)$ shown in (4.18).

$$\hat{y}(t|\theta) = \boldsymbol{\theta}^T \boldsymbol{\phi}(t) = \boldsymbol{\phi}^T(t)\boldsymbol{\theta} \tag{4.18}$$

In this case, optimal parameters ($\boldsymbol{\theta}$) are estimated using a least squares method.

It follows that the elements of (4.1) can be populated, with $\widehat{\boldsymbol{T}} = [T_{si}(t), T_{sw}(t)]^T, \boldsymbol{I} = [I_a(t), I_f(t)]^T$ and , $\boldsymbol{G} = \begin{bmatrix} G_{I_a 2T_{si}}(\boldsymbol{\theta}_{I_a 2T_{si}}) & G_{I_f 2T_{si}}(\boldsymbol{\theta}_{I_f 2T_{si}}) \\ G_{I_a 2T_{sw}}(\boldsymbol{\theta}_{I_a 2T_{sw}}) & G_{I_f 2T_{sw}}(\boldsymbol{\theta}_{I_f 2T_{sw}}) \end{bmatrix}$, with the individual transfer function elements being calculated independently of each other and being of the form

$$G(\boldsymbol{\theta}) = \frac{B(z)}{A(z)} \tag{4.19}$$

The input and output data of the system are required and were hence gathered using the generator rig. Two sets of inputs and two sets of outputs were collected, these are the RMS excitation current, RMS average phase current, stator iron temperature and stator winding temperature, respectively.

Different methods of system identification were employed, and their results were compared to ensure the closest accuracy of fit whilst having a suitably low order system, such that real time operation penalties are low. A state space model was estimated using the gathered data. The model was created as a 2 input - 2 output model, to ensure cross coupling effects are considered; this was achieved by using the subspace method [55]. Different methods and number of input- output pairs were tested to derive a model that is of low complexity but at the same time describes all dynamics effectively. First a 2 input - 2 output model is created, then a multiple input single output is constructed using an autoregressive exogenous (ARX) [9, 24] model, lastly a single input - single output approach is explored, where the best I/O pairs are calculated and then the transfer functions are approximated.

In all cases some data manipulation was conducted before estimating the systems. Firstly, zero initial conditions were preferred, so the ambient temperature was subtracted from all values of the output data; hence the output variable became temperature difference in both cases of stator iron and windings. Then the choice of input data was considered: the excitation current and armature current can be used (without any pre-processing) or the input data can be integrated first, and then the integral of the input data can be used as an input to the system identification algorithm. As it can be seen in the Fig. 4.6 and 4.7 there is no substantial improvement in the goodness of fit therefore the raw (non- integrated) currents should be used.

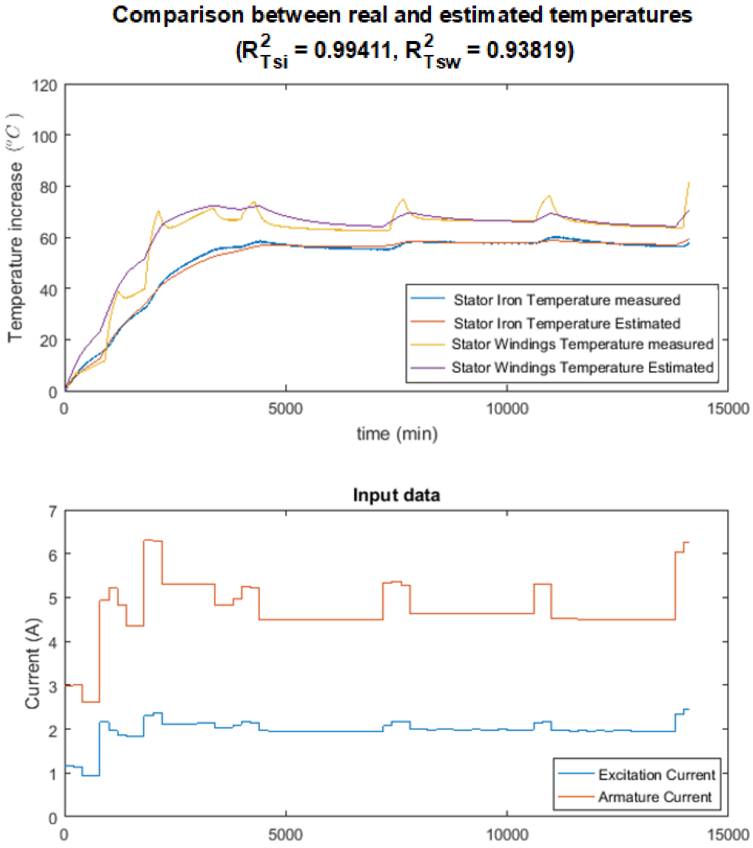

Fig. 4.6 Temperature of stator iron and windings using currents as inputs.

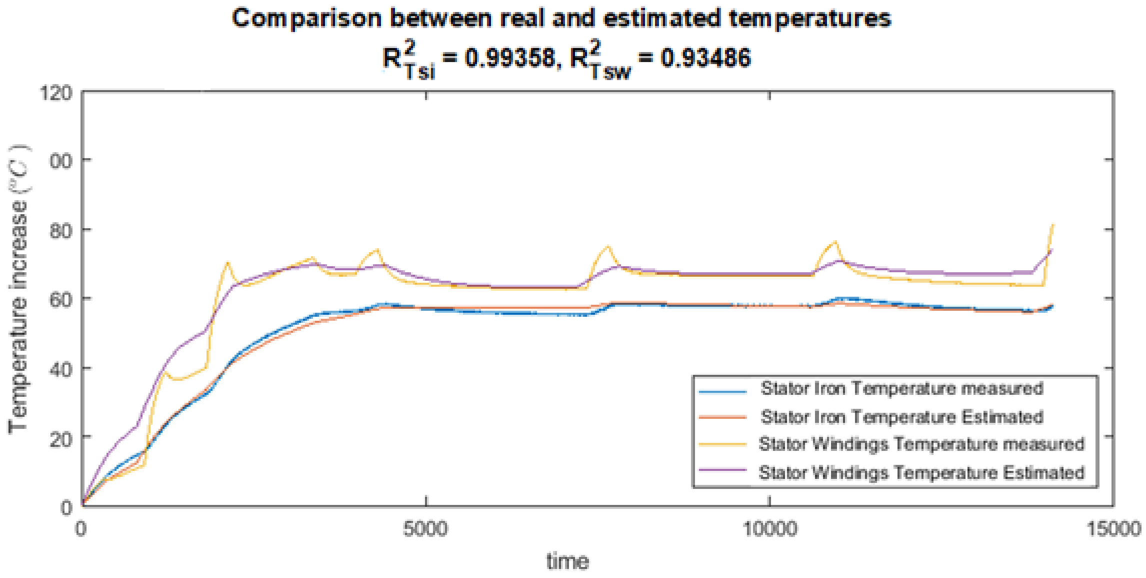

Fig. 4.7 Temperature of stator iron and windings using the integral of currents as inputs.

4.3.1 Multi-Input Multi-Output System

The MIMO system is defined and estimated in continuous state space as described in (4.2, 4.3) and then discretised using bilinear transform as discussed in the introduction. The estimation is done using MATLAB's "ssest()" function and the discretisation is done using "c2d()". The system is assumed to be time invariant, and the coefficients of A, B and C are free.

Models of order 1 to 10 were constructed and their responses were compared based on their R_T^2, adjusted R_T^2 ($\bar{R}_T^2$) and their normalised Akaike information criterion [3, 55] (nAIC) (4.22). Coefficient of determination (CoD or R_T^2) is the square of the correlation between the measured values and the predicted values; it is defined as (4.20). The $\bar{R}_T^2$ is adjusted based on the degrees of freedom (DoF) of the residuals. The residuals DoF is defined as v = N − m, where N is the sample size and p is the number of predictors. These criteria are used as follows: R_T^2 and $\bar{R}_T^2$ are used for assessing the curve fitting efficacy, R_T^2 measures the proportion of variation in the dependent variable explained by all independent variables, whereas $\bar{R}_T^2$ has a penalty for adding variables that do not help in the prediction; nAIC is a measure that assesses model overparameterisation, a high magnitude of nAIC suggests that the model has been overparameterised.

Table 4.2 System identification MIMO order ranked by order of decreasing $R^2_{T_{si}}$ as a means of deciding for the optimal set.

Order n	$\mathrm{R}^2_{\mathrm{T_{si}}}$	$\mathrm{R}^2_{\mathrm{T_{sw}}}$	$\bar{\mathrm{R}}^2_{\mathrm{T_{si}}}$	$\bar{\mathrm{R}}^2_{\mathrm{T_{sw}}}$	nAIC
10	0.9981	0.9802	0.9565	0.8593	13.095
9	0.9956	0.9581	0.934	0.7954	13.037
7	0.9956	0.9583	0.9339	0.7959	12.846
8	0.9956	0.9611	0.9334	0.8027	12.884
5	0.9954	0.9625	0.9321	0.8013	11.612
2	0.9859	0.933	0.8814	0.7412	10.147
1	0.9479	0.9572	0.7718	0.7932	1.9011
6	0.856	0.8939	0.6205	0.6742	11.466
3	0.3268	0.2463	0.1795	0.1319	9.6471
4	0.0456	0.4491	0.0226	0.2038	10.224

$$R_T^2 = \frac{\sum_{i=1}^{N}(\hat{y}_i - \bar{y})^2}{\sum_{i=1}^{N}(y_i - \bar{y})^2} \tag{4.20}$$

$$\bar{R}_T^2 = 1 - \frac{(1 - R_T^2)(N-1)}{N - p - 1} \tag{4.21}$$

$$nAIC = \log\left(\left|\frac{1}{N}\sum_{1}^{N} \epsilon\left(t, \hat{\theta}_N\right)\epsilon^T\left(t, \hat{\theta}_N\right)\right|\right) + \frac{2n_p}{N} \tag{4.22}$$

From Table 4.2 it is obvious that high order system (10) gives a good match with $\mathrm{R}^2_{\mathrm{T_{si}}}$= 0.9981 and $\mathrm{R}^2_{\mathrm{T_{sw}}}$= 0.9802. That said, it is highly complex and that would incur a computational time penalty. On the other hand, a model of order 5 is much faster to compute and the results yielded are not significantly worse, as shown in Fig. 4.8. Order 7,8 and 9 do not provide an increase in $\bar{R}_T^2$ and can hence be deduced that the added complexity does not result in an increase in performance.

Comparing the models of order 10 with the order 5, the main reason for the decrease in $\bar{R}_T^2$ of the 5th order is the disparity at the initial warmup transient (Fig. 4.8). This part of the model is less important as the since the purpose is to be able to detect overheat. At the high temperature transients, the two models perform closely and the small increase in $\bar{R}_T^2$ that using an order 10 model would provide, does not justify doubling the order of the model. It should be noted that only the first two states correspond to physical quantities: the first is the stator iron temperature and the second one is the windings temperature; the rest of them are mathematical constructs that aid in the system identification process and the creation of the model.

$$\boldsymbol{A}=\begin{bmatrix} 0.9993 & 0 & 0 & -0.002 & 0.003 \\ 0 & 0.9998 & -0.00124 & 0 & 0.207 \\ -0.003 & 0.0094 & 0.3131 & -0.958 & 0.05342 \\ 0.0026 & -0.003 & -0.6363 & -0.2631 & -0.732 \\ -0.0015 & 0.0023 & 0.6628 & 0.1936 & -0.6836 \end{bmatrix}$$

$$\boldsymbol{B}=\begin{bmatrix} 0 & 0 \\ -0.0001993 & 0.0001398 \\ -0.005675 & 0.006258 \\ -0.0002821 & 0.00446 \\ 0.01321 & -0.007494 \end{bmatrix}$$

$$\boldsymbol{C}=\begin{bmatrix} 925.9 & 251.8 & -6.722 & -3.325 & 7.392 \\ 1179 & -122.3 & -0.8632 & -1.96 & 1.212 \end{bmatrix}$$

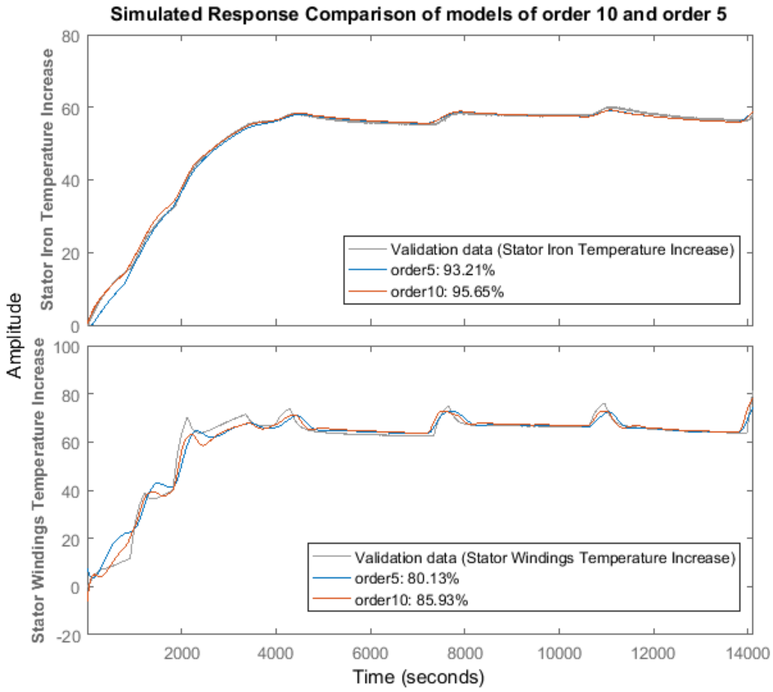

Fig. 4.8 Comparing the order 10 and order 5 models based on their $\bar{R}_T^2$.

4.3.2 Single Output Systems

In a similar manner to the previous method, the output sets (temperatures) are related to the input sets. Contrary to above, this is done for each output at a time. If there is no significant decrease in goodness of fit, there is no reason to use a MIMO system. The model estimation is done using the “arx()” function from MATLAB. Single input - single output and 2 input - single output systems are calculated and compared based on their $R_T^2$and $\bar{R}_T^2$. The MISO system is modeled in an ARX (4.23) [56]

$$y(z) = \frac{B(z)}{A(z)} U(z - n_k) \tag{4.23}$$

where $y(z)$ signifies the model output, in this case the stator iron and stator winding temperatures; B(z) and A(z) are as defined in (4.14, 4.15); $U(z - n_k)$ is the model input, in this case the excitation and armature current, with n_k signifying the number of delays, n_a and n_b are the number of $A(z)$ and $B(z)$ terms used. The models are ranked based on their goodness of fit to the measured temperatures. The number of numerator, denominator and inherent delay coefficients are altered sequentially for both transfer functions.

Table 4.3 shows the different coefficient sets and their goodness of fit when compared to the measured data using the R_T^2 as a primary criterion and $\bar{R}_T^2$ as a secondary criterion for the windings. The same iterative process, although not shown, is repeated for the stator iron as well. It should be noted that the notation is as follows: $n_{a_{If}}$ and $n_{a_{Ia}}$ refer to the number of denominator coefficients for the excitation current input and armature current input respectively, $n_{b_{If}}$ and $n_{b_{Ia}}$are the numerator coefficients for the aforementioned inputs and $\mathrm{n_c}$ is the number of delays.

In order to assist in the decision-making process, the best performing model was compared to the simplest one in order to deduce if the increase in performance is worth the increased model complexity, as shown in Fig. 4.9.

As it can be observed, the simple model behaves almost as well as the complex one for modelling the stator iron temperature, having less than 2% difference in normalised coefficient of determination, hence the simple model is preferred. For modelling the stator winding temperature, although the simple model is able to accurately model the steady state temperatures, it has difficulty modelling the sharp transients, which are the most important part of the model. This is reflected in the plot of the residuals (Fig. 4.10).

In this case, in order to accurately model the transients, a more complex model is needed; further increasing the complexity may yield even better results. The same process was repeated for ARMAX models with no improvement (this can be found in Appendix 1). Equation (4.24) shows the resultant multi-input multi-output system when the two MISO systems are joined.

Table 4.3 System identification coefficients ranked by order of decreasing R_T^2 as a means of deciding for the optimal set of coefficients for a MISO model for the stator windings temperature.

n_a	n_b	n_c	R_T^2	$\bar{R}_T^2$	$nAIC$
7	6	3	0.9835	0.8715	195.815
7	7	3	0.986	0.8818	168.974
6	6	3	0.9829	0.8692	16.7677
. . .	. . .	. . .	. . .	. . .	. . .
2	1	0	0.9743	0.8397	1.9181

6	6	2	0.9726	0.8345	6.462
2	2	0	0.9693	0.8247	2.097
1	1	0	0.9577	0.7944	2.4159
. . .	. . .	. . .	. . .	. . .	. . .
6	1	2	0.8875	0.6645	21.8872
4	2	0	0.3428	0.1893	5.1601

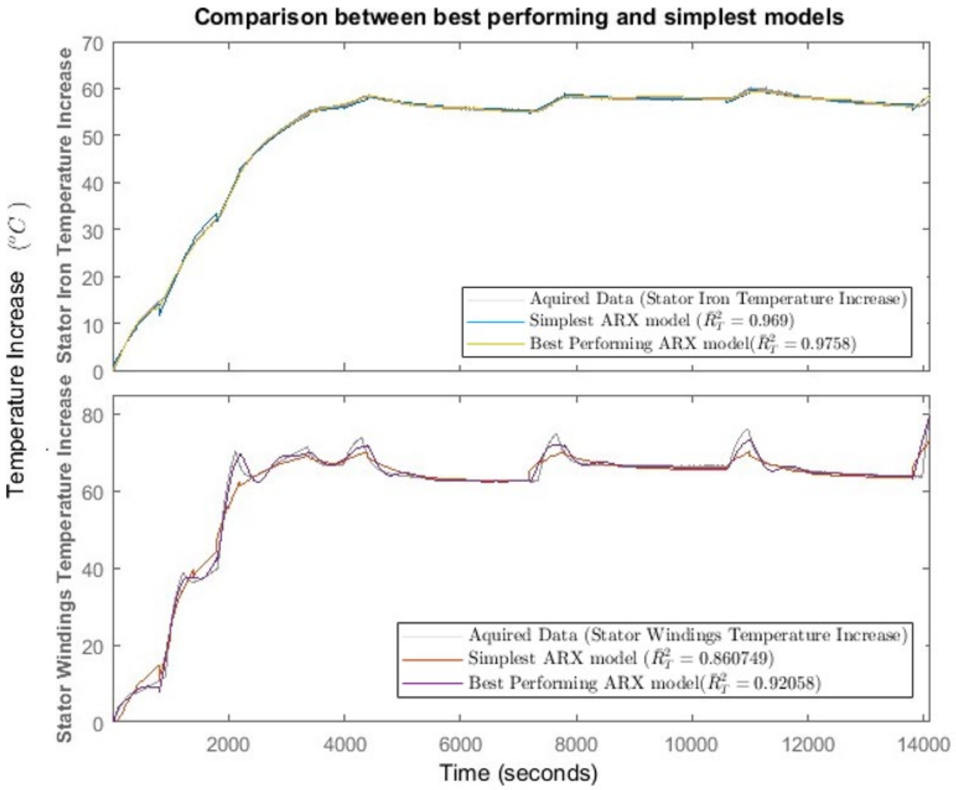

Fig. 4.9 Comparing the best performing with simplest models based on their $\bar{R}_T^2$, (for windings $n_a = 1, n_b = 1, n_c = 0$ and $n_a = 6, n_b = 6, n_c = 3$; and for stator iron they are $n_a = 1, n_b = 1, n_c = 0$ and $n_a = 5, n_b = 3, n_c = 0$).

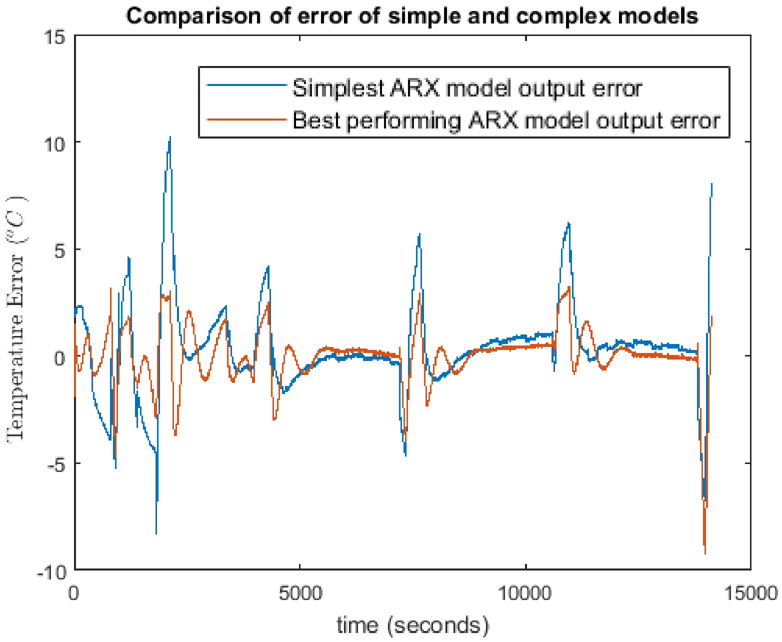

Fig. 4.10 Error in winding temperature of the simplest and best performing ARX models.

$$\begin{bmatrix} T_{si} \\ T_{sw} \end{bmatrix} = \begin{bmatrix} G_{I_a 2T_{si}} & G_{I_f 2T_{si}} \\ G_{I_a 2T_{sw}} & G_{I_f 2T_{sw}} \end{bmatrix} \begin{bmatrix} I_a \\ I_f \end{bmatrix} \tag{4.24}$$

$$G_{I_a 2T_{si}} = \frac{-0.5115 + 0.5115z^{-1}}{1 - 1.000z^{-1}}$$

$$G_{I_a 2T_{si}} = \frac{-0.8588 + 0.8671z^{-1}}{1 - 0.9993z^{-1}}$$

$$G_{I_a 2T_{si}} = \frac{-0.0005436z^{-3} + 0.0005925z^{-4} + 0.0004474z^{-5} - 0.0004962z^{-6}}{1 - 3.757z^{-1} + 5.273z^{-2} - 3.274z^{-3} + 0.7583z^{-4}}$$

$$G_{I_f 2T_{sw}} = \frac{-0.5013z^{-2} + 1.53z^{-3} - 1.556z^{-4} + 0.5271z^{-5}}{1 - 2.993z^{-1} + 2.987z^{-2} - 0.9935z^{-3}}$$

As previously mentioned, the MIMO transfer function can be constructed by using two SISO functions, both inputs are related to both outputs and the most suitable input for each output is chosen.

It can be observed that all transfer functions related to stator iron take a form close to an integrator, which does justify the suggestion of about using the integral of current as an input. That idea was not pursued as it provided a smaller coefficient of determination when compared to real data, but the estimated parameters are close to an integrator form.

Table 4.4 System identification coefficients ranked by order of decreasing R_T^2 as a means of deciding for the optimal set for the stator winding transfer function by using I_f as an input using ARX.

n_a	n_b	n_c	R_T^2	$\bar{R}_T^2$	$nAIC$
7	6	3	0.9835	0.8715	195.815
7	7	3	0.986	0.8818	168.974
6	6	3	0.9829	0.8692	16.7677
. . .	. . .	. . .	. . .	. . .	. . .
2	1	0	0.9743	0.8397	1.9181
6	6	2	0.9726	0.8345	6.462
2	2	0	0.9693	0.8247	2.097
1	1	0	0.9577	0.7944	2.4159
. . .	. . .	. . .	. . .	. . .	. . .

6	1	2	0.8875	0.6645	21.8872
4	2	0	0.3428	0.1893	5.1601

When considering the stator iron temperature, a simple system ($n_a = 1, n_b = 1$) is sufficient for its modelling providing an R_T^2> 0.99. On the other hand, when modelling the stator windings, a higher order system ($n_a = 6, n_b = 6, n_c = 3$) is necessary to model the initial transient dynamics, but there is still poor fit when attempting to model the later transients. It should be noted that this issue is not present when using two inputs for this model. Equations (4.25) and (4.26) model the temperature of the stator iron and windings. The one pole- one zero model has been chosen for the stator iron since there is a minimal change in the coefficient of determination when higher order systems are chosen.

$$T_{si}(z) = \frac{-0.7655 + 0.773z^{-1}}{1 - 0.9994z^{-1}} I_a(z) \tag{4.25}$$

$$T_{sw}(z) = \frac{\begin{gathered}(-0.8042 + 4.845z^{-1} - 12.16z^{-2} + 16.29z^{-3}\\ -12.26z^{-4} + 4.925z^{-5} - 0.824z^{-6})z^{-3}\end{gathered}}{\begin{gathered}1 - 0.5994z^{-1} + 14.97z^{-2} - 19.94z^{-3} +\\ 14.94z^{-4} - 5.972z^{-5} + 0.9943z^{-6}\end{gathered}} I_f(z) \tag{4.26}$$

The preferred model structures contain three delays on the numerator although delays have not been explicitly modelled in the nonlinear model. There are two reasons behind this: firstly, thermal masses in thermal circuits have mathematical properties akin to those of capacitors in electrical circuits, i.e. they create a lag in the response, this lag in response in turn manifested as a delay in the ARX model. The alternative explanation is that the model chosen is overparameterised as hinted by the nAIC of Table 4.4.

4.4 Discussion

Figures 4.4, 4.5 demonstrate that the linearised model is a good approximation for the system and the higher order dynamics do not influence the system for the operating ranges defined previously. It cannot be understated that the approximation of the transient behaviour (for the stator winding temperature) description is still suboptimal.

The white box models have a difficulty in describing the initial heating up dynamics, both in linear and nonlinear cases. This might be the case because of assuming the losses are larger than they are, or because of the cooling action taking place. Once the generator is warm though, the transient behaviour of the winding temperature is very accurately modelled by the nonlinear model with a maximum error of 3.7^{o}C; this error is doubled for the linear model. With regards to the stator iron, both linear models are able to describe its behaviour after the initial transients have completed. The nonlinear model describes the initial transient dynamics more accurately, but this part of the model is less important for the task at hand.

4.4.1 Black box analysis

From the information presented in the black box modelling section, it can be observed that the only information needed to model the stator iron temperature is the armature current. On the other hand, for the winding temperature estimation, if only one input is used, the transient behaviour is not properly encapsulated; therefore, information on both the armature current and the excitation current is necessary. The model can accurately be described by (4.27). It is possible to further simplify the transfer functions describing the winding temperature, but that would compromise the accuracy of fit, especially at the transient segments.

$$\begin{bmatrix} T_{si} \\ T_{sw} \end{bmatrix} = \begin{bmatrix} G_{I_a 2T_{si}} & 0 \\ G_{I_a 2T_{sw}} & G_{I_f 2T_{sw}} \end{bmatrix} \begin{bmatrix} I_a \\ I_f \end{bmatrix} \tag{4.27}$$

where

$$G_{I_a 2T_{si}} = \frac{-0.7655 + 0.773z^{-1}}{1 - 0.9994z^{-1}}$$

$$G_{I_a 2T_{si}} = \frac{-0.0005436z^{-3} + 0.0005925z^{-4} + 0.0004474z^{-5} - 0.0004962z^{-6}}{1 - 3.757z^{-1} + 5.273z^{-2} - 3.274z^{-3} + 0.7583z^{-4}}$$

$$G_{I_f 2T_{sw}} = \frac{-0.5013z^{-2} + 1.53z^{-3} - 1.556z^{-4} + 0.5271z^{-5}}{1 - 2.993z^{-1} + 2.987z^{-2} - 0.9935z^{-3}}$$

Similarly to Ch.3, the preferred model is validated against acquired data for the cases of step input of 1A and 4A as well as for transient conditions. This is to ensure that the performance of the linear model adequately describes the system at hand. The nonlinear model response is added for completion. These tests are shown in Figs. 4.11 – 4.16.

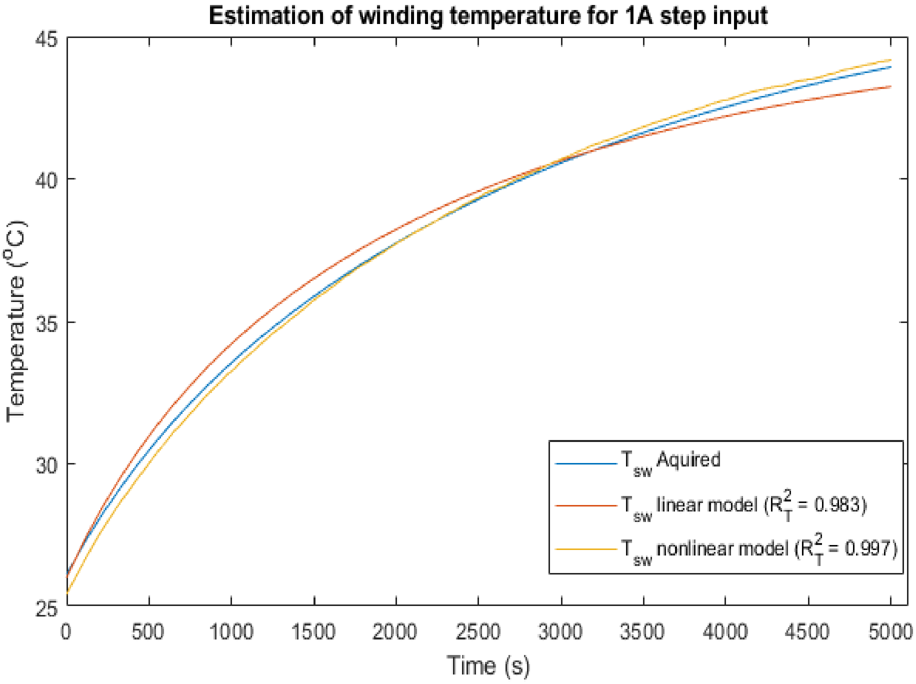

Fig. 4.11 Model fit comparison for winding temperature between the acquired data and the linear model for a step input of 1A.

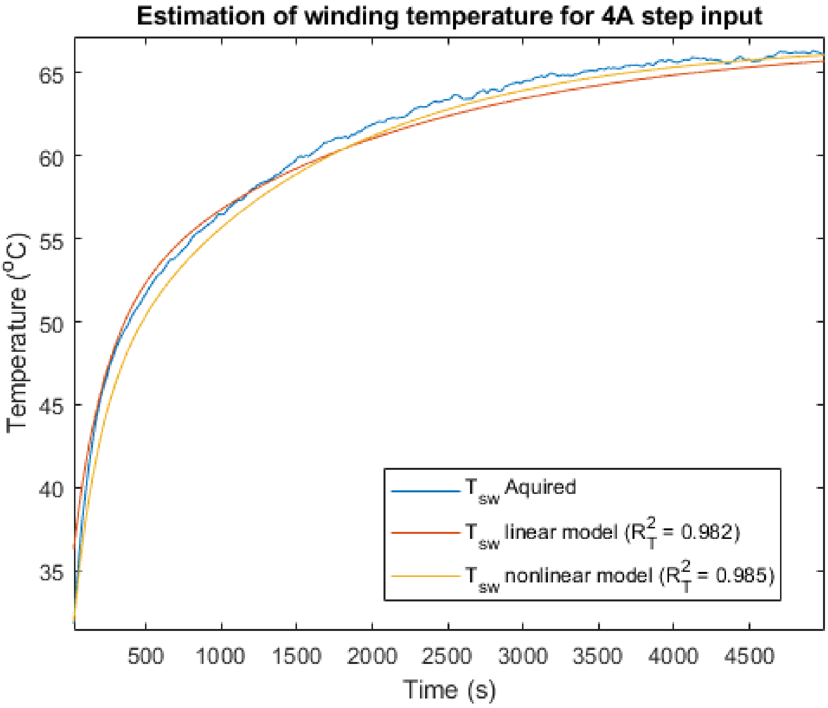

Fig. 4.12 Model fit comparison for winding temperature between the acquired data and the linear model for a step input of 4A.

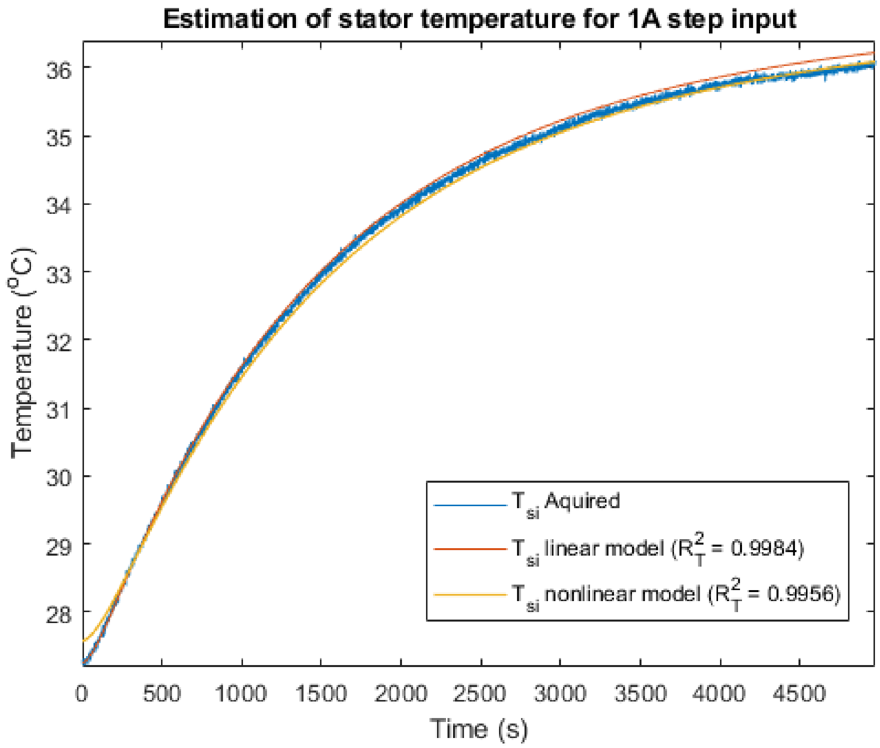

Fig. 4.13 Model fit comparison for stator temperature between the acquired data and the linear model for a step input of 1A.

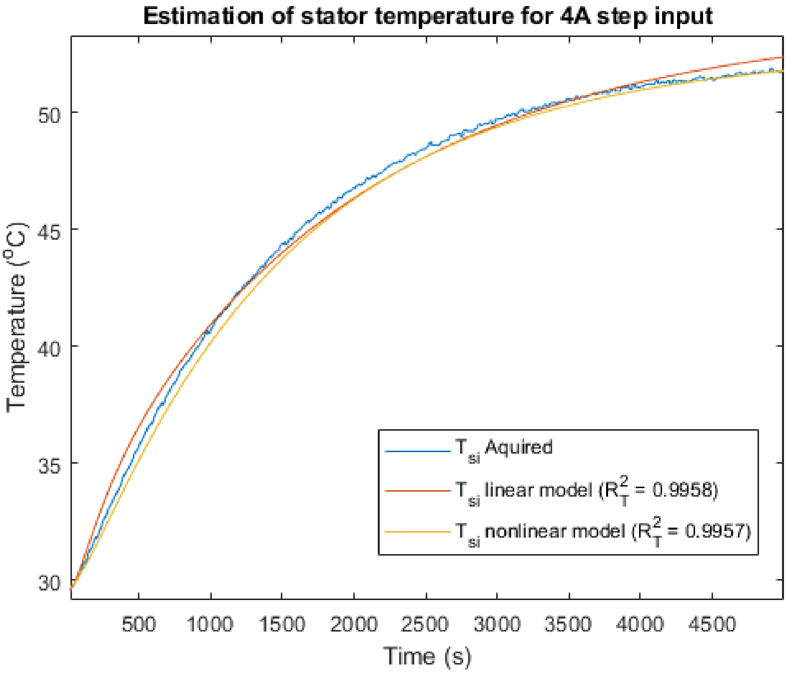

Fig. 4.14 Model fit comparison for stator temperature between the acquired data and the linear model for a step input of 4A

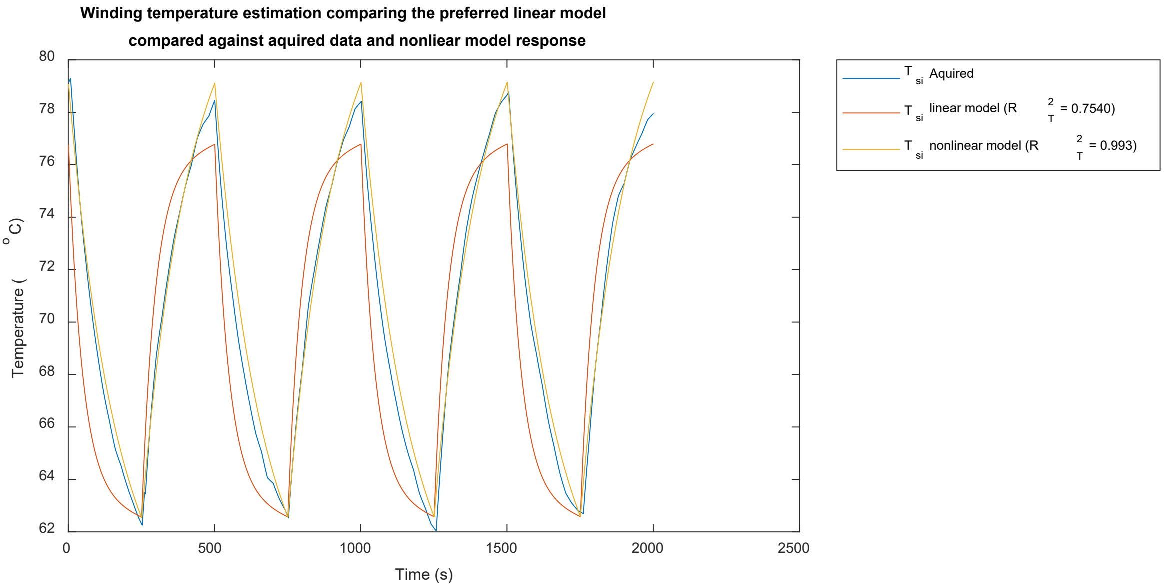

Fig. 4.15 Model fit comparison for winding temperature between the acquired data and the linear model for the varied load test (40% - 80% of full load).

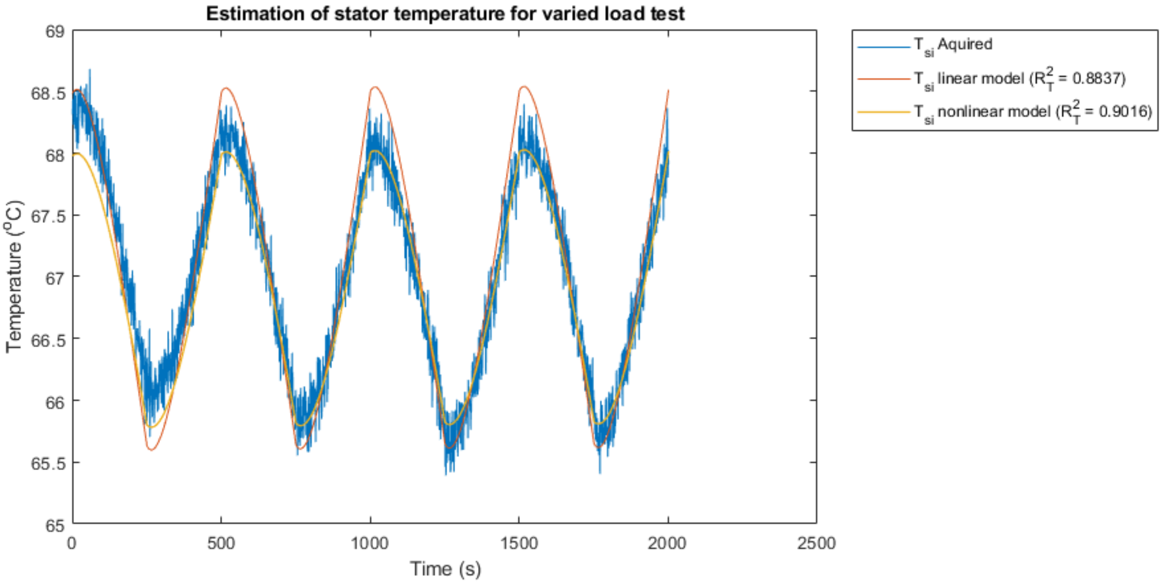

Fig. 4.16 Model fit comparison for stator temperature between the acquired data and the linear model for the varied load test (40% - 80% of full load).

Table. 4.5 Model fit comparison for stator temperature between the acquired data for the black box model.

Test	$R^2_{T_{sw}}$ Black Box	$R^2_{T_{sw}}$ Nonlinear	$R^2_{T_{si}}$ Black Box	$R^2_{T_{si}}$ Nonlinear
1A Step	0.9830	0.997	0.9984	0.9956
4A step	0.9820	0.985	0.9958	0.9957
Transient test	0.7540	0.9933	0.8837	0.9016

Table 4.5 summarises the results of Figs. 4.11- 4.16. When comparing the response of the linear ARX model to the acquired data, it can be observed that for steady state cases it performs on-par with the nonlinear model from Ch.3. The main drawback of the linear model is the description of the transient conditions of the windings, where there is a slightly higher rise time and an error on the maximum temperature. This data further supports the response shown in Figs. 4.8-4.10.

In a further attempt to capture the transient dynamics of the winding temperature (using a black box approach), one can pick a more suitable training window which only includes points from the system after it has completed its initial transient. Figure 4.17 demonstrates how an input that does not include the initial dynamics can reduce the error at the further transients. A model like this one has better fit at the transient dynamics even compared to the nonlinear white box model [4] with a maximum error of 3.2^{o}C.

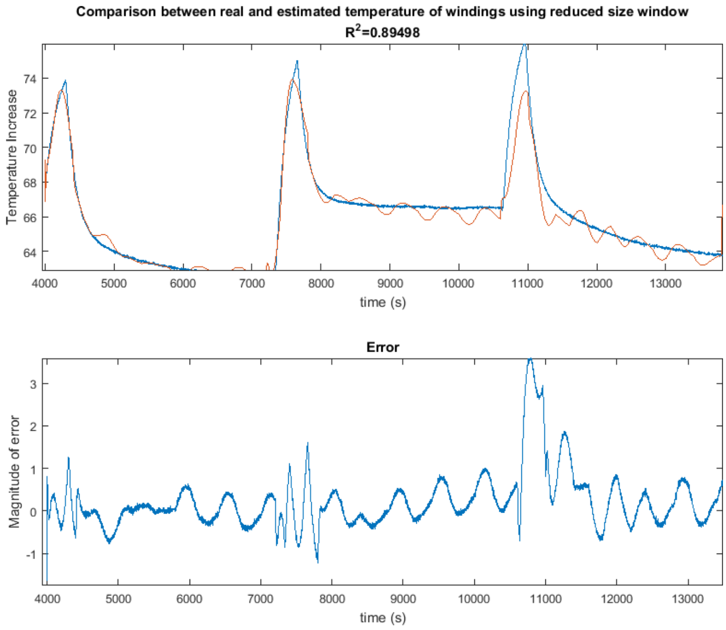

Fig. 4.17 Response for a Black Box Model using a window that excludes initial transients in the parameter estimation.

Based on this, another approach can be theorised. Having several transfer functions that accurately describe the dynamic of specific behaviours of the system. For example, let these transfer functions be $G_1(z), G_2(z)$ … $G_n(z)$ based on the inputs (I_f and I_a) received, the relevant transfer function is chosen in order to model a specific behaviour. Another way of improving this, is by using a dynamic/ adaptive approach; there are several adaptive modelling approaches [56, 71, 100]. The input to the training of the transfer function can be a moving window of either set or variable size. The data describing the initial transients of the system is not relevant for describing the further transients or the steady states; so when that stage is reached, a new transfer function can be calculated which better fits that behaviour. Another improvement to the accuracy of fit can occur by more intelligent sampling of data. Currently all data gathered had a sample time of 1s. This results to a surplus of data describing steady states and less data describing transients, which in turn results to transients being poorly described in comparison.

4.4.2 Model Comparison and Suggested Model Uses

It can be observed from Table 4.6 that the system identification model outperforms the linearised white box and therefore it is a better candidate to be used as a basis for the predictive algorithms. The black box model also has the advantage of being easily created from gathered data without full knowledge of the system. Having said that, the white box model offers the advantage of clarity and modifiability. It allows for easier testing of different scenarios, such as faults which can be implemented at different parts of the generator.

Table 4.6 Comparing the goodness of fit of the linear white box and black box models developed in the realistic mission test.

Model Type	R_T^2 Stator Iron	R_T^2 Stator Windings
Linearised White Box	0.9746	0.9617
Linear Black Box	0.9975	0.9937

4.5 Conclusion

In this Chapter, two approaches, Black box (ARX and state space) vs linearised white box model, for developing a linear model for the estimation of the temperatures of vulnerable components of the generator have been developed and discussed.

The use of an ARX model-based on measurements of currents and temperatures provides an improvement, both in terms of goodness of fit and model complexity, when compared to its white box counterpart and the state space approach.

Furthermore, it can be used in situations where limited information about the generators at hand is accessible.

It has been demonstrated that using a linear black box system identification approach (ARX) is a valid alternative for calculating the temperature of the heat sensitive components of the generator, whilst being comparable in most cases to the performance of the nonlinear model.

Therefore, the black box approach is preferable when applied as a basis for controller design and prediction algorithms, whereas the white box linearised model provides more customisation options which allow for easier simulation of faults.

CHAPTER 5

ADAPTIVE MODELLING AND TIME VARYING SYSTEMS

5.1 Introduction

The purpose of this chapter is to discuss the necessity and development of adaptive models as part of a fault tolerant prediction algorithm. Adaptive models are necessary for integrating the fault behaviour in the model. Two main approaches are explored:

- Linear time varying models based on the ARX models of Chapter 4

- Nonlinear adaptive models based on neural networks (NNARX)

These two approaches are compared based on their response time, prediction accuracy and complexity. The merits and drawbacks of both methods are mentioned, and specific uses are suggested for each.

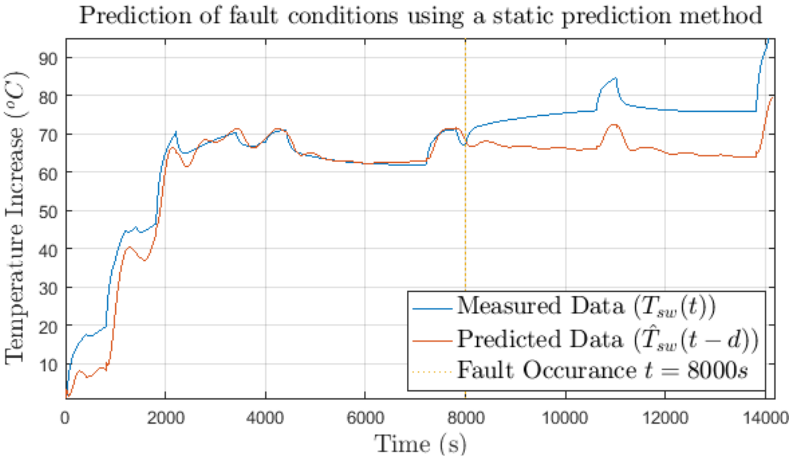

Fig. 5.1 Static model behaviour before and after fault occurrence.

5.2 Top Level Design

The models demonstrated in Chapter 4, although excellent at predicting the future temperature during normal operating conditions (no fault), they are unable to accommodate for potential faults. It should be noted that the term fault is used widely in this body of work to describe a change in input-output relationship due to factors not considered in the model. This can vary from change of environmental conditions in a short time, insulation degradation, blockage in the cooling pathway etc.

When a fault occurs, it can be assumed that the system changes, and so do the input-output relationships used to approximate the black box model. As it can be observed in Fig. 5.1, although the model is able to predict the temperature before the fault occurs, after t = 8000s the model is unable to accurately predict the generator temperature.

Due to sensing limitations, faults can be undiagnosed and undetected, but nonetheless, they need to be accommodated for in real time. In this body of work, this is achieved by sampling the relevant inputs and outputs (currents and temperatures) and in real time estimating a best performing model-based on most recently collected information, further explained in section 5.3.

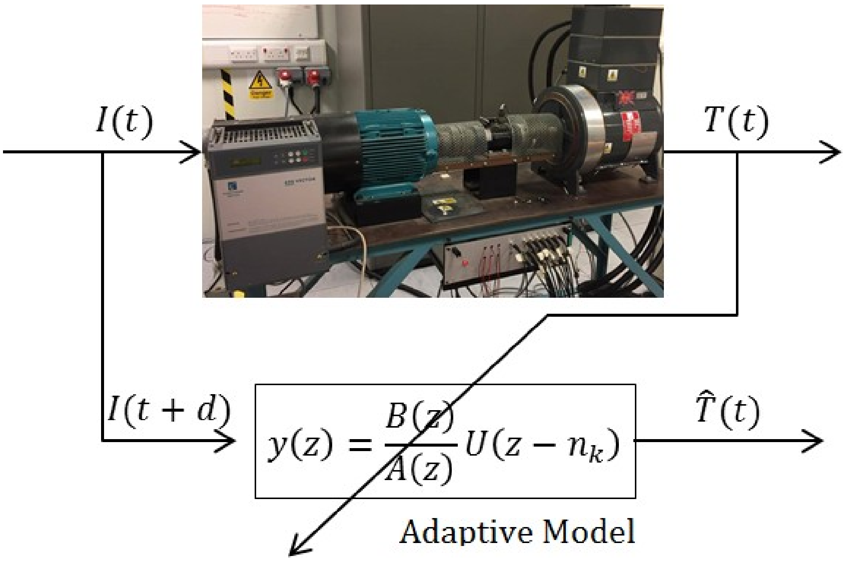

Fig. 5.2 Top level schematic of the adaptive model.

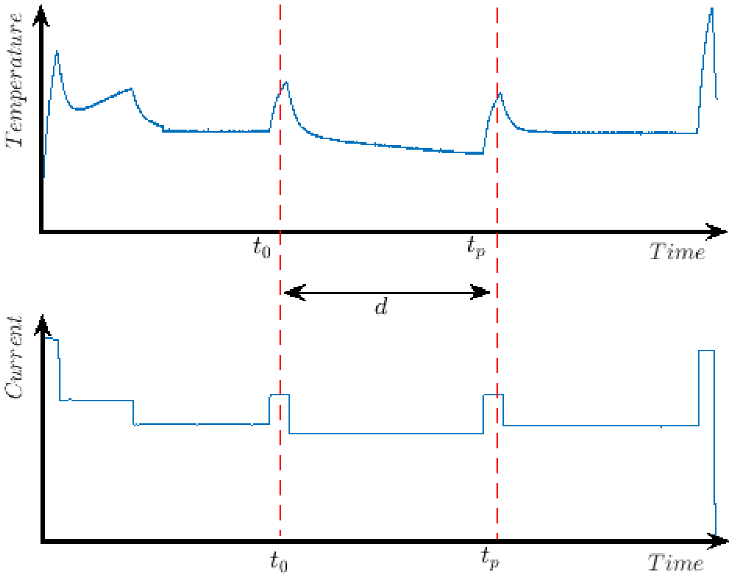

Fig. 5.3 Schematic outline of the current point in time t_0 and the end of prediction t_p.

5.3 Adaptive ARX

Adaptive ARX has been used for economic forecast [53], environmental applications and materials engineering [10]. Estimating the temperature of generator components though, is not often treated as a time varying system online.

In Chapter 4, offline ARX models were explored for temperature predictions. It was demonstrated that in no fault conditions they perform very well, having a coefficient of determination of R_T^2> 0.99. In Fig. 5.1 this does not hold. The structure chosen for the adaptive model is two SISO transfer functions, as outlined in Chapter 4 section 3, because SISO models provide simplicity during online adaptation. A necessary assumption to make the system run in real time, is that the structure of the transfer function must remain constant through time with the same number of numerator and denominator parameters. This circumvents the need for calculating a set of models (as shown in Chapter 4) and choosing the optimal one for the task.

The black box models described in Chapter 4 are used as a baseline. They provide a criterion for model accuracy, as it is the worst case scenario where the model has not adapted to accommodate for the change in conditions. It is also assumed that the input $(u(t))$ is known for all relevant points in time. In practical terms this means that any change/ shift in load current is predetermined and planned. The relevant points in time include all past values and future values at least until the end of the prediction horizon. Referring to Fig. 5.3, the current demand is known for $I_d(t) \in [0, t_p]$ as shown in (5.1).

$$I_d(t) = \begin{cases} u(t), & t \in [0, t_0] \\ \hat{u}(t), & \text{otherwise} \end{cases} \tag{5.1}$$

This ensures causality in the prediction system. Hence information from the input signals (i.e. the excitation and load current) populates the vectors $u(t)$ and $\hat{u}(t)$.

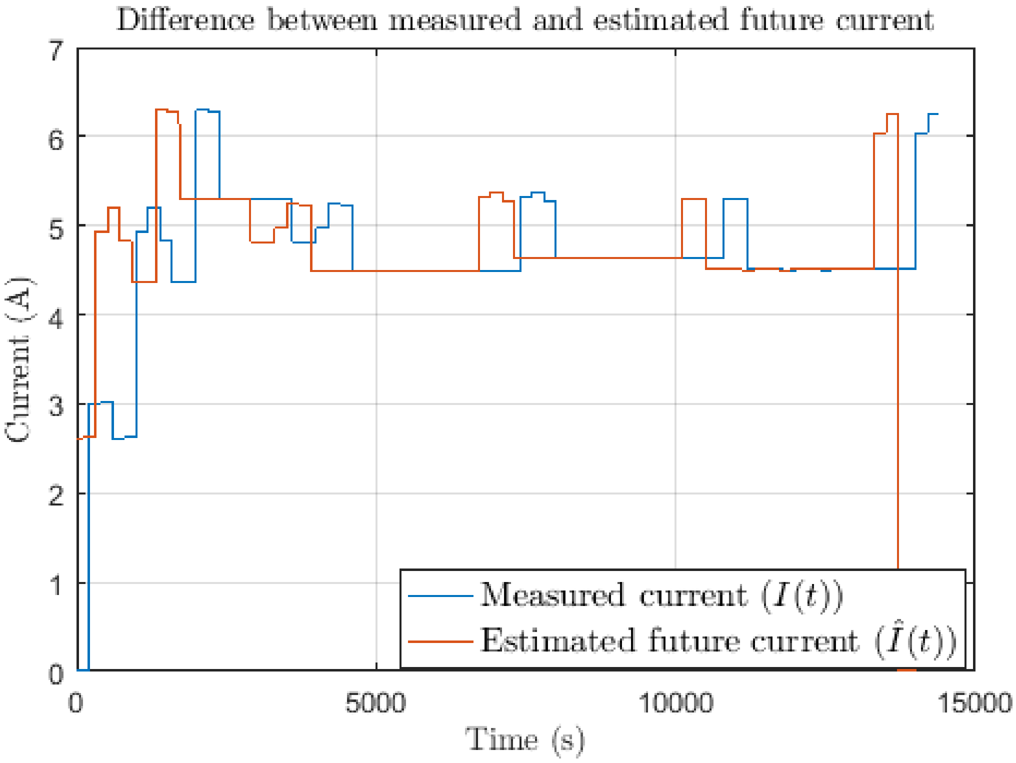

Fig. 5.4 Time difference between measured and estimated future current.

During normal operating conditions $\hat{u}(t)$ holds the future values of $u(t)$, i.e. $\hat{u}(t+d) = u(t+d)$. Separating the two is done for two reasons, firstly, $u(t)$, is based on past measurements, whereas $\hat{u}(t)$ is a desired signal that has not yet occurred and hence cannot be measured; $\hat{u}(t)$ can be modified, if needed, to avoid overheating faults. Figure 5.4 visually showcases how the “future current” needs to be known d time units before it occurs.

The adaptive ARX process is conducted as follows:

1. Selection of the desired structure of the transfer function and initial conditions of the parameter vector $\boldsymbol{\theta}$ via offline estimation: This allows a baseline for prediction to be available as well to have the model usable from the beginning of the flight. This is identical to the offline estimation that was explained in section 4.3. That said, the requirements can be considered to be less scrutinous because of the adaptive nature of the algorithm.
2. Online parameter estimation: By continuously measuring the input(s) and output(s) the parameters of A(z) and B(z) can be estimated and adapted in real time.
3. Transfer function population: These parameters are, in turn, used to update the transfer function that was previously defined.
4. Temperature Prediction: By using information of the future load demands (and hence currents) the future temperatures can be predicted.

5.3.1 Parameter estimation

There are several ways of dynamically estimating the A(z) and B(z) parameters [56], including forgetting factor; Kalman filter; and Least Mean Squares (LMS), which is the method employed in this application.

$$\widehat{\boldsymbol{\theta}}(t) = \widehat{\boldsymbol{\theta}}(t-1) + K(t)[y(t) - \hat{y}(t-1)] \tag{5.2}$$

$\widehat{\boldsymbol{\theta}}(t)$ is the parameter vector predicted at t. $y(t)$ is the measured output and $\hat{y}(t)$ is the estimated output based on the data gathered until $(t-1)$. The gain, $K(t)$, determines the extent that the prediction error between the measured and predicted outputs $y(t) - \hat{y}(t-1)$ affects the update of the estimated parameter vector. The overall aim is to minimise the error between measured and predicted data.

$$K(t) = Q(t)\boldsymbol{\psi}(t) \tag{5.3}$$

$$\hat{y}(t) = \boldsymbol{\psi}^T(t)\widehat{\boldsymbol{\theta}}(t-1) \tag{5.4}$$

$$Q(t) = \frac{\gamma}{\left|\left|\boldsymbol{\psi}(t)\right|\right|^2 + \beta} \tag{5.5}$$

$\boldsymbol{\psi}(t)$ is the gradient vector of the estimated output $\hat{y}(t|\theta)$ with respect to the parameter vector. The normalised LMS algorithm scales the adaptation gain by γ at each iteration by the two-norm squared of the $\boldsymbol{\psi}$. At small gradients, transients can be caused.

To prevent sharp transients, a bias term (β) is added in the denominator of scaling factor. Based on the choices of $Q(t)$, the parameter vector is updated in a direction opposite to the gradient.

5.3.2 Model Implementation

As previously stated, for the algorithm to be able to predict future temperatures, the future load of the generator is required. Implementing this in a Simulink environment can be achieved by delaying signals. To achieve this, one must first define a ‘frame of reference’ for the time variable, which specifies when the signals occur. The information the models receive regarding the temperatures is limited due to time. Although the current/ load is known for all time, the temperatures can only be considered accurate enough up to the present moment of measurement.

The parameter vector $\boldsymbol{\theta}$ is calculated and the model is adapted for $t < t_0$, where t_0 is the present moment of prediction. Although obvious, this is limiting the capabilities of the model since the latest update of the parameters might not be accurate enough for a large prediction horizon.

For simplicity, let the input and output variables be put in matrix form, $\boldsymbol{I}(t) = \left[I_a(t), I_f(t)\right]^T$, $\boldsymbol{T}(t) = [T_{si}, (t)T_{sw}(t)]^T$, where the superscript T denotes their transposition.

Hence, let $\boldsymbol{I}(t)$, $\hat{\boldsymbol{I}}(t)$, $\boldsymbol{T}(t)$ and $\hat{\boldsymbol{T}}(t)$ be the input, predicted input, output and predicted output variables respectively; the hat (ˆ) notation refers to predicted data, so that:

where t_0 is the present point in time (i.e. when the prediction is made) and d is the size of the prediction horizon.

In this case, the predicted current $\hat{\boldsymbol{I}}(t)$ is equivalent to $\boldsymbol{I}(t + d)$ for any instance before the point of prediction ($t \leq t_0$). As such, values are based on the load profile and measurements. For values of $t > t_0$ the value of $\hat{\boldsymbol{I}}(t)$ can change and deviate from the initial load profile if it is necessary to avoid generator overheat (further explored in Chapter 6). This is best described in Fig. 5.4 where $\hat{I}_a(t)$ provides the information of $I_a(t)$, d time units before it occurs. In this case they would coincide given the appropriate shift by d time units. It should be noted that both the prediction horizon and delay are denoted as d since their sizes are equivalent.

The prediction occurs as follows: Using information from the relevant current and temperature measurements ($\boldsymbol{I}(t)$ and $\boldsymbol{T}(t)$) parameters $\widehat{\boldsymbol{\theta}}(t)$ are adapted (5.5).

In order to simulate this, the input signal is delayed by d time units, which in turn causes the prediction output to be shifted as well in order to be comparable to the actual output. It is worth noting that the same result can be achieved by delaying the parameter update instead of the inputs and outputs. This is shown diagrammatically in Fig. 5.5.

As previously mentioned, the adaptive model is only relevant for after a fault occurs, judging its performance before a fault occurs, will misleadingly inflate the goodness of fit between measurements and prediction. Hence the relevant region of comparison should only be defined for $t \geq t_{fault}$.

It is important to note the size and contents of the aforementioned variables. Looking for example at $\boldsymbol{T}^T(t) = [\boldsymbol{T}_{si}(t), \boldsymbol{T}_{sw}(t)]$ where $\boldsymbol{T}_{si}(t) = [T_{si}(t),\ T_{si}(t-1) \ldots T_{si}(1)]$, so, $\boldsymbol{T}_{si}(t)$ contains all past information of T_{si} until time t; the same idea is valid for the other variables as well . This is best visualised if $\mathbf{T}$ and $\mathbf{I}$ are 1 × 2 × n and $\mathbf{G}$ is 2 × 2 × n matrices where n is the number of time samples (5.6).

$$\therefore T^{T(2,3)} = \begin{bmatrix} T_{si}(n) & T_{si}(n-1) & \ldots & T_{si}(1) \\ T_{sw}(n) & T_{sw}(n-1) & \ldots & T_{sw}(1) \end{bmatrix} \tag{5.6}$$

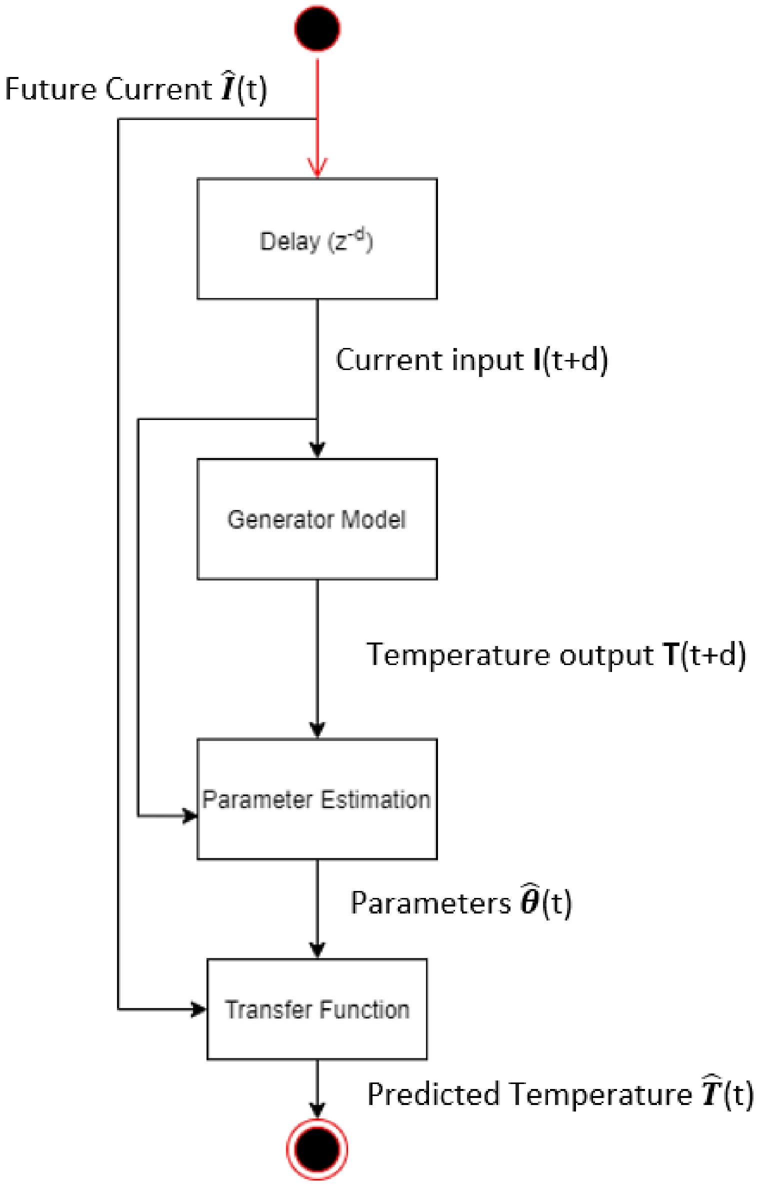

Fig. 5.5 Diagrammatic representation of the simulation of the prediction process.

5.3.3 Prediction Horizon Tradeoff

Imagine the scenario where a fault occurs at t=8000s, similarly to Fig. 5.1. By using the techniques described in section 5.3, the initial parameters $\boldsymbol{\theta}_0$ are adapted in real time populating $\boldsymbol{G}(\hat{\theta}|t)$. $\hat{T}(t)$ is predicted by treating $I_d(t)$ (from (5.1) as an input to $\boldsymbol{G}(\hat{\theta}|t)$.

Prediction is best understood by starting at the point that is being predicted. Consider predicting the peak at $t = 11000s$, let $t_p = 11000s$. This peak is being predicted from points $\mathrm{t} = \mathrm{t}_0$where $\mathrm{t}_\mathrm{p} - t_0 = d$. Namely, when $t_0 = 9000s$, the prediction horizon for predicting $t_p = 11000s$, $d = 2000s$ and so on. This is done for every point $t_p \in (1, t_{end})$ and from every point $t_0 \in (0, t_p - 1)$ (Fig 5.3). The values of prediction horizon d are discrete and are chosen in a fashion that the corresponding outputs are useful. This can be observed in Fig. 5.3, where a segment post fault occurrence is examined and the pronounced peak of $T_{sw}(t)$, at $t_p = 11000s$, is predicted with decreasing size of prediction horizon. It should be noted that all other points are also predicted, but attention is drawn to that specific one for simplicity.

$\hat{T}(t)$ occurs d time units before $T(t)$. Therefore, in order for the predicted temperature to be comparable with the measured temperature, a delay of size of the prediction horizon (d) needs to be implemented. This is demonstrated in Fig. 5.6, where the signals are delayed by d time units, in order to be temporally comparable to the measured data.

As it can be observed, a large prediction horizon results to a decrease in accuracy of prediction. This is due to two main reasons: firstly, $G(\hat{\boldsymbol{\theta}}|t)$ being tuned for values of $I(t)$ and not $\hat{I}(t)$, and secondly, not having enough data to fully adapt after the fault occurs at $t = 8000s$. This increase in prediction error is best detected when describing the error as a function of the prediction horizon, see Fig. 5.7. This plot is showing the error for the peak value of $t = 11000s$, but a similar description would be applicable for any point t_p that satisfies the aforementioned conditions.

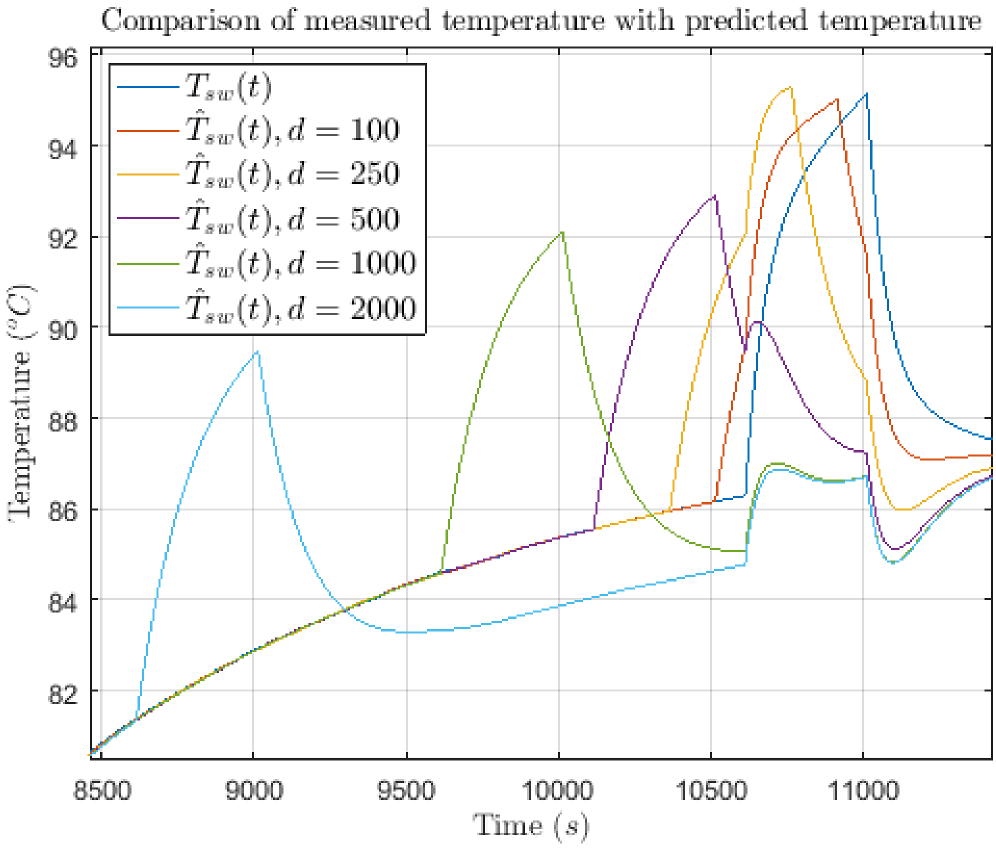

Fig. 5.6 Comparison of measured stator winding temperature to predicted ones, using increasing prediction horizons using adaptive system identification.

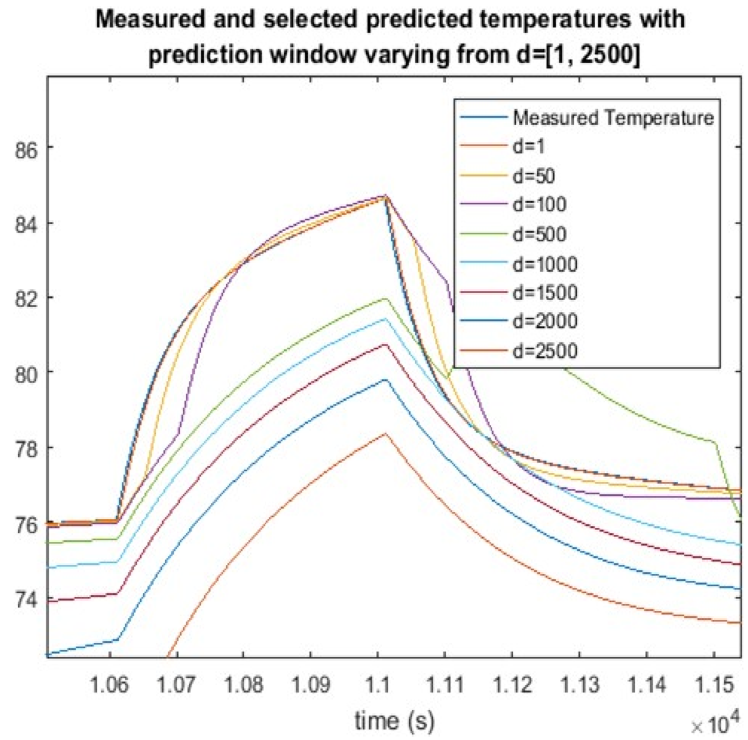

Fig. 5.7 Comparison of measured stator winding temperature to predicted ones, using increasing prediction horizons. A delay of size equal to the prediction horizon d is introduced to all $\hat{T}_{sw}(t)$.

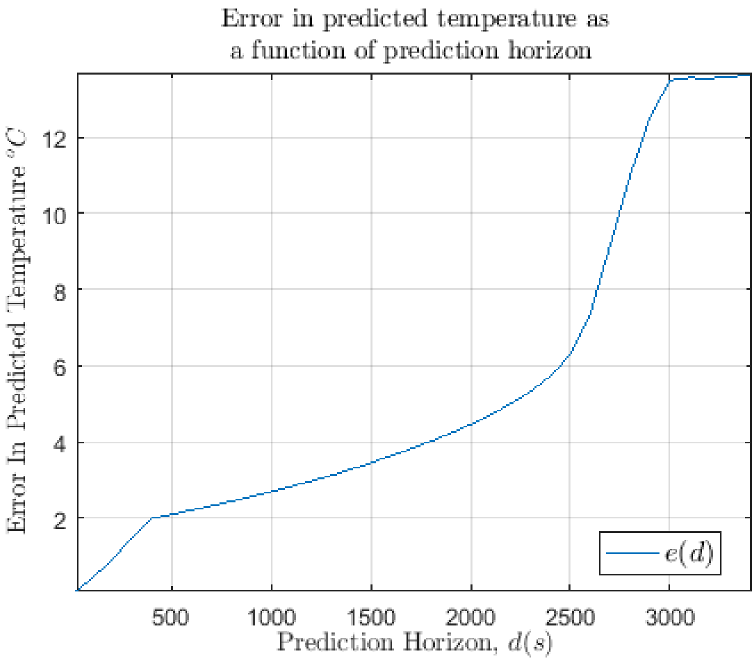

Fig. 5.8 Prediction error as a function of the prediction horizon.

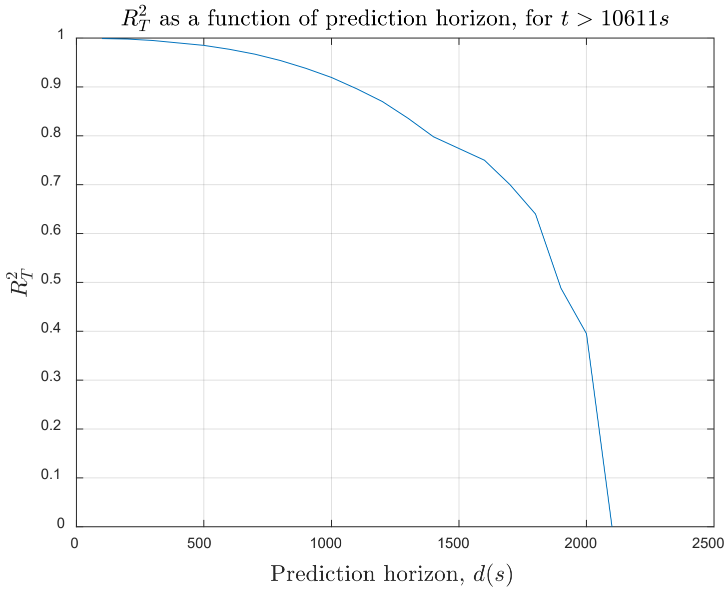

Fig. 5.9 Model fit as a function of the prediction horizon.

There are four main segments in Fig. 5.8; they are discussed in ascending order of d: first, a linear increase in error between $1s < d < 450s$, this increase is due to the discrepancy between $I(t)$ and $\hat{I}(t)$; after that, the lack of training data starts to become apparent $451s < d < 2500s$, nonetheless, there is enough data for the model to be adapted and provide an improvement to the static model; between $2501s < d \leq 3000s$ the lack of data is detrimental to the model accuracy with its rate of change increasing; lastly for $d > 3000s$ a pseudo-steady state is reached, as these systems only contain information before the fault had occurred and hence are unable to adapt to it.

Fig. 5.9 demonstrates the degradation of the model fit as the prediction horizon increases, this does not make the model useless for prediction horizons $d > 2500s$ as the maximum temperature error is still smaller than using the static model. Close to the fault occurrence there is limited information for a new model to be created, therefore the error of the system with the large prediction horizon is significantly larger. Essentially there is a prediction "dead zone" of size d after a fault occurs. This lack of information poses a threat when the potential overheat point is close to the point of fault.

Different scenarios where the fault occurs closer to the point of potential overheat are explored in Chapter 6. Such as an example is demonstrated in Fig 5.10 with prediction horizon of $d = 500s$

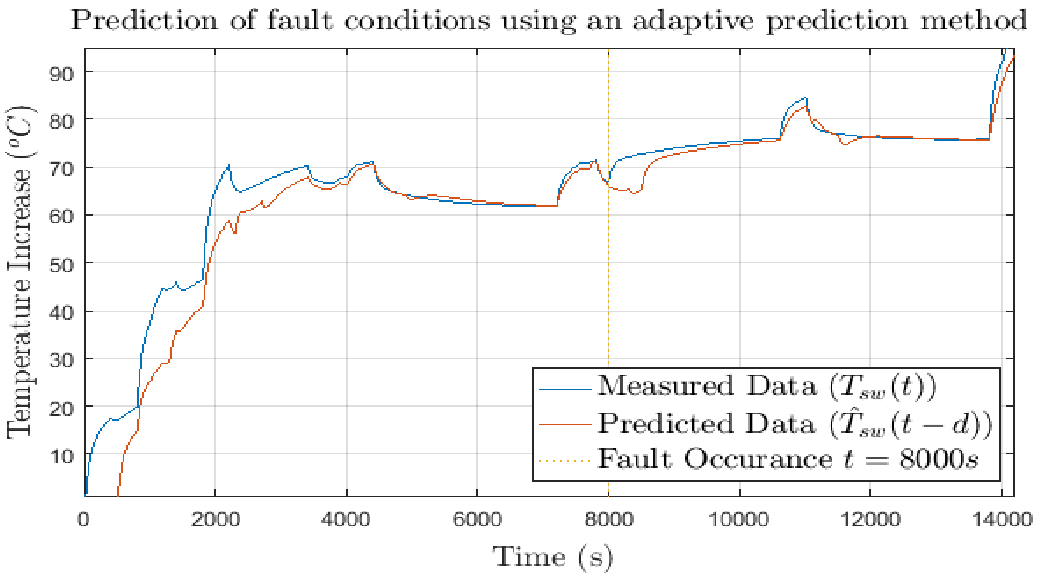

5.4 Neural Network Based Adaptive Modelling

Artificial neural networks refer to complex nonlinear relationships within numeric data. They have been often avoided for real time tasks as they are computationally demanding, especially when the training occurs online, but with the progress in computing power, this limitation is starting to lift. They are often used in timeseries problems such as Economic forecasting, and yield projection [5]. Neural Networks have several advantageous characteristics, such as their ability to fit nonlinear data and their relative immunity to noise.

The architecture of the neural network chosen is Nonlinear Autoregressive Exogenous (NARX). NARX networks are often used for time series analysis. They are recurrent dynamic networks with feedback paths spanning several layers.

$$\hat{y}(t) = f(y(t-1), y(t-2), \dots y(t-n), u(t-1), u(t-2), \dots u(t-m), \qquad (5.7)$$

where $m, n \in \mathbb{N}$,

A NARX system is defined as (5.7), where the predicted value of the output variable $\hat{y}(t)$ depends on previous values of: a) output signal, and b) values of an exogenous signal which does not depend on y, namely $(u(t))$. Neural networks can be used to approximate the function $f(.)$ also allowing a vector implementation of the model with multidimensional inputs and outputs.

The output of the NARX can be considered to be the output of the nonlinear system being modeled. There exists a feedback loop between the output and the input of the feedforward network. But, as the measured output is available during the training of the network, a series- parallel architecture can be used (Fig. 5.11(b)). This means that the measured output can be used directly instead of its estimation.

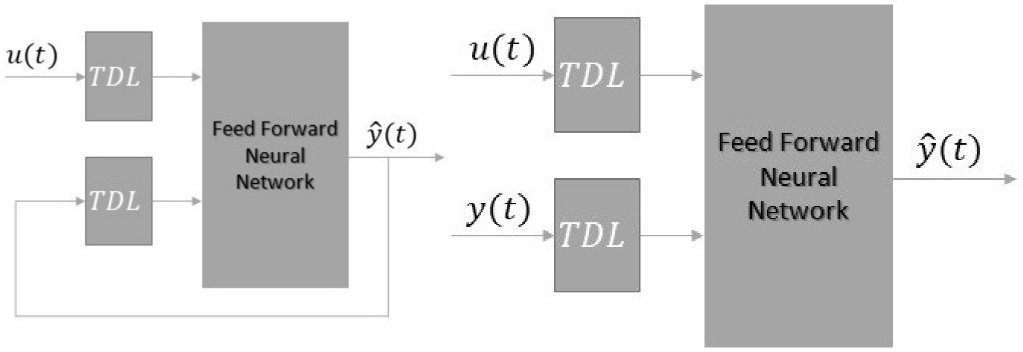

(a) Series Architecture (b) Series- Parallel architecture

Fig. 5.11 Comparison of the architecture of a Series to a Series- Parallel network.

This has two advantages. Firstly, measured data ensures increased accuracy of inputs to the network. The second is that the resulting network has a purely feedforward architecture, which means static backpropagation can be used for training.

5.4.1 Neural Network Training

Similarly to the ARX approach, the initial training occurs offline using a large dataset of the generator during healthy operating conditions Fig. 5.12. This assists with the prediction of the early stages of operation.

The same requirements for adaptation from Section 5.3 are still present here; the time varying essence of the system needs to be considered. This is tackled, in this section, by manipulating the input data training vector.

The question of data sufficiency can be answered by checking the goodness of fit between the predicted data and the acquired data. If the coefficient of determination is sufficient then the data set is large enough; if it is not, the window can be increased for the next instance. If it is sufficient, a moving window can be used. This allows for a sufficiently small data set when a change in the input/output relationship occurs. This is demonstrated diagrammatically in Fig 5.12.

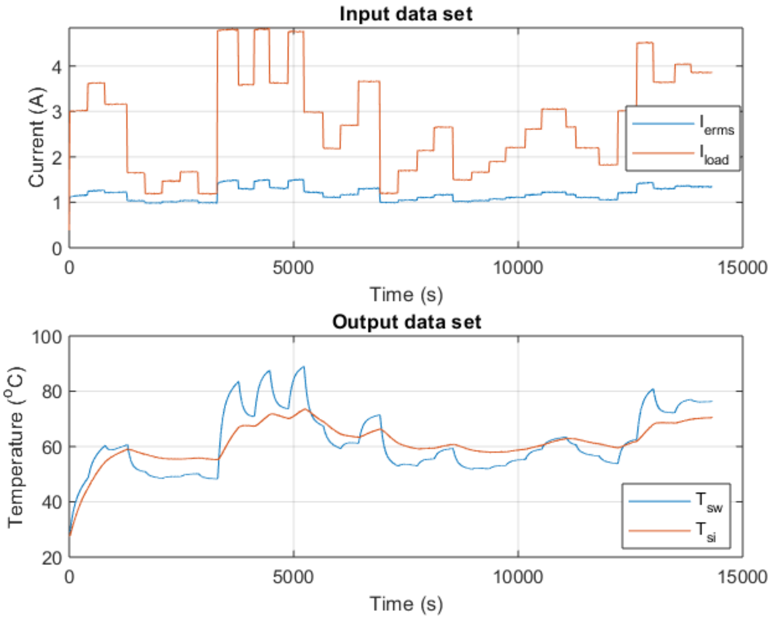

Fig. 5.12 Initial training input and output data.

Training algorithm

The training approach used is Bayesian Regularisation Back-propagation. Bayesian Regularization is a training algorithm that updates the weights and biases according to the Levenberg-Marquardt algorithm (further discussed in the next chapter). The aim is to minimise the terms of sum of squared errors and weights; following that, the appropriate combination that produces a network that generalises the data appropriately is determined. Bayesian Regularization introduces the network weights into the training objective function (5.8).

$$F(\omega) = \alpha E_{\omega} + \beta E_d \tag{5.8}$$

where E_ω is the sum of squared error of network weighs and E_D is the sum of network errors. α and β encompass the objective function parameters. In this framework, the assumption that is made, is that the weights are random variables, hence both the training datasets, and weights can be assumed to be normally distributed. The objective function parameters can be defined using Bayes' rule (5.9).

$$P(A|B) = \frac{P(B|A)P(A)}{P(B)} \tag{5.9}$$

In order to optimise the weighting, the objective function is minimised. This is identical to maximising the probability function as expressed in (5.10).

$$P(\alpha, \beta|D, N) = \frac{P(D|\alpha, \beta, N)P(\alpha, \beta|N)}{P(D|N)} \tag{5.10}$$

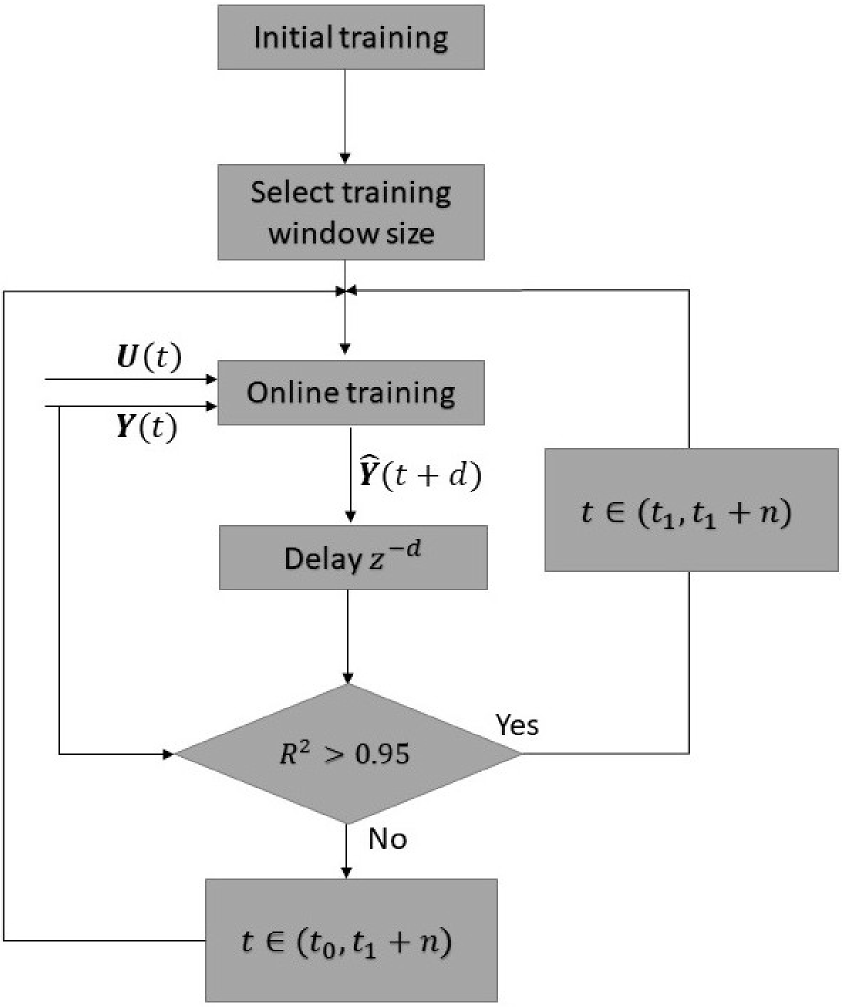

Fig. 5.13 Diagrammatic representation of the choice of window size in an online fashion.

α and β are the objective function parameters that are being optimised, D is the distribution of weights, with N the specific network architecture. $P(D|N)$ is used as a normalisation factor, $P(\alpha,\beta|N)$ the density for the regularisation parameters and $(D|\alpha,\beta,N)$ is the probability of D; given α,β and N. Maximising $P(\alpha,\beta|D,N)$ follows the same process as maximising $P(D|\alpha,\beta,N)$ as they are proportional. Hence, optimal values are calculated for the objective functions for a given weight space. The training process then moves onto the Levenberg-Marquardt (6.5- 6.8) phase where the Hessian matrix is approximated, and the objective function is minimised. In order to ensure convergence, new values for α and β are estimated whenever convergence is not reached.

Activation Transfer function

A Hyperbolic tangent ($tanh(.)$) (5.11) activation function is chosen for this application. When it was compared to the performance of using rectified linear units (ReLU) (6.5), it was shown that it was performing significantly better. ReLU is an excellent activation function for large networks, such as machine vision [66, 91]. Large gradients can cause ReLU neurons to update the weights in a manner that the neuron will never activate again. If this happens, then the gradient flowing through the unit will result to a zero for all inputs.

When considering the current input, large gradients are very common, they occur every time the current changes.

$$\tanh(z) = \frac{e^{z} - e^{-z}}{e^{z} + e^{-z}} \tag{5.11}$$

5.4.2 Predictor Implementation

The ANN based predictor is implemented with an increasing prediction horizon. This is demonstrated in Fig. 5.11, where it can be observed that the prediction error is decreased when compared to the ARX approach in Fig. 5.6. There is less data necessary to adapt the ANN to accurately predict the future winding temperature. The issue that is presented with the ANN approach is the potential discontinuities in prediction between prediction blocks (e.g. $t = 11000s$). These are due to the change of neuron weights between iterations. Tests with prediction horizons ranging from $t = 100s$ to $t = 3000s$ were run with their results showing that the maximum error of prediction before saturation is $3^{o}C$ (excluding discontinuities) but as less information is present the discontinuity between iterations is larger. This is also supported in Fig 5.14 with the curves of d = 1000s and d = 2000s performing similarly.

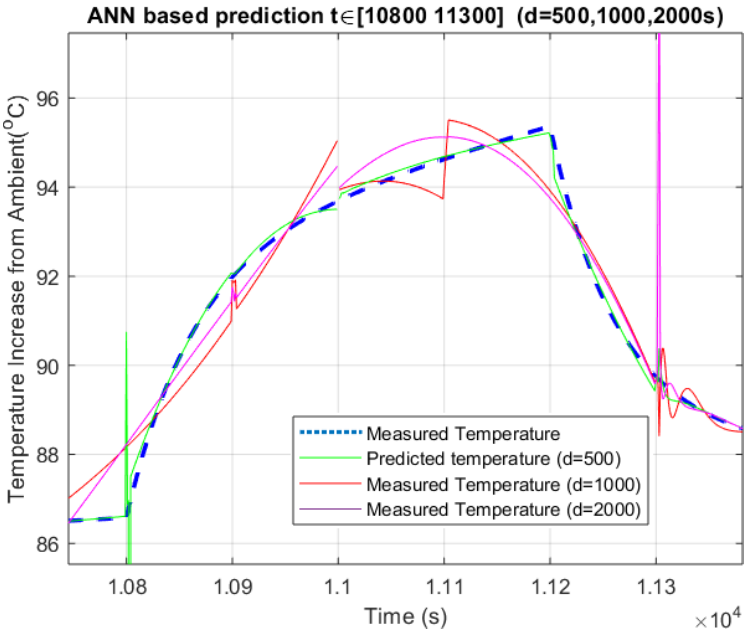

Fig. 5.14 Comparison of measured stator winding temperature to predicted ones, using increasing prediction horizons a neural network approach.

To assess the discontinuities the metric of maximum change of temperature in consecutive steps is also considered ($\Delta\hat{T}(t) = \hat{T}(t) - \hat{T}(t-1)$). It is important for the prediction to be accurate at high temperatures and minimise false reports of overheat due to modelling artifacts. Table 5.1 compares ARX and Neural Networks based on R_T^2 and max $\Delta\hat{T}(t)$. It can be observed that at high prediction horizons, neural networks achieve an increased goodness of fit, but they suffer discontinuities. Adaptive ARX outperform the neural networks in shorter prediction horizons and do not exhibit similar modelling artifacts that may be mistaken for overheats.

Table 5.1 Comparison of Adaptive ARX and Neural Network approaches.

Prediction horizon (d)	Adaptive ARX		Neural Network	
	R_T^2	max $(\Delta\hat{T}(t))$	R_T^2	max $(\Delta\hat{T}(t))$
500	0.985	0.19	0.937	4.6
1000	0.920	0.18	0.681	1.2
2000	0.394	0.19	0.575	11.6

5.5 Conclusion

Implementing the fault in the training process allows for more accurate prediction in the case of an undiagnosed fault. In this chapter, two prediction approaches have been explored, namely Adaptive ARX and Neural Network based prediction. Compared purely based on performance, the ANN based prediction performs significantly better. When softer factors are considered, such as ease of implementation and adjustments, ANNs require more specialist knowledge for troubleshooting. Furthermore, although accurate prediction is important, large prediction horizons are less important. This becomes apparent when considering the larger picture: predicted temperatures are used as a guidance or criterion to adjust the loads. It is often not feasible to make optimal decisions 45 minutes in advance to prevent an overheat. For the aforementioned reasons and due to the computational ease, the Adaptive ARX is the preferred option of prediction for this application.

CHAPTER 6

MODEL-BASED LOAD MANAGEMENT

6.1 Introduction

The purpose of this chapter is to introduce and explore the concept of model-based load management as well as discuss the development of load management techniques. Two techniques are discussed:

1. Inverse modelling load management through linear models (G^{-1}LM) and through neural networks (NNLM).

2. Controller based load management (KGLM).

Their advantages and drawbacks are discussed, as well as their preferred cases of application. They are compared based on: accuracy of load management, size and speed of response, as well as complexity of implementation. Two loading scenarios are explored, both of which have fault and no-fault cases. Firstly, the "realistic load profile" that is based on the k-values and loading during a normal mission, this profile is designed in a way that overheat does not occur under no-fault conditions. The second one is less realistic, introducing more aggressive transients. In this case, overheat occurs both due to overloading and due to potential faults.

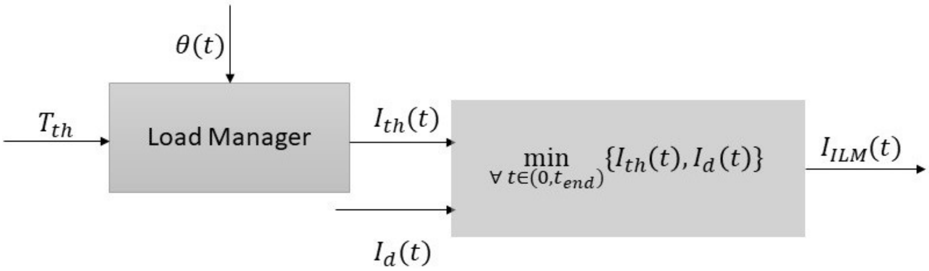

Fig. 6.1 Top level representation of the load management algorithm as considered by one generator in isolation.

Its purpose is to test the adaptive algorithm and the load management in both fault and no-fault conditions.

6.2 Load Management Algorithm

In both techniques the algorithm in which they are integrated is the same. Let T_{th} be the hard threshold temperature when the thermal fuse takes action isolating the generator. This temperature can not be exceeded. A steady state of the threshold temperature corresponds to a set magnitude of current, named threshold current (I_{th}). It can be assumed that if $I_{load}(t) > I_{th}$ an overheat is imminent and hence action needs to be taken. For safety to be ensured, the current being drawn cannot exceed $I_{th}(t)$.

It should be mentioned that although the threshold temperature is a constant (for each instance of the algorithm), the threshold current is not. $I_{th}(t)$ greatly depends on the description of the system at hand, so if the system varies, so may the threshold current. This is especially important in a time varying system such as the one at hand.

Figure 6.1 shows a top-level schematic representation of the algorithm for a single system of interest. The difference between techniques is what populates the "load manager" box and how $I_{th}(t)$ is extracted.

It is after the load manager provides a threshold current, $I_{th}(t)$ is compared to the current demand from the flight profile. Under normal operation, $I_{th}(t)$ should exceed $I_d(t) = I_{load}(t)$ as no overheat should be present. When the derived threshold current is exceeded, it is assumed that an overheat is imminent and only load drawing up to $I_{th}(t)$ is allowed. In a multi-generator system, remaining load $I_d(t) - I_{th}(t)$, assuming it is non-negative, is added onto the load profile of the next generator and the same procedure is repeated sequentially, this is shown in section 7.2.

Formally the minimisation is defined as follows in (6.1). It states that the suggested load management current $I_{ilm}(t)$ is the minimum of the load current $I_{load}(t)$ and the extracted threshold current $I_{th}(t)$.

$$I_{ilm}(t) = \min_{\forall t \in (0, t_{end})} [I_d(t), I_{th}(t)] \tag{6.1}$$

6.3 Inverse Modelling Load Management

The inverse modelling method $(G^{-1}LM)$ builds upon the ideas explored in Ch. 4 and Ch. 5. A black box modelling approach is used, where a temperature to current model is created. Estimating this model directly through online linear system identification (as in Ch. 5) is difficult due to the lack of an autoregressive link in the output $(I(t))$; future currents do not depend on past currents, resulting to low R_T^2.

Two approaches have been developed under the inverse modelling.

- Firstly, using the recursive estimation of the temperature to current relationship, assuming the model is invertible, the already estimated parameters of the temperature predictor can be used for creating a difference equation that takes temperatures as inputs and produces current as an output.
- Secondly, a feed-forward time delay neural network model (TDNN) can be created if the current and temperature are manipulated temporally. This approach circumvents the need for an actual predictor, although using one is still advisory.

As this is a feed-forward system, it is highly sensitive to noise; hence the inputs to it need to be noiseless (i.e. not measurements).

Figures 6.2 and 6.3 demonstrate the effectiveness of $G^{-1}LM$ for limiting the temperature, below the pre-set threshold (80°C above the ambient).

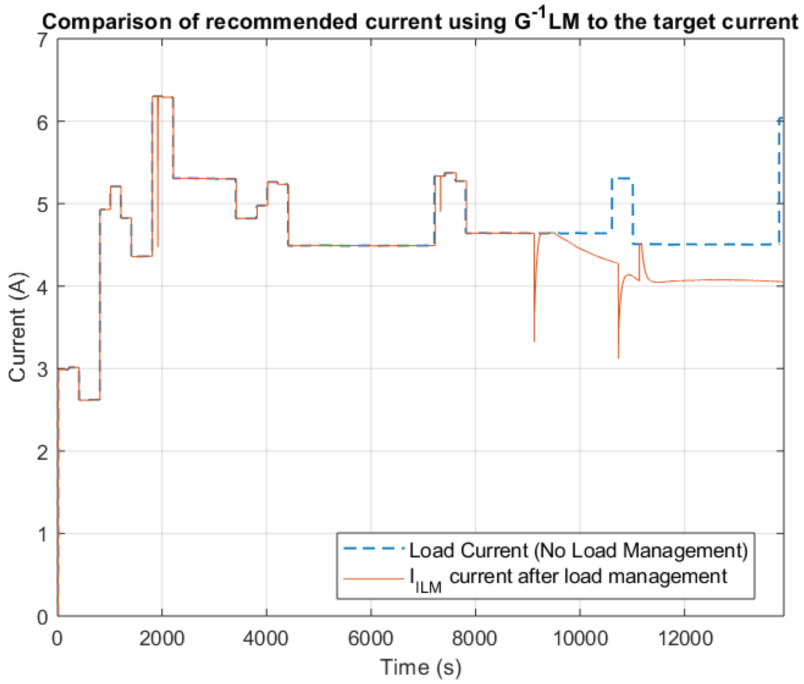

Fig. 6.2 Recommended current $I_{ILM}(t)$ as compared to the initial target load current.

6.3.1 Assessment of *G*$^{-1}$ LM

Three criteria are considered in order to assess the quality of the load management. The first metric used is the charge lost due to load management (6.2). This is defined as the difference of integrals between the realised current I_{ILM} and the initially demanded current (I_{Load}).

(I_{ILM}) is best defined in (6.3) and by using that definition it is ensured that the difference between I_{ILM} and I_{Load} at each time step is non-negative.

$$C_1 = \int_{t_0}^{t_{end}} [I_{ILM}(t) - I_{load}(t)]dt \tag{6.2}$$

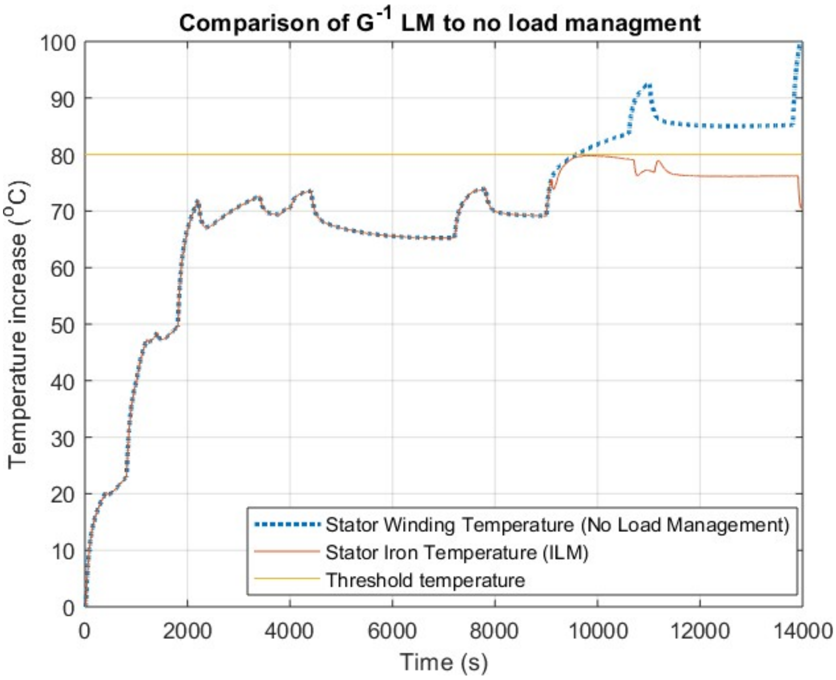

Fig. 6.3 Resulting temperature post load management compared to the temperature of the windings without load management present.

The second metric is the temperature steady state difference from the threshold (post ILM); theoretically the current is allowed to be slightly higher, as the resulting temperature is below the threshold. The third criterion is the maximum instantaneous current dip, i.e. how much of the current is to be reduced in consecutive timesteps; this shows the feasibility of adaptation of such profile.

The calculated threshold current is very sensitive to the change of the parameter vector $\boldsymbol{\theta}(t)$. Therefore, large change in the input, such as the one observed between $t \in [1800, 2200]$ in Fig. 6.2, can cause a dip in the recommended current. This has minimal effect to the change in temperature, but if the recommended current is followed at all times, such a dip is difficult to achieve; it does not affect the current and it rebounds to the initial value in a span of 15 timesteps.

As such, the minimisation should have a temperature criterion as well. It is defined as follows in (6.3). It states that the suggested load management current $I_{ILM}(t)$ is the minimum of the load current $I_{load}(t)$ and the extracted threshold current ($I_{th}\,(t)$), as in (6.1). This minimisation occurs for all time steps of the mission, while the predicted temperature ($\hat{T}_{sw}(t)$) exceeds the threshold temperature $T_{th}(t)$. The temperature clause, although may seem superfluous, is added in order to ensure that large transient currents do not influence the output. This situation is more prevalent in the inverse modelling approach due to the larger sensitivity to the parameter vector.

$$I_{ILM}(t) = \min_{\forall t \in (0, t_{end}) | \hat{T}_{sw}(t) > T_{th}(t)} [I_{load}(t), I_{th}(t)] \tag{6.3}$$

Table 6.1 Assessment criteria for the considered scenarios using $\mathbf{G}^{-1}LM$

Scenario	$\int \Delta I dt\ (C)$	$\Delta T\ (^{o}C)$	max dI dip (A)
No Fault in realistic	43.1	-1.1	-1.04 (t=13950)
Fault in realistic	1920	-3.8	-2.19 (t=10715)
No Fault aggressive overcurrent	588	-3	-0.8 (t=12950)
Fault aggressive overcurrent	4440	-12	-3.75 (t=12030)

Three criteria are used for assessment of the load management strategies they assess performance, accuracy, and safety. They are as follows: $\int \Delta I dt$, which signifies total charge loss due to the ILM – this metric aims to assess the loss of system efficiency due to the ILM intervention. ΔT is the maximum temperature difference between actual and desired temperature - it aims to assess the accuracy of the correction of ILM – a perfect correction has a $\Delta T = 0$. Lastly, max dI dip assesses the maximum size of a spike in current that is caused due to load management, subjecting avionic subsystems to large current dips and spikes may cause electronic failures. From Table 6.1 it can be observed that the inverse modelling feed forward approach performs very well in the no fault scenarios. The reason is the small $\nabla\boldsymbol{\theta}$ and the lack of need for adaptation. The system remains largely the same hence the parameters do not need to change. As it is a feed forward system it is sensitive to parameter change. This is reinforced by identifying when the maximum current dip occurs. In all cases it occurs very close to a large change in current, which implies a change in parameters. This is accentuated when this change in current is accompanied by new temperatures due to fault or other disturbances.

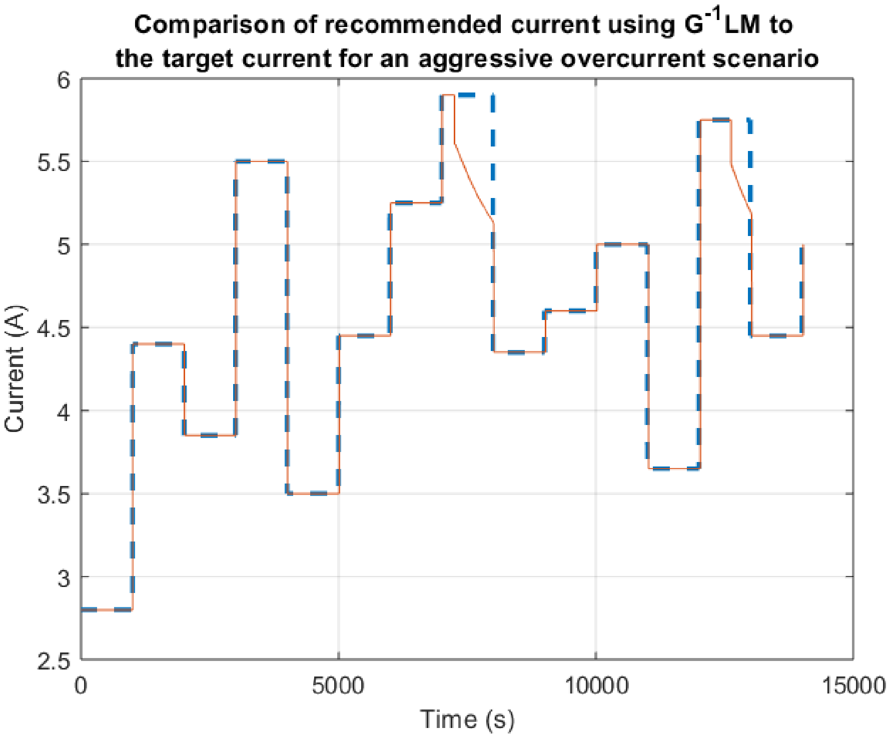

Fig. 6.4 Comparison between I_{Load} and I_{ILM} in the aggressive transient scenario with no faults present.

This is most clearly supported by the 3rd scenario shown in Figs. 6.4 and 6.5. Scenarios where a large current dip occurs suggest against using this approach, as the recommended action is too extreme for it to be implemented.

Overall, this approach gives a system that works best under normal operation, but it struggles with quick change of $\boldsymbol{\theta}(t)$. It provides a working baseline with the requirement to decrease the current dips.

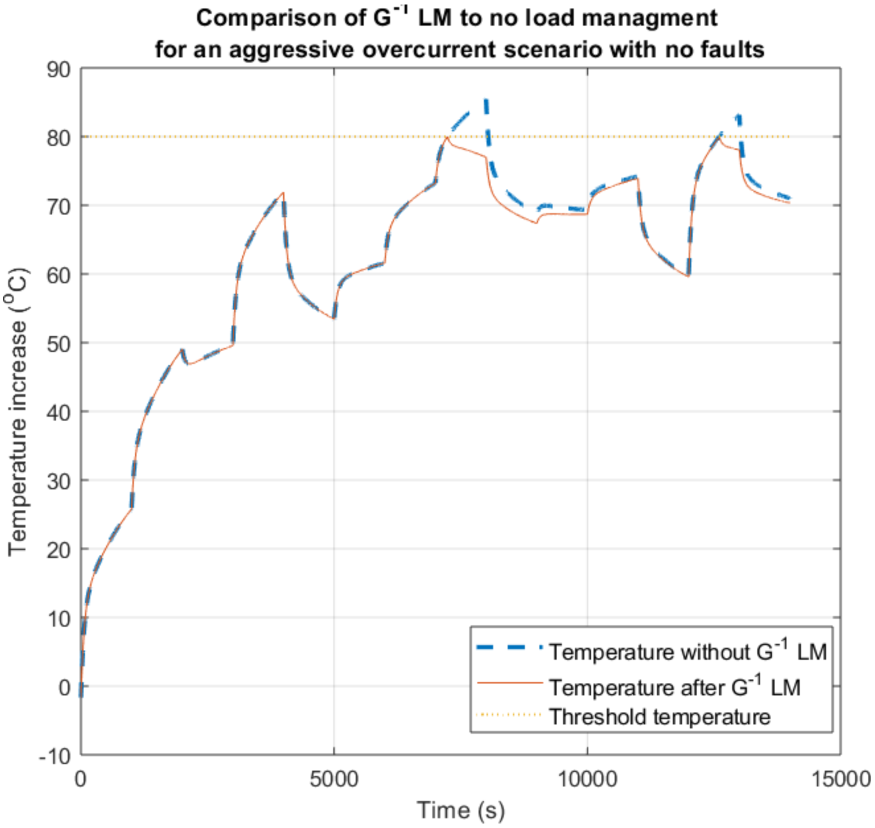

Fig. 6.5 Comparison of resulting temperatures after inverse modelling load management for the aggressive transient no-fault scenario.

6.3.2 Neural Network Based Load Management (NNLM)

The approach of a dynamic neural network can be employed for managing the threshold current. It provides a nonlinear approach that does not necessarily require an associated predictive model to operate. In this case, the temperature measurements are directly related to currents, without feedback or auto regression of such currents. Although initially attempted, autoregressive feedback led to overtraining of the model and worse results in the fault scenarios.

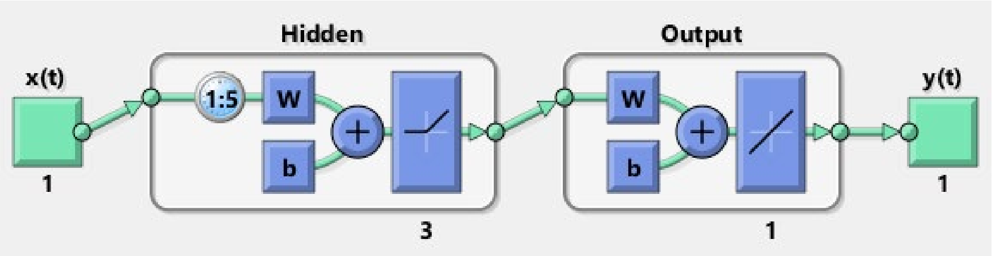

Fig. 6.6 Architecture of the feed-forward network using ReLU for the hidden layer activation function and linear for the output layer.

The model at hand is still adaptive, as it updates online using new measurements in order to improve the estimation of the current. Due to the higher computational demand, this adaptation does not occur at each time step, but each 50 timesteps (this is subject to the processing power). Although not strictly required, more accurate outputs are produced when future predicted values of the temperature are utilised as training data. Therefore the training data set can be defined in (6.4), whilst the load profile is used as the target data.

$$u_{train} = \begin{cases} T_{sw}(t), & if \ \ t < 0 \\ \widehat{T}_{sw}(t), & otherwise \end{cases} \tag{6.4}$$

The network comprises of three parts: a delayed input layer, where the temperatures are used as inputs, three hidden layers necessary for capturing nonlinear dynamics and an output layer. The architecture of the network is shown in Fig. 6.6.

The hidden layers utilise a Rectified Linear Unit activation function (ReLU) as defined in (6.5). It has been shown that ReLU trains faster than $tanh(.)$ and sigmoids without compromising accuracy. ReLU activation function is used instead of a purely linear activation function to add nonlinearity to the network and its estimations. As this is a real time operation the speed of ReLU assists in the online estimation.

$$ReLu(t) = \begin{cases} x, & if\ \ t < 0 \\ 0, & otherwise \end{cases} \tag{6.5}$$

The training method chosen is the Levenberg-Marquardt algorithm. This algorithm also provides high speeds as it does not compute the Hessian matrix; instead an approximation is done using the Jacobian (6.6), under the assumption of the performance function being a sum of squares.

$$\boldsymbol{H} = \boldsymbol{J}^T\boldsymbol{J} \tag{6.6}$$

with the gradient

$$\boldsymbol{g} = \boldsymbol{J}^T\boldsymbol{e} \tag{6.7}$$

where $\boldsymbol{H}$ is the Hessian approximation, $\boldsymbol{J}$ is the Jacobian matrix that contains derivatives of the network residuals with respect to the corresponding biases and weights, and $\boldsymbol{e}$ is a vector of network errors. The Hessian matrix is then used in an iterative, Newton-Raphson-like method.

$$\boldsymbol{x}_{k+1} = \boldsymbol{x}_k + [\boldsymbol{J}^T\boldsymbol{J} + \mu\boldsymbol{I}]\boldsymbol{J}^T\boldsymbol{e} \tag{6.8}$$

For μ equal to zero, (6.8) is identical to the iterative Newton-Raphson method. When μ is large, this method is just a steepest descent algorithm with a small step size. Newton-Raphson has increased accuracy and iteration speed when approaching a minimum error, hence the aim is to ensure that this method is reached after minimal iterations. After each successful iteration, μ is decreased. This results to iteratively minimising the function.

Table 6.2 Assessment criteria for the considered scenarios using NNLM.

Scenario	$\int \Delta I dt\ (C)$	$\Delta T\ (^{o}C)$	max dI dip (A)
No Fault in realistic	203	-0.5	0
Fault in realistic	2800	-1.8	0
No Fault aggressive over-current	233	-4	0.1
Fault aggressive overcurrent	3510	-8	-0.7

As it can be observed from Table 6.2, the time delay neural network yields similar results when it comes to charge loss compared to the linear ARX method. Where it excels though, is on the feasibility and ease of implementation, i.e. the current overshoot transients. The recommended currents are provided in an extremely discretised format with no fluctuation. This can allow the user to just shed a set amount of load once without the need to manage it continuously. The performance of this approach can be ameliorated by increasing the adaptation rate or adding more inputs or delays. An example of this method is shown in Figs. 6.7 and 6.8.

6.4 Controller Based Load Management (KGLM)

Feedback systems are more robust and less sensitive to disturbances in the parameter vector. A closed loop system, where the time variable transfer function $G(\boldsymbol{\theta}|t)$ which describes the generator is used as a plant, is employed in order to decrease the size of current dips in scenarios where a fault is present, i.e. highly variable $\boldsymbol{\theta}$. A controller is used in series with the plant and the output of the controller is extracted. The input of such controller is the threshold temperature; hence the controller strives to bring the system to this threshold temperature.

A top-level representation of the load management system is portrayed in Fig. 6.9. Let $I(t)$ and $T(t)$ be the measured current and temperature signals from the generator (at time t). They are used in a system identification algorithm to calculate a set of parameters $\boldsymbol{\theta}$ describing a linear system $G(\widehat{\boldsymbol{\theta}}|t)$ at each time step. A future desired current $\hat{I}(t+d)$ is fed into $G(\widehat{\boldsymbol{\theta}}|t)$ to produce a future temperature $\hat{T}(t+d)$. Meanwhile, a $G(\widehat{\boldsymbol{\theta}}|t)$ is also used in a control loop that provides information required to prevent overheating. Let $T_{th}(t+d)$ be a the desired output signal, $I_{th}(t+d)$ be the controller output and input of $G(\widehat{\boldsymbol{\theta}}|t)$, which in turn provides an output $\hat{T}_{th}(t+d)$, the difference between $T_{th}(t+d)$and $\hat{T}_{th}(t+d)$ is defined as an error signal $e_{T_{th}}$. It should be noted that the prediction algorithm is not depicted in Fig. 6.9 for the sake of space, more information on that can be found in Ch. 4 and 5.

The static linear models discussed in Ch. 4 are used as a basis for controller design. The purpose of the controller is to provide a current demand signal that makes the generator reach its threshold temperature.

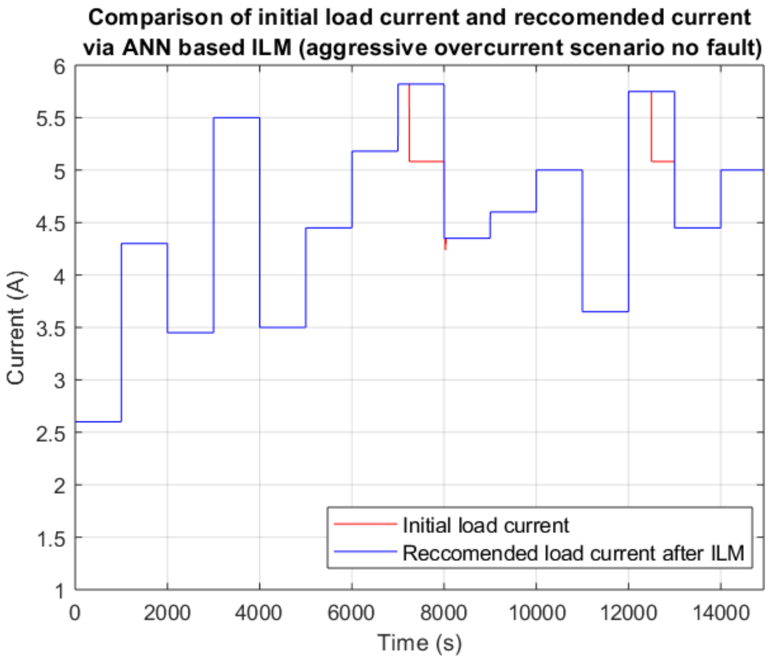

Fig. 6.7 Demonstration of the ANN based load management limiting the load current in the no-fault aggressive over-current scenario.

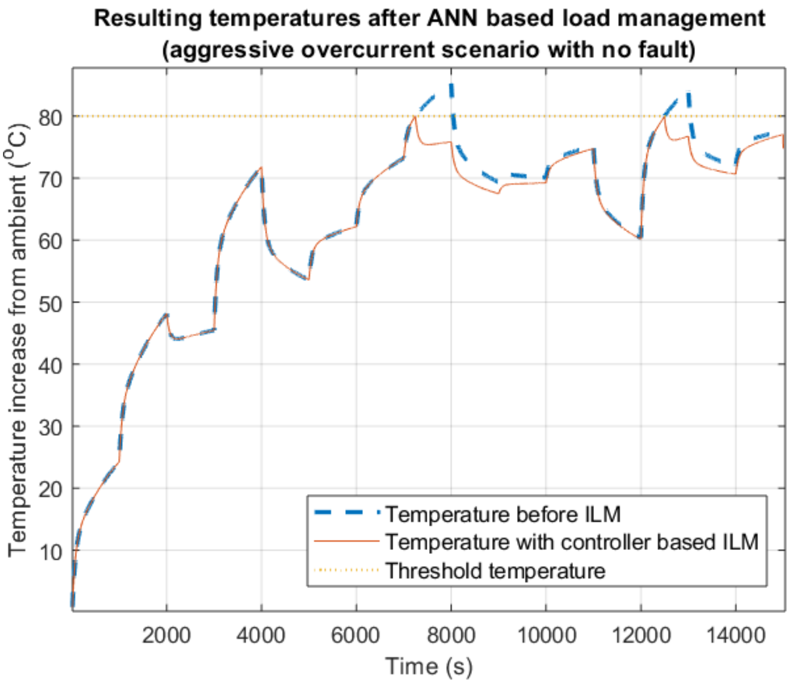

Fig. 6.8 Resultant temperatures with and without the load management has been implemented.

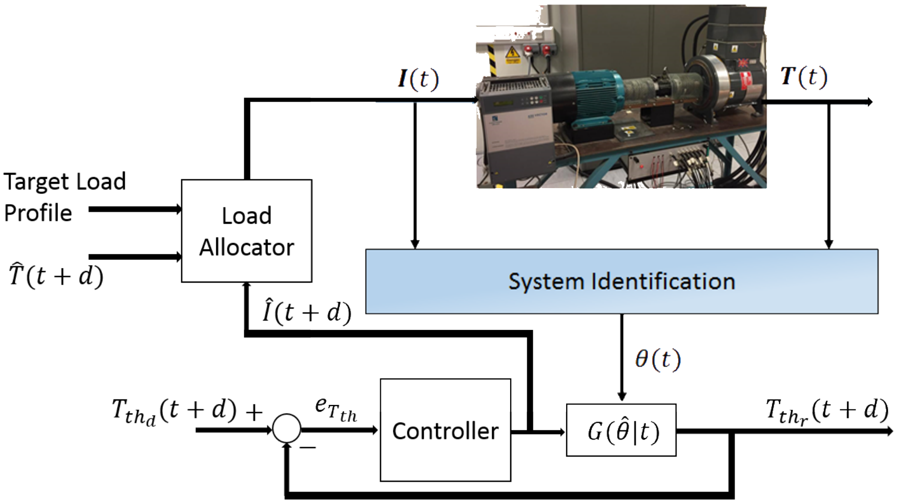

Fig. 6.9 Top level representation of the load management algorithm as considered by one generator in isolation.

6.5 Establishing Controller Requirements

The minimum and maximum requirements of the controller can be estimated by using the time response of the time-invariant linear transfer function $G(\widehat{\boldsymbol{\theta}})$. The reader should be reminded that the linear model is tuned for a specific range of current responses, hence for using this model an assumption needs to be made: the linear model describes the system adequately for such responses.

It is also assumed that the relevant use of this controller is as a means to a cooling down action, therefore oscillations are only relevant at the bottom part of the response.

Since the controller provides information of the future current $\hat{I}(t+d)$ and how such current should fluctuate to avoid overheat, its characteristics should be expressed as a function of the prediction horizon d. It should be noted that there is a minimum time-advance (d_0) that the control action is useful for. This time advance is based on the forced cooling time of the machine, i.e. the time needed for the temperature to decrease after the load is switched off. Action after that point would not be sufficient to prevent the overheat. This estimation of d_0 can be assumed to be aggressive since a healthy generator in laboratory condition is used for its estimation.

For consistency, a set of specifications are hereby established. The closed loop system's temperature is not to exceed the threshold temperature. It is assumed that the threshold temperature is the point at which the thermo-mechanical fuse trips the generator offline. It should be noted that the threshold can be lowered and treated as a soft limit, but that would lower the efficiency of the overall system as action would be taken in unnecessary situations, too. Another requirement is the first current oscillation not exceeding 15% of the initial desired value (whichever is smaller in terms of magnitude). This limitation is set, so that the load management is performed in a smooth manner and the need for repetition is lowered.

6.5.1 Controller Design

For this application, a proportional plus integral controller is chosen. The main reason is the simplicity of design and ease of implementation and it is used as a proof of concept for this algorithm.

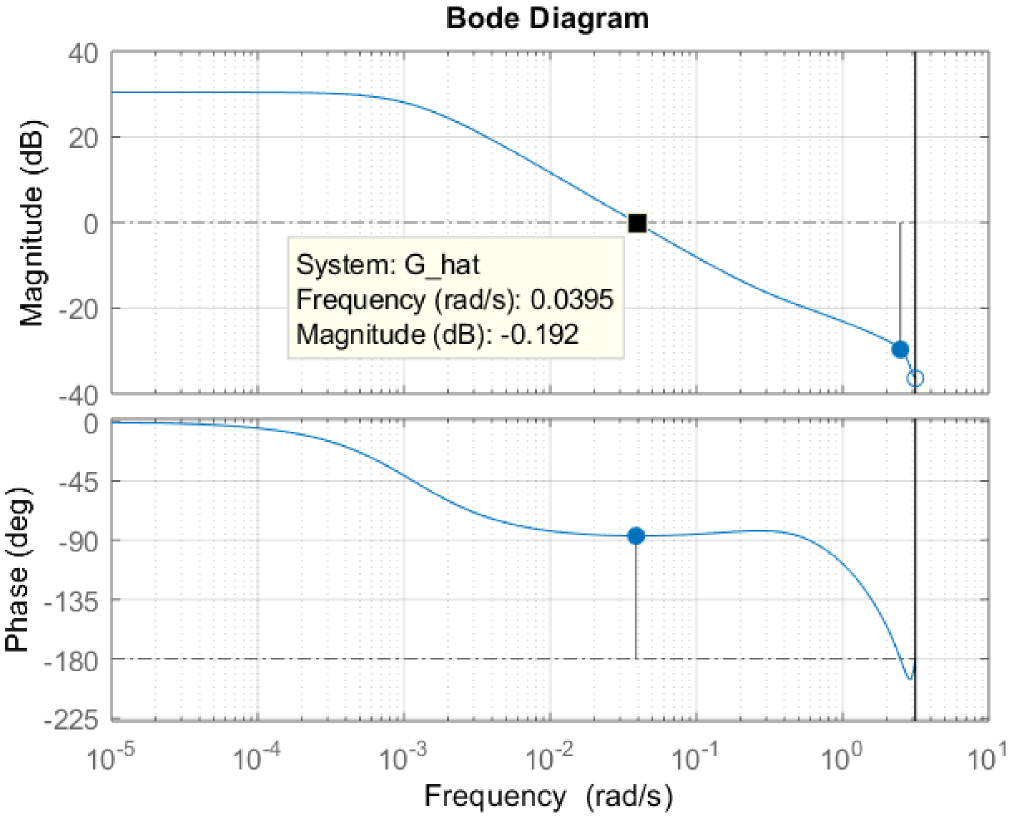

Fig. 6.10 Bode plot of $\hat{G}$.

The requirements of the controller change based on when action can be taken. If a large prediction horizon is employed action can be taken in advance, hence there can be smoother controller action (which implies the ability of gradually shedding loads). Vice versa, small prediction horizons imply an aggressive controller action, where a larger immediate load shedding is necessary. The manner this tradeoff is dealt with, is discussed in the following subsection (6.5.2).

The requirements are no overshoot, minimal steady state error and a rise time that matches the prediction horizon, whilst the phase margin does not exceed 90^o.

The controller is designed offline and hence a static model designed in Ch. 4 is used. Firstly, the system is analysed in the frequency domain and key parameters are identified as shown in Fig. 6.10.

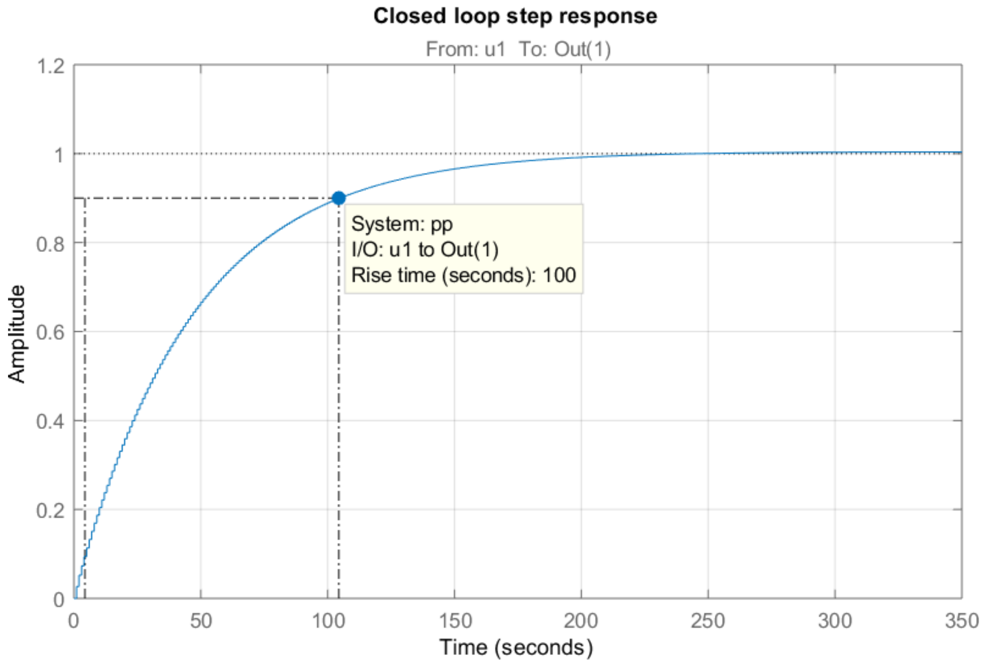

Fig. 6.11 Step response of $K\hat{G}/\ (1+K\hat{G})$.

The proportional gain is introduced in order to find the maximum allowable gain that does not violate the 90^o phase margin requirement. Then a small integral action is employed based on the crossover frequency $(0.061\ rad/s)$. The proportional action is modified in order to ensure that the phase margin and rise time criteria are met for the specific prediction horizon chosen.

This is demonstrated in the Fig 6.11 and 6.12 for a prediction horizon and rise time of 100 seconds. Fig 6.11 shows the rise time of the closed loop with a PI controller with proportional gain $P = 0.358$ and integral gain $I = 0.0005$, the rise time is 100s which matches the prediction horizon. Fig 6.12 compares the compensated $K\hat{G}$ to the plant $\hat{G}$ and highlights that the phase margin requirement is not breached when the compensator is added. The same procedure can be repeated for any rise time chosen.

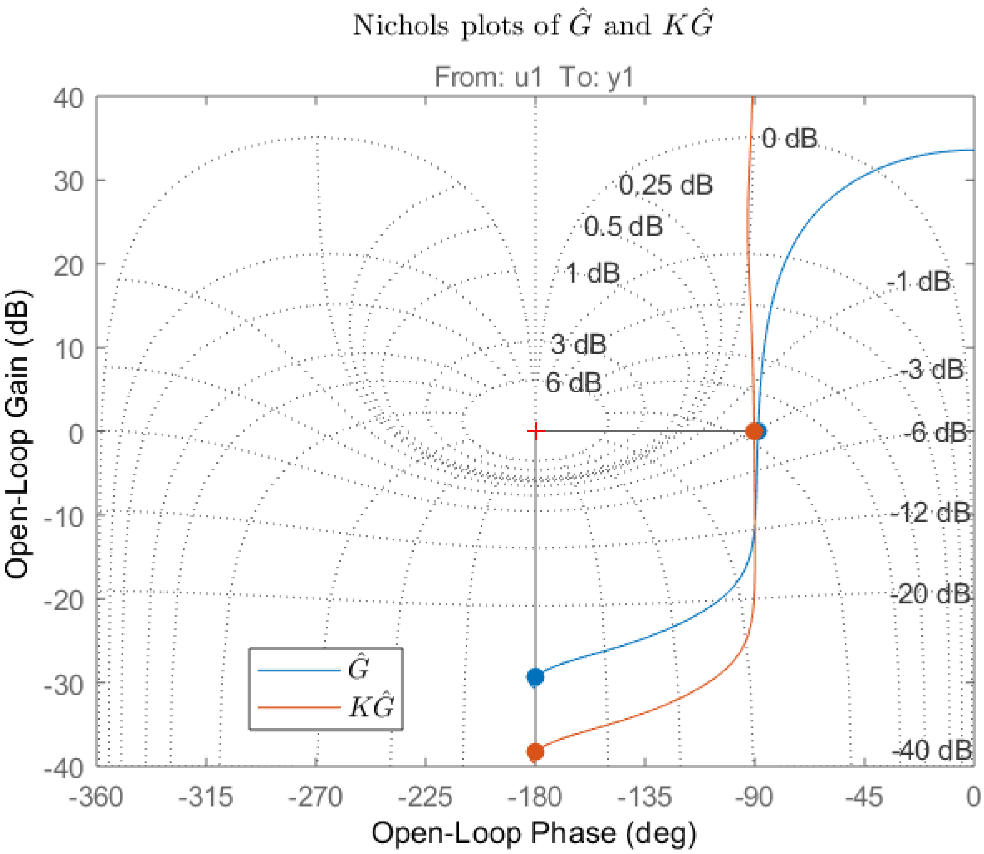

Fig. 6.12 Nichols plot of $K\hat{G}$.

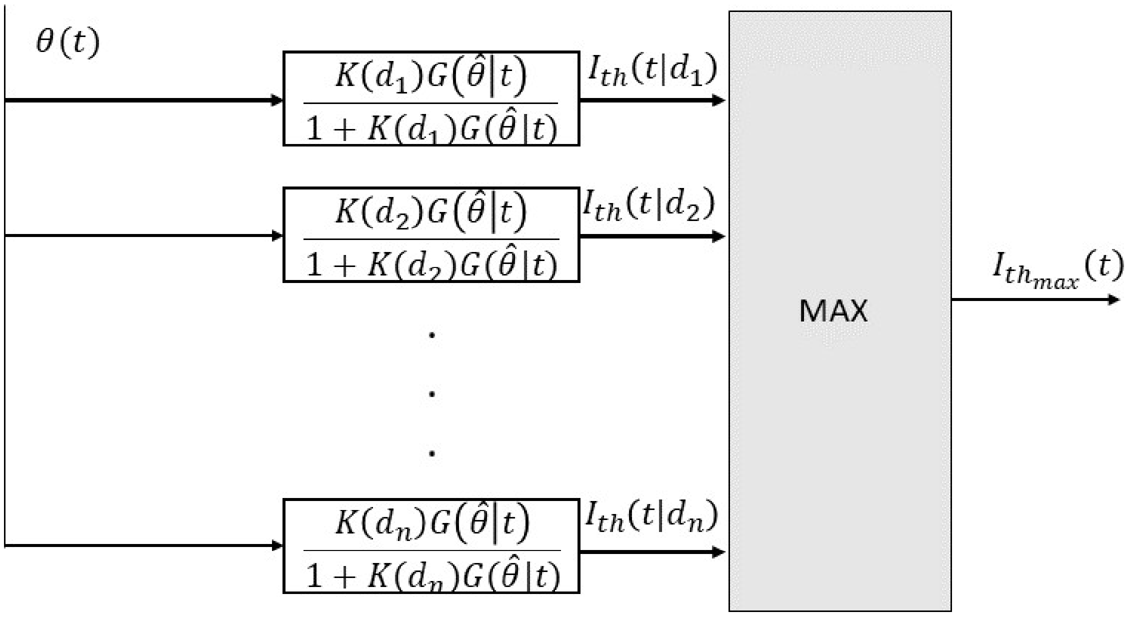

Fig. 6.13 Pictorial representation of the controller bank.

6.5.2 Controller Bank

An advantage of the controller based load management is that several instances of the prediction model $\hat{G}(\boldsymbol{\theta}|t)$ can be used by being coupled with different controllers. It should be kept in mind that the rise time of the closed loop system is linked to the prediction horizon of the estimation. By using this information, actions of different speed can be examined simultaneously and the most applicable can be chosen at each time step. The same minimisation function as previously (6.3) is used for deriving $I_{ILM}(t)$ in this case though $I_{th}(t)$ is the maximum permitted current of all the instances (6.9).

$$\max_{\forall t \in (0, t_{end})} \{I_{th}(t, d = d_1), I_{th}(t, d = d_2) \ldots I_{th}(t, d = d_n)\} \tag{6.9}$$

This is also shown pictorially in Fig 6.13.

In section 5.4, the way the increased prediction horizon affects maximum error of prediction was discussed. Since the same $\widehat{\boldsymbol{\theta}}(t)$ parameters are used, it is expected that there will be an overshoot equal to the magnitude of the error for that prediction horizon.

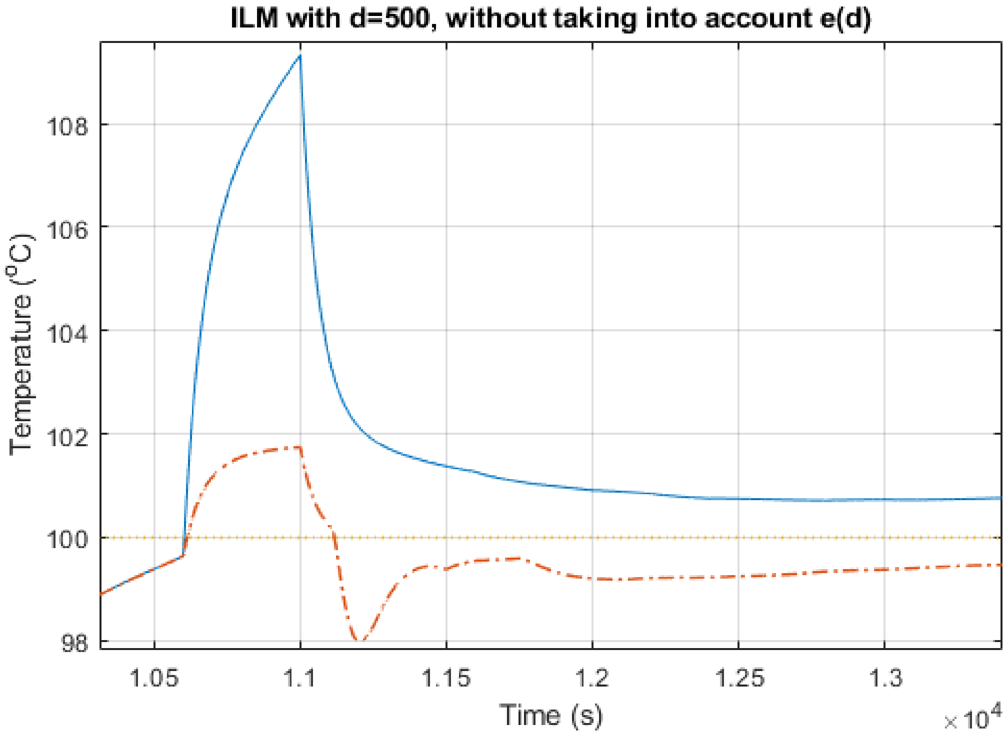

Fig. 6.14 Resultant temperature after ILM action with a prediction of 500s ahead.

Figure 6.14 demonstrates an example of overshoot, with a 500 second predictor. As it was established from Fig. 5.7, a 500s prediction is coupled with an error of approximately $2^{o}C$.

This overshoot can be reprimanded by biasing the threshold temperature in the control loop by the expected error from the $e(d)$ graph. This results to a steady state error instead, as per Fig. 6.15.

The trade-off that is to be considered is the prediction horizon resultant error versus the amplitude of the input signal, i.e. the suggested current. Since ILM is not an automated process and needs user approval, time should be allocated for such approval. This places extra importance on the large prediction horizon.

The alternative is using several predictors with different horizons. With an increasing prediction horizon, large prediction horizons allow early action to be taken. As it was pre-stated, the controllers are tuned to have rise time equal to the prediction horizon, this makes the smaller prediction horizon controllers compensate for the remaining load management.

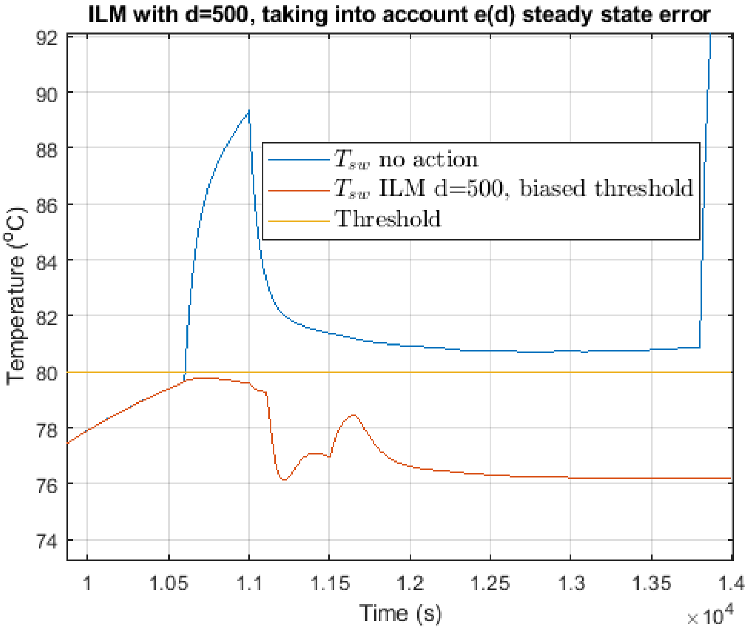

Fig. 6.15 Resultant temperature after ILM action with a prediction of 500s ahead after taking into account the expected error.

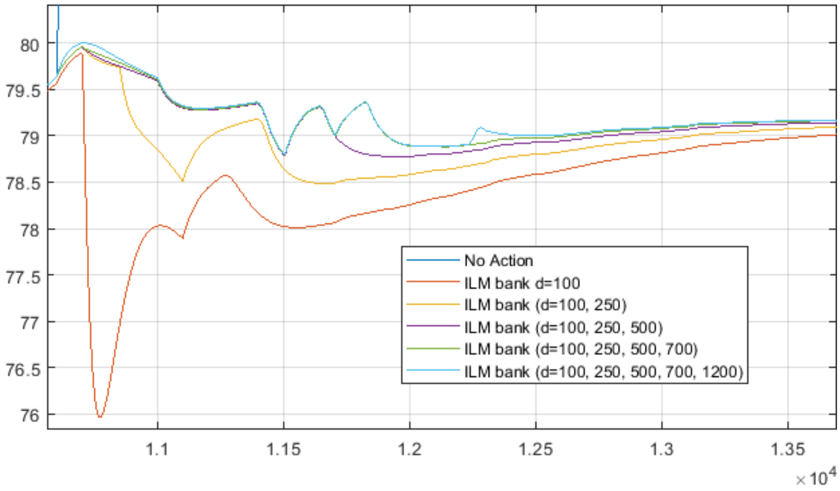

Fig. 6.16 Resulting temperature after using ILM with bank of controllers of increasing size.

Using a bank of controllers is demonstrated in Fig. 6.16, where predictors with larger horizons are added sequentially and the resulting temperature is examined.

As it can be observed, the bank with predictors ranging from 100s to 1200s has a gentler temperature decrease and its steady state error is 0.8 °C. The suggested load currents are presented in Fig. 6.17. An argument on diminishing returns can be made when adding increasing number of controllers. Having two controllers, one with high prediction horizon and one with low, could suffice, if both predictors detect the overheat. As an example, if the overheat is to occur 900s after the fault, then the predictor of 1200s is unable to detect it. The number of controllers chosen and the appropriate horizons are ultimately up to the designer and the complexity allowed by hardware limitations.

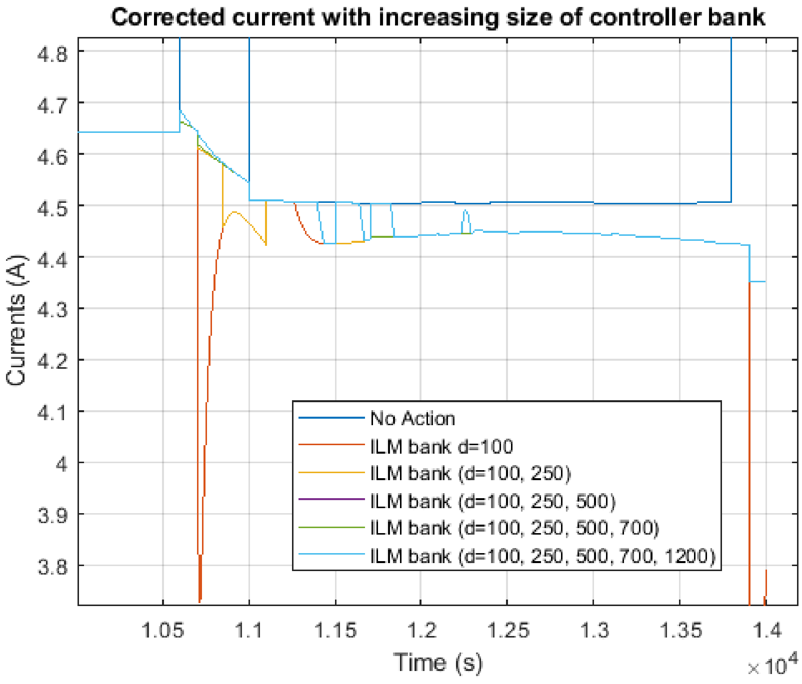

Fig. 6.17 Currents suggested by the ILM using an increasing size controller bank.

6.5.3 Assessment of Feedback Controller Method

Using the same criteria as when assessing the inverse modeling approach, Table 6.3 can be constructed.

Table 6.3 Assessment criteria for the considered scenarios using a controller bank.

Case	$\int \Delta I dt$ (C)	ΔT (^oC)	max dI dip (A)
No Fault in realistic	222	-0.85	-0.12
Fault in realistic	1840	-3.8	-0.49
No Fault aggressive overcurrent	279	-0.5	-0.05
Fault aggressive overcurrent	3810	-8	-0.7

The main requirement for using this feedback approach was to minimize the current dips post load management. This is achieved by using the aforementioned controller bank. The results from the Table 6.3 further support this, performing particularly better in the fault scenarios by having a gradual current decrease with no intense spikes. Changes in the parameter vector $\boldsymbol{\theta}(t)$ still affect the steady state temperature after faults occur (last case in the table). It is possible that higher efficiency can be achieved with either more, or better controllers. This simple, and limited approach is chosen in order to ensure low computational effort to ensure real time running.

Table 6.4 summarises the results shown in Tables 6.1 – 6.3. It can be observed that due to it being open loop $G^{-1}LM$ is inferior to the other two approaches especially due to its large steady state error. That suggests that the ILM correction was not optimal. NNLM and the controller bank approach perform overall similarly. NNLM has a slight edge on the performance in the aggressive overcurrent scenarios, but KGLM performed better in the realistic profiles with a fault occurrence; without significantly compromising the performance when a fault does not occur.

6.6 Comparison of Load Management Methods

A metric driven insight on the pros, cons and applicability of each method is provided in Tables 6.1, 6.2 and 6.3. It can be deduced that the ARX inverse load management only provides comparable results in the no-fault scenarios. Changes in the parameter vector increases the error, as there is no feedback loop. The advantage of this method lies on the simplicity of the design and ease of implementation. Assuming an autoregressive exogenous model that links current to temperature exists, inverting that model is all that is required. This procedure would be identical regardless of the machine at hand, as long as a linear model is sufficient for temperature prediction. This can save valuable time in an industrial setting.

The time delay feed forward neural network expands on the inverse modelling idea but does not utilise a pre-existing model. The network is trained directly for current estimation from the data gathered. Depending on which minimisation function is used (6.1) or (6.3) a prediction model might not be necessary at all.

That said, the existence of an accurate temperature prediction model greatly assists when there is a lack of input data; so although not necessary, a temperature prediction model is encouraged. The neural network approach is the most versatile one, as it does not require linear models. The generator used for this project is a constant speed machine and assumptions regarding their losses can be made (Ch. 4) in order to linearise them.

Table 6.4 Summary of performance of different load management algorithms.

Case	$\mathbf{G}^{-1}LM$ (Inverse model)			NNLM (Neural network)			KGLM (controller bank)		
	$\int \Delta I dt$	ΔT	max dI dip	$\int \Delta I dt$	ΔT	max dI dip	$\int \Delta I dt$	ΔT	max dI dip
No Fault in realistic	43.1	-1.1	-1.04	203	-0.5	0	222	-0.85	-0.12
Fault in realistic	1920	-3.8	-2.19	2800	-1.8	0	1840	-3.8	-0.49
No Fault aggressive overcurrent	588	-3	-0.8	233	-4	0.1	279	-0.5	-0.05
Fault aggressive overcurrent	4440	-12	-3.75	3510	-8	-0.7	3810	-8	-0.7

Variable speed machines have variable iron losses that need to be taken into account at all times. Addition of extra inputs is effortless with this approach. On the other hand, the tuning and implementation can be difficult as some prior knowledge is required. The user needs to avoid common pitfalls such as over-fitting, under-fitting or other data related issues, when designing such network. There needs to be some understanding regarding activation functions and which function is preferred for the application at hand; ReLU is most likely applicable in all these situations. It should be noted that the recommended ILM currents are the easiest ones to implement in a real scenario, as they are discrete and largely constant.

The controller based approach performs equally well as the neural network based ILM on the aforementioned metrics of Tables 6.1 - 6.3. Similarly to the ANN approach, some prior knowledge of controller design is necessary. The controllers need to be tuned by having certain specifications in mind, such as the lack of overshoot and the fast rise time. In this body of work it was demonstrated that a PI controller is sufficient, but more accurate and robust controllers can be utilised instead. The current response is not as "clean" as the one produced by the ANN approach, but there is minimal overshoot and can still be implemented. The unique advantage of this approach is that different instances of the models can be used in parallel and decisions can be made based on the responses of such instances.

In order to choose the appropriate methods to be employed, two main questions should be answered first:

- When/ why do overheats occur? If faults that can cause overheat are extremely rare, the designer could use the $G^{-1}LM$ARX approach to deal with mostly potential overloading issues. If faults are likely to occur though, a more robust technique should be used.

- What machine is there at hand? If the generator at hand cannot be described accurately with linear models, then the techniques that rely on them cannot be used.

6.7 Conclusion

In this chapter, different load management techniques have been demonstrated and compared against pre-set metrics that gauged the effectiveness and applicability of such methods. Softer factors such as ease of implementation and design were also considered, as well as prerequisite knowledge of the field. Therefore, it has been concluded that a controller-based load management is the preferred approach for a constant speed constant frequency machine. The relative ease and transparency of design as well as the good performance make $KGLM$ the preferred load management technique for the generator at hand.

CHAPTER 7

VALIDATION AND IMPLEMENTATION

7.1 Introduction

In this chapter the preferred approaches discussed in Chapters 3, 4, 5 and 6 are integrated together and validated. In Ch. 3, a model of a generator system was developed based on the physics of the system; its purpose was to be used as a simulation model that mirrors the behaviour of a generator. Due to its tunable parameters different conditions and faults can be modeled. In Ch. 4, linear models as a basis for the prediction system were developed. It was concluded that ARX models are the best candidates for this task. In Ch. 5, the prediction method was developed based on the models of Ch. 4. In Ch.6, different techniques of load management were discussed with the prime candidate being a controller based approach.

This is initially done in a software only environment where two simulation models are used in parallel. After that, a hardware in the loop (HiL) approach is employed and one of the simulation models is replaced by the laboratory generator. The ILM system is tested both in healthy and faulty conditions. Furthermore, ILM is discussed as a single system. The process of its implementation on a new generator system is explored.

7.2 Implementation Steps

Before ILM can be implemented on a new generator the steps below need to be conducted.

- Firstly, the system of interest needs to be defined, as well as what the load management algorithm should do. Hence an objective function should be defined.
- Exploration of data should occur. Understand what quantities are measurable and observable. Potential sensor locations should also be identified at this stage.
- A functioning data set should be constructed for training purposes. This can require pre-processing of the gathered data.
- Variable selection: The important variables are identified, and the potential model is simplified if possible.
- Using different data sets the models created are validated offline.

7.3 Concept of Operation; Implementation on a Two-Generator System

The implementation of Intelligent Load Management for a multi-generator system is described in this section. The case where two generators work in parallel is shown schematically in Fig. 7.1.

Each generator has its own prediction and processing module subsystems, as they both depend on the system of interest at hand, as described in Ch. 5 and 6.

The adaptive prediction models $G_n(\theta|t)$ adapt from a known baseline model created offline ($G(\boldsymbol{\theta})$), by taking into account current ($\boldsymbol{I}_n = \left[I_a, I_f\right]^T$) and temperature ($\boldsymbol{T}_n = [T_{sw}, T_{si}]^T$) information online. The processing modules estimate the maximum safe current that can be provided by the generators by using the collected data ($\boldsymbol{\theta}$) and predicted temperature ($\hat{T}_n(t+d)$). If the desired current $\hat{I}_n(t+d)$ exceeds the max allowed current $\hat{I}_{n_{max}}(t+d)$, load is shed from that generator and it is attempted to be run by the rest of the system. The process is repeated for all generators sequentially. Subscript n denotes which generator the quantities refer to, e.g. $\boldsymbol{I}_1 = \left[I_a, I_f\right]^T$ is the measured current vector associated to generator 1.

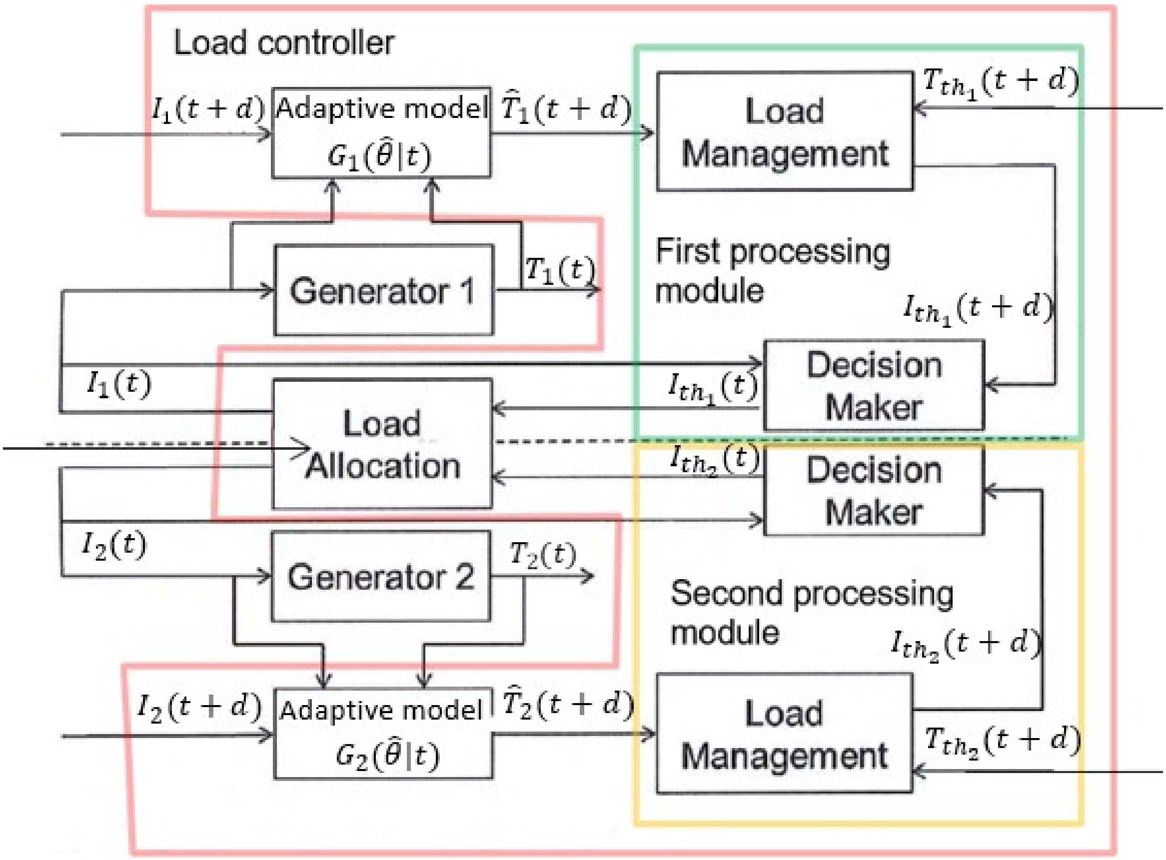

Fig. 7.1 Top level schematic description of ILM algorithm.

$$I_{net} = \sum_{k=1}^{n} I_k + I_{shed} \tag{7.1}$$

with

$$I_{n+1} = \hat{I}_{n+1} + (\hat{I}_n - I_n) \tag{7.2}$$

This means that the shed current from each generator is added onto the desired load of the next one in the sequence, resulting to a net shed current (I_{shed})

7.3.1 Preferred Methodology

The items on the schematic of Fig. 7.1 are populated by appropriate subsystems depending on the system requirements. For the three-phase system that has been used to prototype this method, the recommended path is using linear models (Ch. 4). Both the adaptive model and the load manager are based on black box ARX offline models. This eases the implementation and reduces the processing speed. Although the other approaches perform at least equally well compared to the linear models, the increase in complexity is not justified for the performance.

7.3.2 Software Implementation

The two generators are tested under the same testing conditions that were discussed in the previous chapters. In this case, one generator is always healthy and the other one is subject to a fault (or not) under the two loading profiles discussed in Ch. 6. The aim is to ensure that neither of the two systems of interest will be subject to overheat.

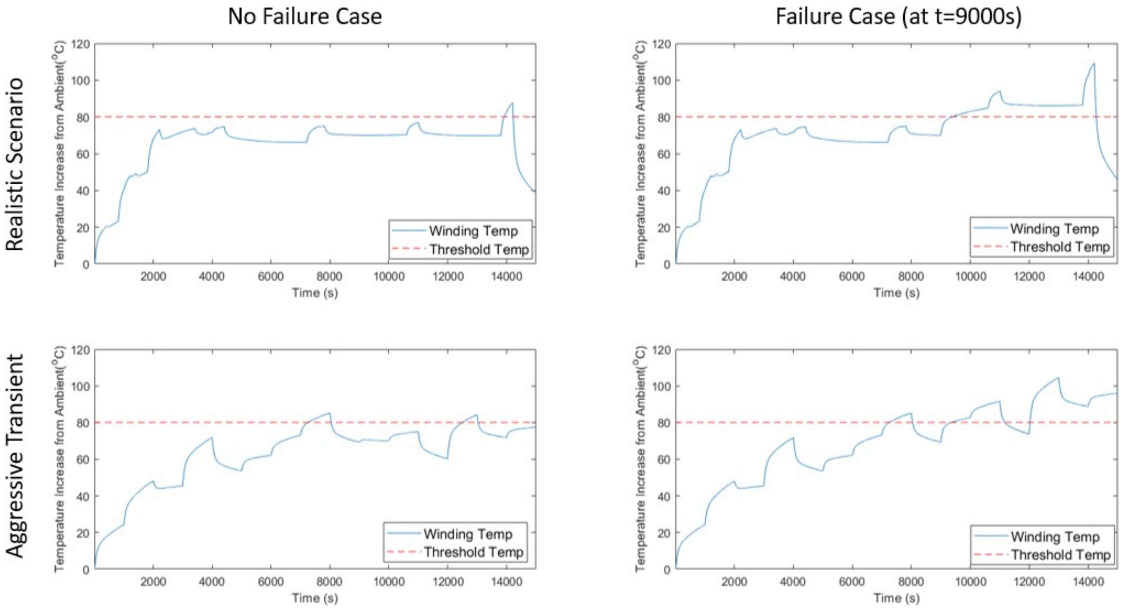

Fig. 7.2 Temperatures during both scenarios under fault and no-fault conditions.

Figure 7.2 shows the temperatures under both scenarios and conditions when no load management is present. This helps to establish a baseline for both generators, against which the responses using ILM are compared. For completion, the corresponding load currents defining such scenarios are provided in Fig. 7.3. The realistic scenario is based on the normal operation of the aircraft, all scenarios that are normally present in a flight are covered. The aggressive transient scenario is aimed to test the behaviour and tolerance of ILM.

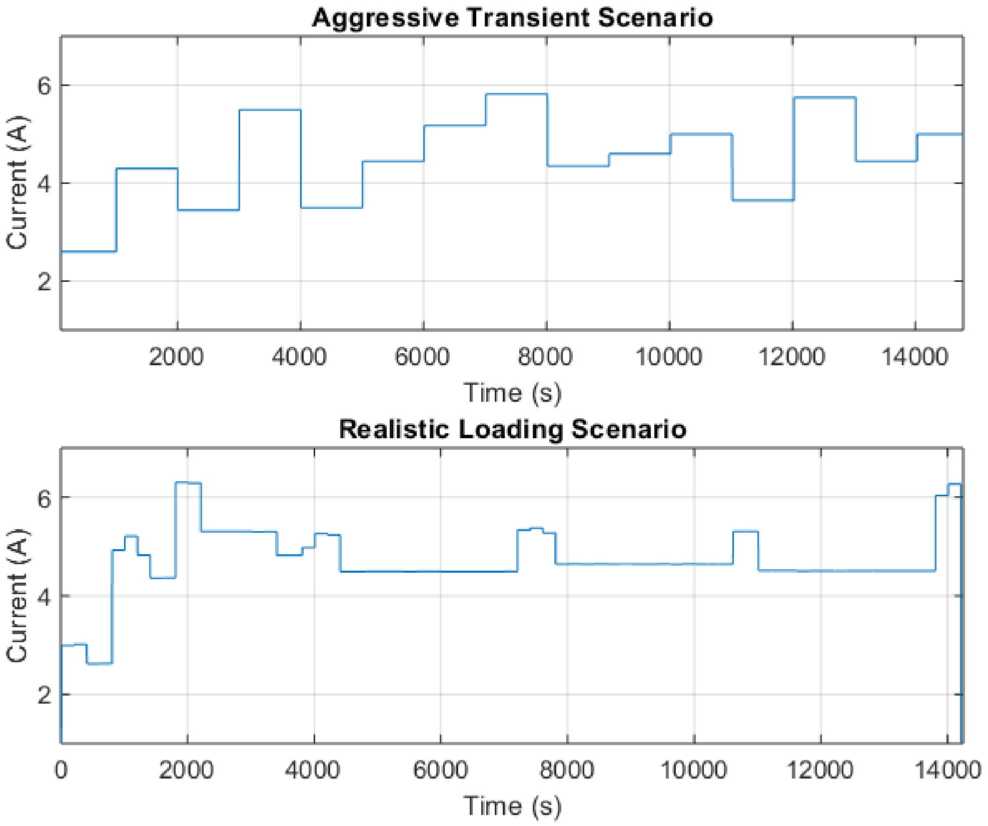
Aggressive Transient Scenario

Realistic Loading Scenario

Fig. 7.3 Load Currents defining both scenarios.

No-Fault Case

This subsection describes and discusses the use of ILM when no failures occur and the overheating occurs normally.

Normal Loading Scenario

When no failures are present the generators behave identically, so overheating issues are tackled in the same fashion as in a single generator system, as any load shifting would result to further overheating of the other machine(s) and would result to being shed by them, too. This is demonstrated in the following cases. Figures 7.4 and 7.5 show the current demands for both generators as well as the actual currents after load management takes place to avoid overheating.

It should be noted that the current demand for the second generator is higher due to the initial shedding from the first generator. The net load shed $I_{shed}(t)$ is shown in Fig. 7.6.

The temperatures of both generators are shown in Figs. 7.7 and. 7.8 both with and without ILM.

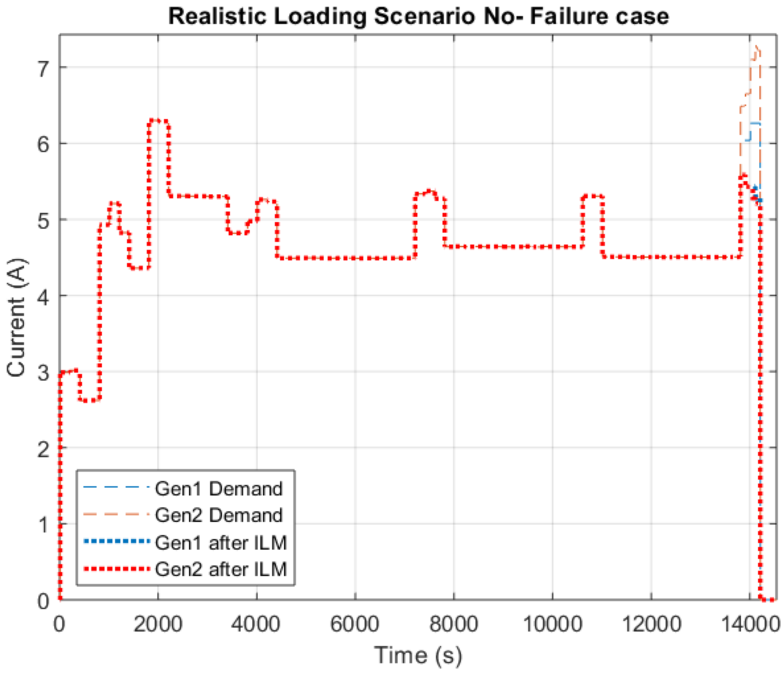

Fig. 7.4 Load Currents before and after load management with realistic loading and no failures.

The predicted temperatures of both generators for $d = 100, 250\,, 500$ are provided in Fig 7.7. The prediction errors for the two generators are identical until the last peak. This is to be expected as the parameter vector ($\boldsymbol{\theta}$) is identical (due to the same inputs and outputs). When the shedding is to occur on the first generator and the loading increase on the second, these inputs and outputs differ, hence so do the prediction errors. This is shown in Table 7.1. This change in prediction accuracy makes the estimation of the threshold current more conservative for the higher current demand of the second generator.

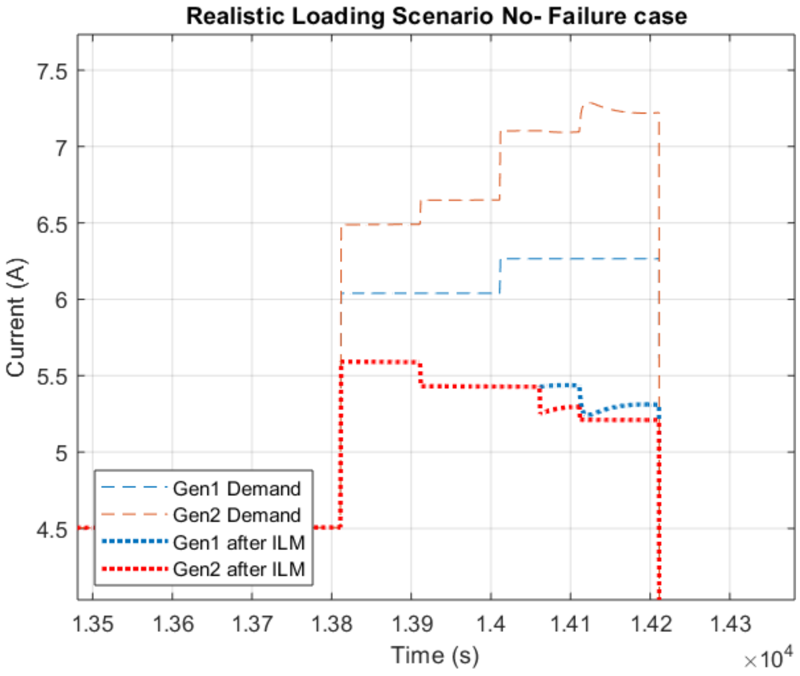

Fig. 7.5 Zoomed in version of Fig. 7.4 at the point where load management takes place.

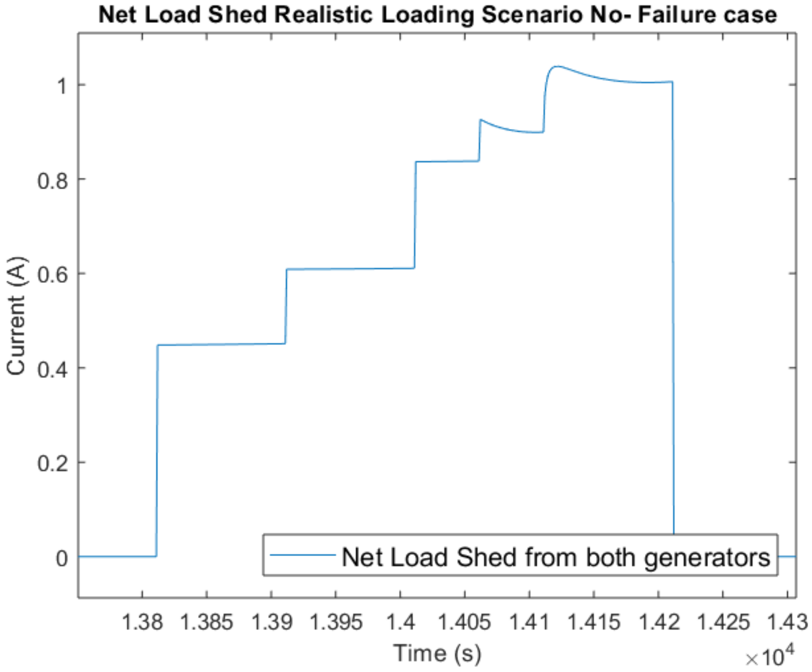

Fig. 7.6 Net current shed from both generators.

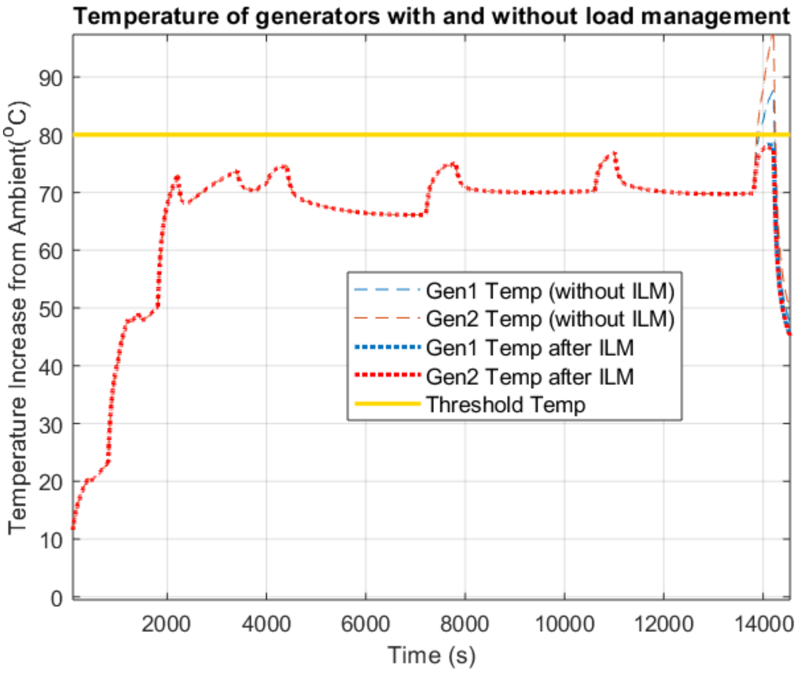

Fig. 7.7 Temperature comparison of between generators in cases where ILM is active and not.

Table 7.1 Predicted errors in the two generators.

	$t \in [13800, 14100]$		$t \in [10500, 11200]$	
	Gen1	Gen2	Gen1	Gen2
d=100	0.25	0.6	0.1	0.1
d=250	0.20	1.2	0.1 (overshot)	0.1 (overshot)
d=500	3.10	6.1	1.2	1.2

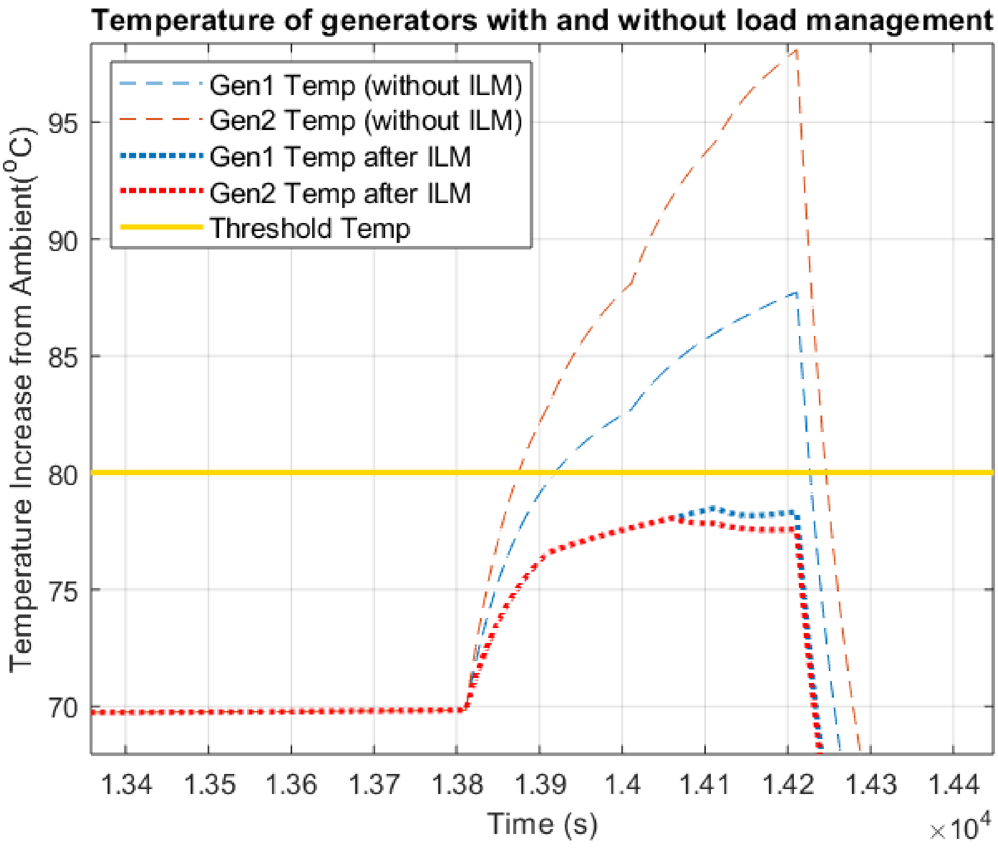

Fig. 7.8 Zoomed in version of Fig. 7.7 at the point where load management takes place.

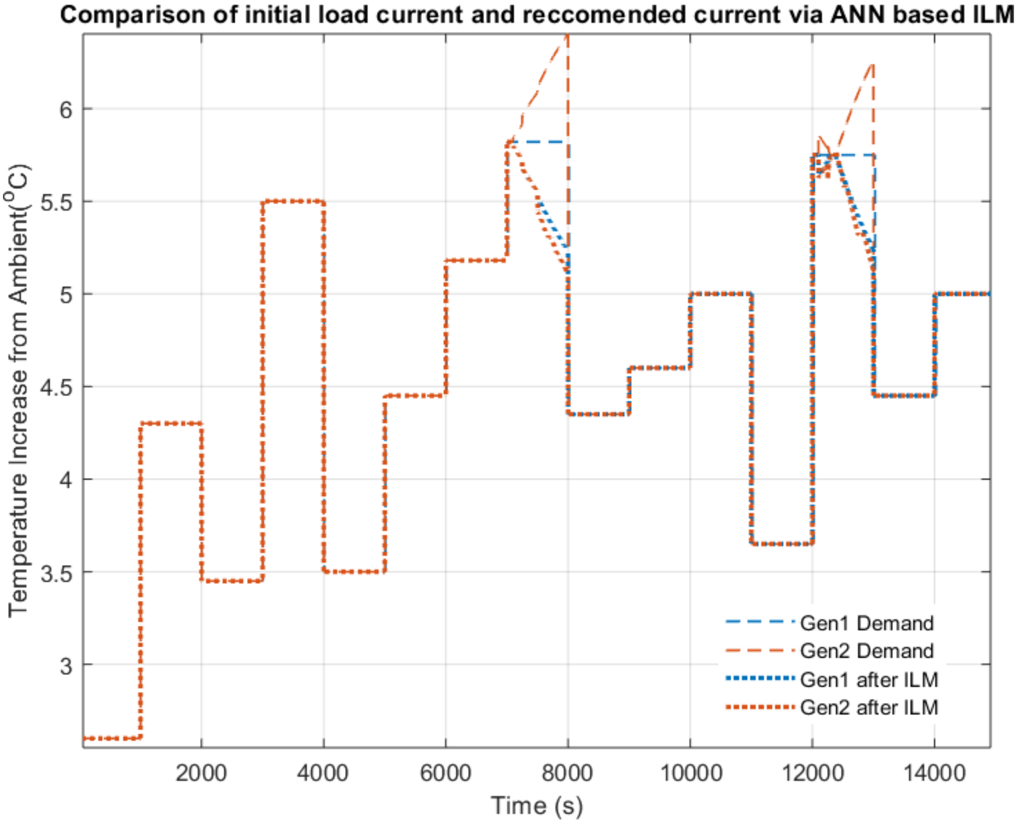

Fig. 7.9 Initial and recommended currents for both generators in an aggressive transient scenario.

Aggressive Transient Scenario

In the aggressive transient scenario, an overheat fault is to occur at two instances during the flight. The change in recommended current can be observed for such points in Fig. 7.9. In similar fashion as before, the second generator has a more conservative estimation of safe threshold current due to its altered load profile. The resulting temperatures can be viewed in Fig. 7.10 and 7.11.

The net shed load is considered and it can be viewed in Fig 7.12.

In Table 7.2 the prediction errors for both generators can be viewed for two different time segments. The first segment ($t \in [7500, 8100]$) is where load is shed from Gen1 and placed on Gen2 due to potential overheating; in the second segment ($t \in [10600, 11200]$), there is no risk of overheating due to the lower load on both machines. Similarly to the previous scenario, the change in load increases the prediction error due to the parameter vector ($\boldsymbol{\theta}$) needing to adapt. The responses are identical for the second segment as the input-output data are also identical.

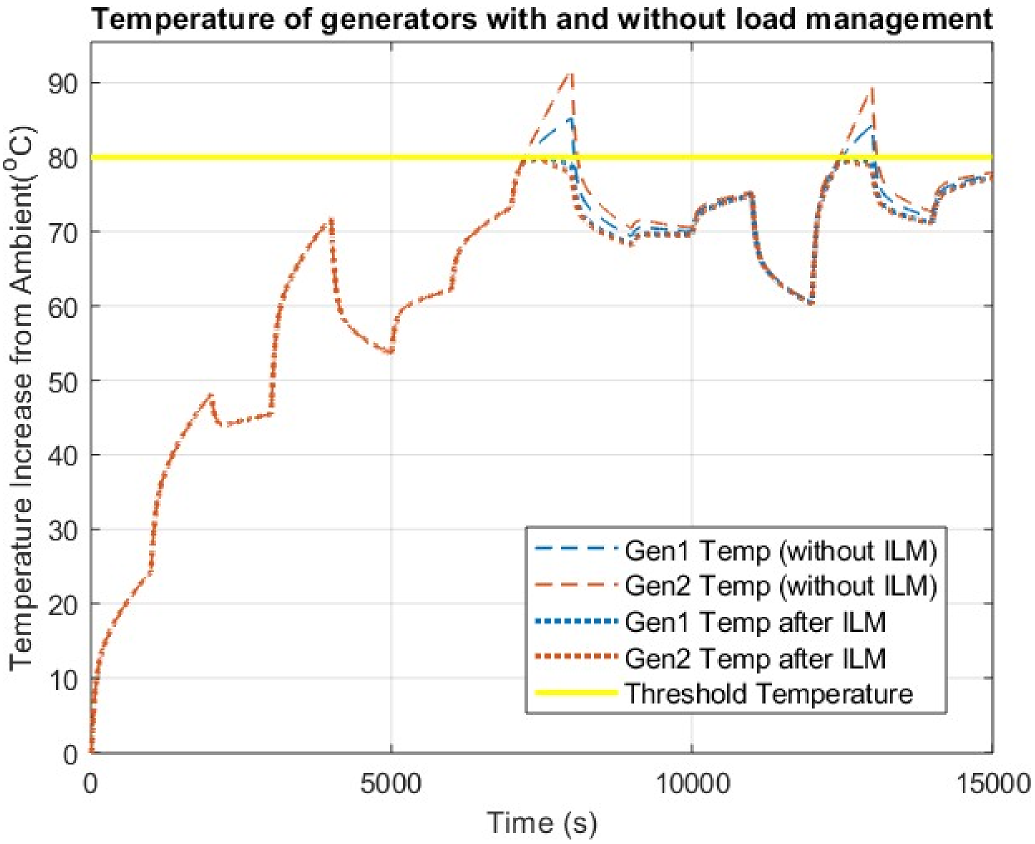

Fig. 7.10 Resulting temperatures for both generators for the aggressive transient scenario.

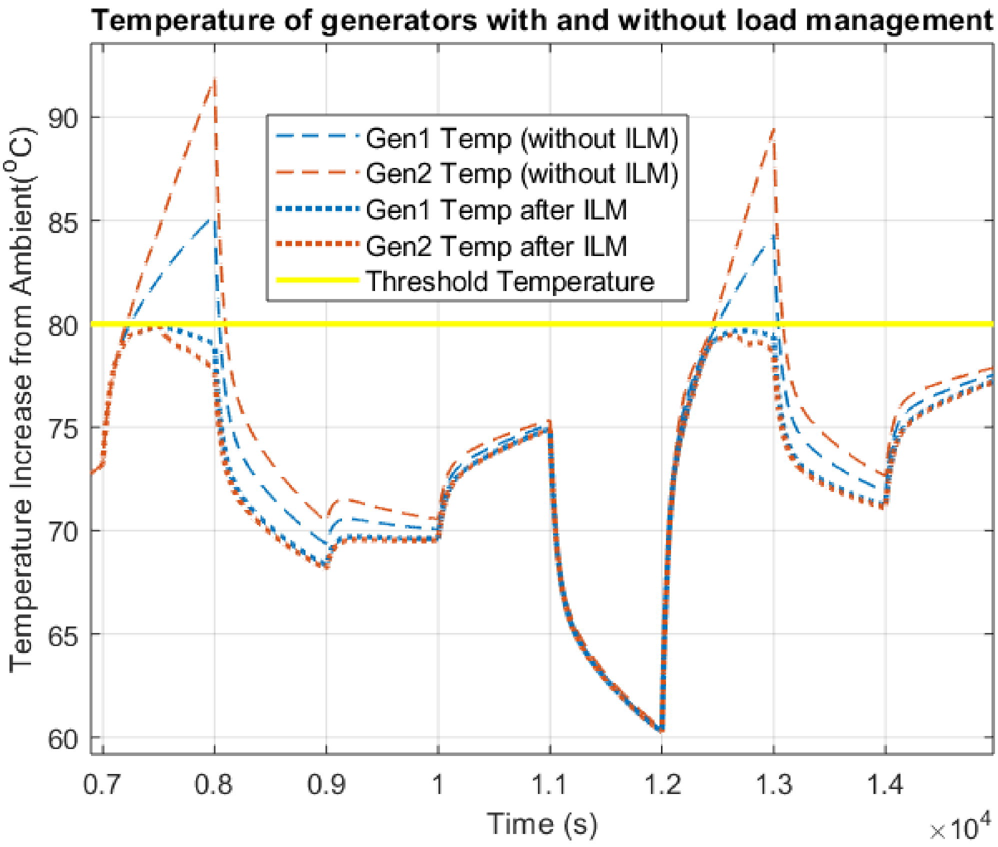

Fig. 7.11 Resulting temperatures for both generators for the aggressive transient scenario zoomed at the points of potential overheat.

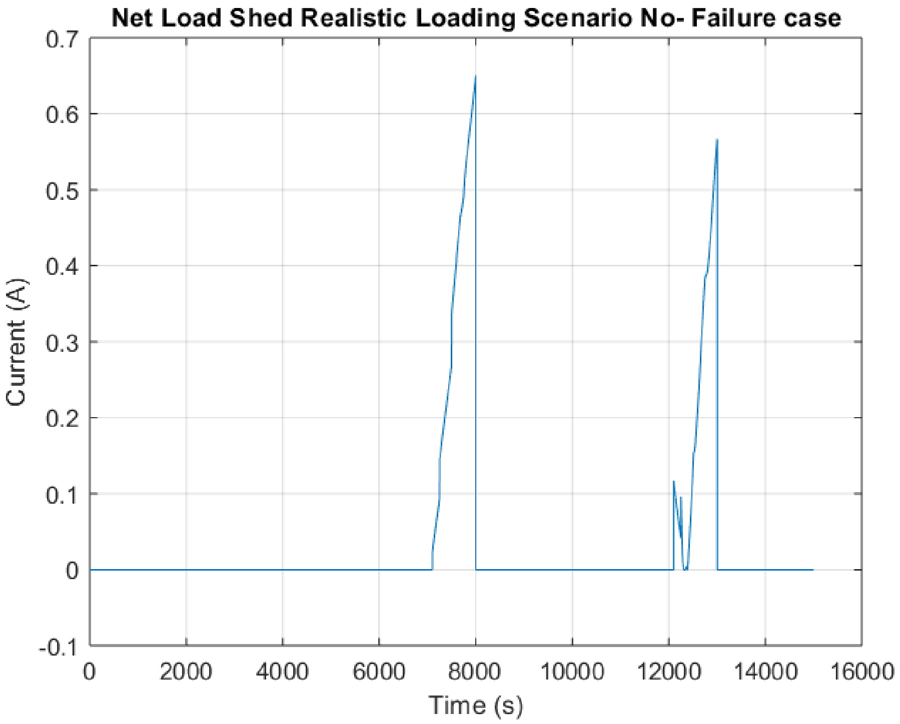

Fig. 7.12 Net shed load for both generators in the aggressive transient scenario with no failures present.

Table 7.2 Prediction errors before and after the occurrence of a fault.

	$t \in [7500,8100]$		$t \in [10600,11200]$	
	Gen1	Gen2	Gen1	Gen2
d=100	0.4	0.8	0.12	0.12
d=250	1.2	1.8	0.4	0.4 (overshot)
d=500	2.5	3.8	0.9	0.9

Load Management With Failures

This section discusses the use of ILM when failures are present in a two-generator system. In this case the first generator is subject to a fault at t=9000s - which results to the increase of the resistance of the windings by 30% (similarly to Ch.5,6 and 7)- whilst the second generator is healthy throughout its operation. Since the generators have different behaviours, there is more room for effective load management.

Normal Loading Scenario

Figure 7.13 shows the recommended currents for both generators after a fault occurs at t=9000s. Load is transferred from the generator subjected to a fault to the healthy one. The load shed from the generators and hence the improvement provided by the use of ILM is shown in Fig. 7.14. Using similar metrics to Ch. 6 to quantify improvement due to ILM, the integral of shed current is shown in Table 7.3. It can be observed that by employing ILM 50% of the load shed from the faulty generator is picked up by the healthy one in this scenario, when possible.

Meanwhile, Fig. 7.15 shows that the temperatures after ILM do not exceed the threshold temperature. Similarly to the previous scenarios, when excess current is added to the generator, more conservative shedding occurs; such is the case at $t \in [11200, 11500]$ for the healthy generator as there is a temperature leeway of approximately 5°C. This conservative management results to a maximum of 0.07A being shed for 1.5 minutes.

Table 7.3 Integral of current over time (charge) loss due to load shedding, under normal loading conditions with a fault occurring at t=9000s.

Generator	$\int \Delta I \, dt \, (C)$
Healthy Generator Shed (No ILM)	509
Faulty Generator Shed (No ILM)	3255
Generator system (No ILM)	3764
Generator system with ILM	1930

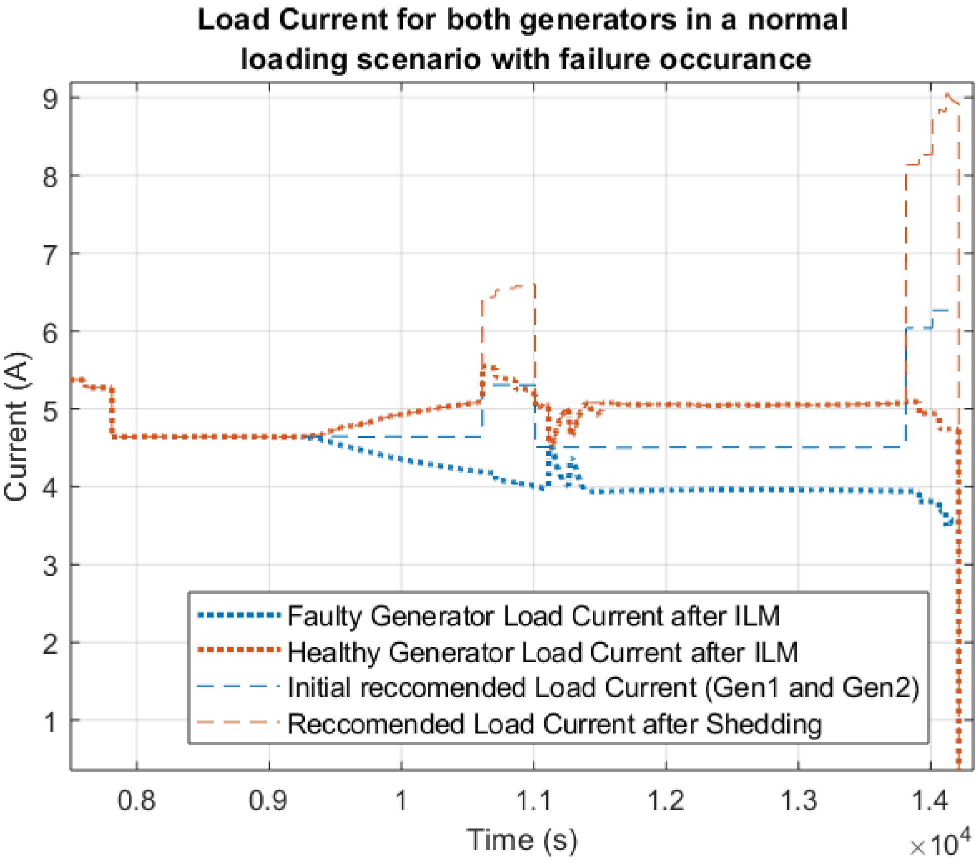

Fig. 7.13 Load Currents before and after ILM for both generators during normal loading scenario with a fault occurring at t=9000s.

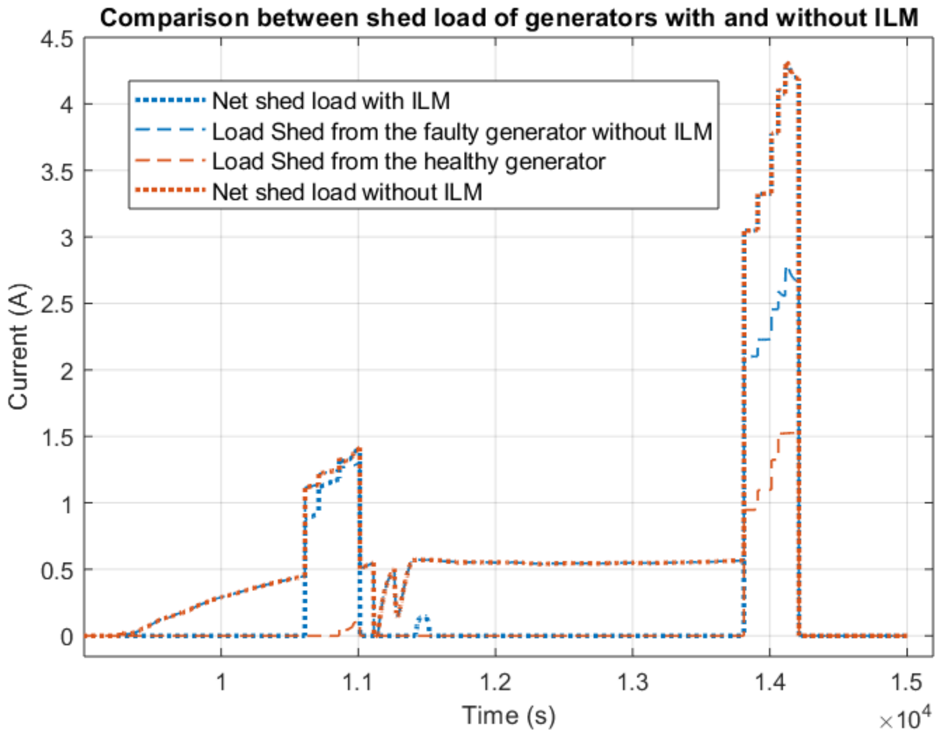

Fig. 7.14 Shed load from the generator system comparing cases with and without ILM.

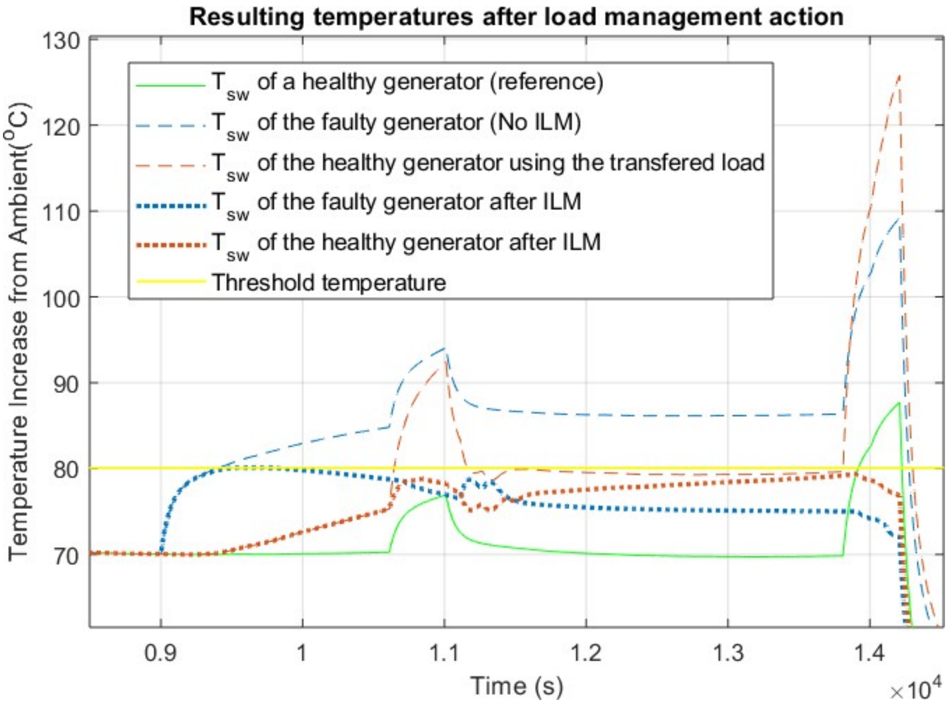

Fig. 7.15 Resulting temperatures with and without ILM.

Aggressive Transient Scenario

The recommended currents for both generators are shown in Fig. 7.16. The load management action at the interval $t \in [7000, 8000]$ is identical to the one described in the previous section, as no fault has occurred yet. The interval $t \in [9200, 11000]$ is a good example of effective load management. The faulty generator load is being progressively shed due to the overheat threat, meanwhile the healthy generator picks up such load increasing its current higher than the initial profile. This can also be observed in Fig. 7.17 where the net shed currents are shown. In this scenario only 7% of the current shed from the faulty generator can be taken on-board the healthy one. This is due to the healthy generator being at risk of overheating due to excess loading. It is evident that a generator can only participate in load management effectively if it has a zero shed current of its own. For completion, the resulting temperatures are presented in Fig 7.18. The observations are consistent with the previous temperatures, as the healthy generator has more conservative load management due to the increased current demand. Furthermore, the overall load management is consistent with the behaviour described in Ch. 6 in the single generator load management.

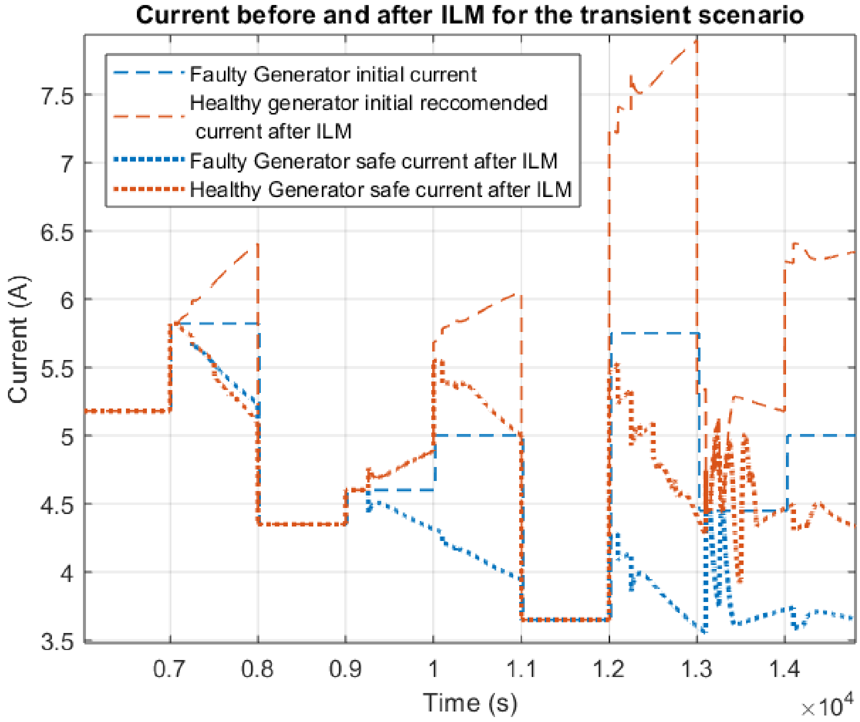

Fig. 7.16 Currents before and after ILM in the transient scenario with a fault occurrence at t = 9000s.

Table 7.4 Integral of current over time (charge) loss due to load shedding in the aggressive transient scenario with a fault occurring at t=9000s.

Generator	$\int \Delta I \, dt \; (C)$
Healthy Generator Shed (No ILM)	1839
Faulty Generator Shed (No ILM)	5143
Generator system (No ILM)	6982
Generator system with ILM	6450

7.4 Hardware in the Loop Validation

In this section the healthy generator model is substituted by the lab-based generator rig and the normal loading test is repeated. This test is chosen so that overheat under normal conditions is avoided on the generator, as that would cause it to trip. The data acquisition is done using an NI PCI-6229 card, with the relevant equipment and their specifications outlined in Chapter 3.

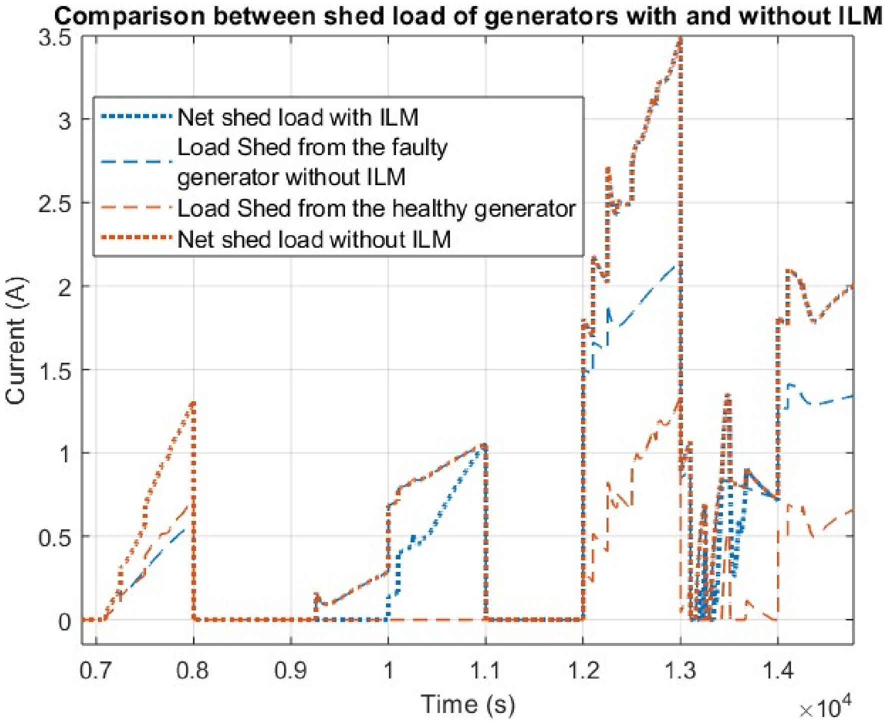

Fig. 7.17 Load Shed from individual generators and generator system in the aggressive transient scenario.

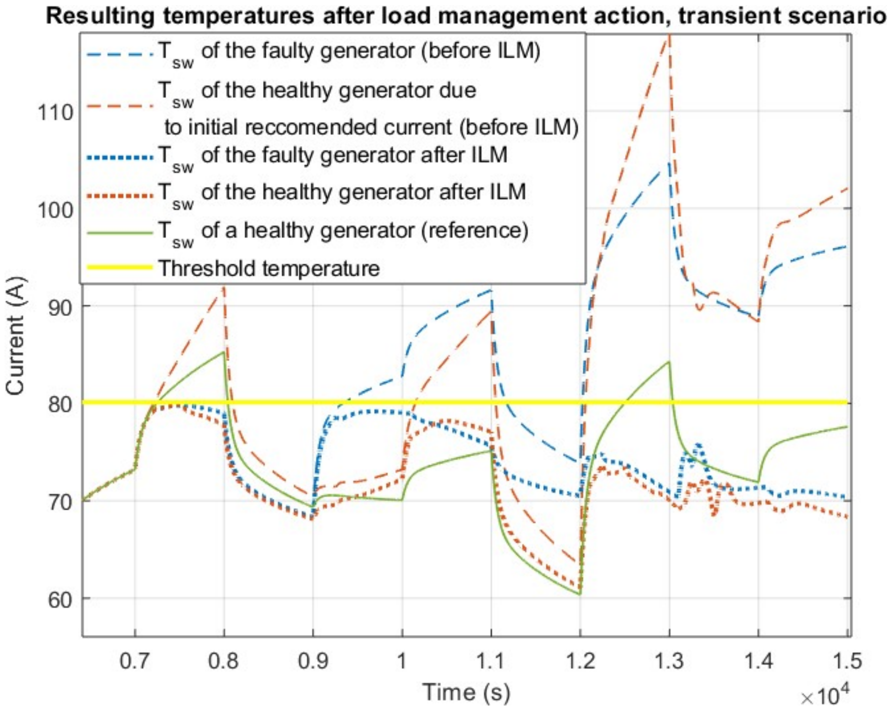

Fig. 7.18 Resulting temperatures due to load currents before and after ILM action.

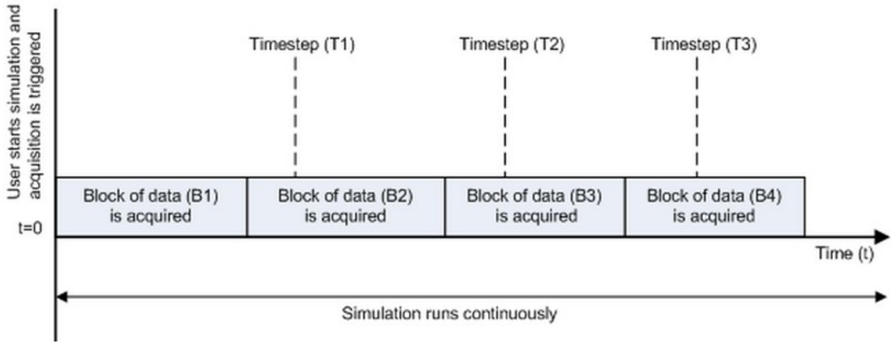

Fig. 7.19 Schematic representation of asynchronous mode [98].

The data acquisition itself occurs fully in MATLAB/Simulink using Asynchronous sampling mode. The Simulink manual states that "the data acquisition from the device and the simulation happen in parallel. The model initiates the acquisition from the device when the simulation starts. Data from the device is continuously acquired into a first in, first out (FIFO) buffer in parallel as the simulation runs. At each time step, the model fetches data from the FIFO buffer and outputs a block of data. The data in the FIFO buffer is contiguous according to the hardware acquisition clock" [98]. A diagrammatic representation can be found in in Fig. 7.19. This is done since the sampling is to outpace the simulation and hence the limiting factor is the speed of the simulation. Furthermore, the speed of the data acquisition needs follow the Nyquist criterion, i.e. the sampling frequency being at least twice of the actual frequency of the signal.

The main limitation of the implementation is the need for manual "shifting" of loads. Although half the load (i.e. the load driven by the faulty generator) is virtual, the other half comes from a load bank that is not in an actuated system. Therefore, any changes in the load need to occur by a person in real time. For this to be feasible, the exact necessary load is provided on an output display in Simulink. These changes might not be exactly achievable due to logistics, such as lack of manual dexterity and obvious inherent delay between observation of the required current and its implementation.

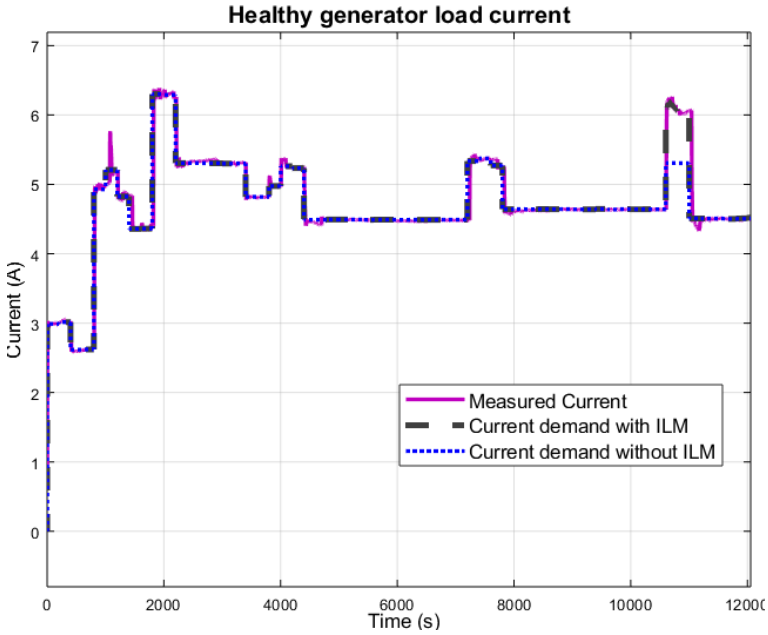

Fig. 7.20 Currents before and after load management for the generator rig.

The behaviour of the faulty generator is the same as the one described in Figs. 7.13, 7.14 and 7.15. Meanwhile, the behaviour of the generator rig is shown in Figs. 7.20 and 7.21.

In Fig. 7.21 it can be observed that the response of the generator rig is comparatively lower than the expected model values, this is attributed to ambient cooling of the room that has not been taken into account. Nonetheless, the different behaviour of the generators does not invalidate the effectiveness of the load management.

Figure 7.20 shows the current of the generator after the load is transferred from the faulty generator. The initial current demand (load profile) of the generator is also shown in order to establish a comparative baseline. The whole of the shed load from the faulty generator can be accommodated in the healthy generator in this scenario.

Table 7.5 Temperature error $e(t)$ in prediction for a given prediction horizon for intervals of $t \in [6700, 8200] \cup [10100, 11400]$.

Prediction horizon (d)	$e(t), t \in [6700, 8200]$	$e(t), t \in [10100, 11400]$
d=1	0.003	0.006
d=100	0.5	0.8
d=300	0.9	3.87
d=500	2.05	9.2

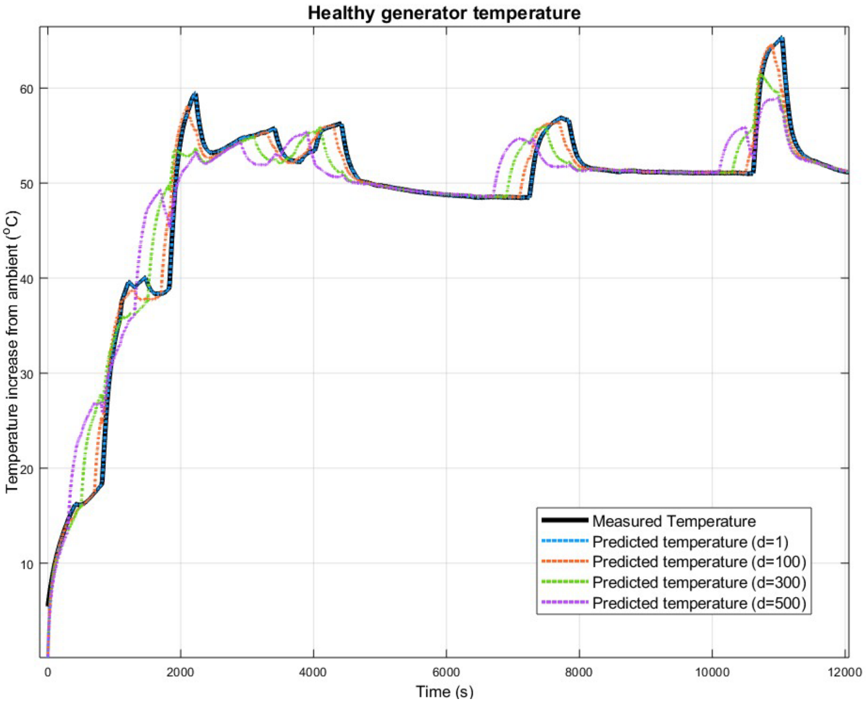

Fig. 7.21 Predicted and actual temperature for the generator rig during load management.

An interesting observation is the prediction errors in the temperature of the generator rig. Two intervals are chosen for analysis, before and after load change. These intervals are $t \in [6700, 8200] \cup [10100, 11400]$ which refer to the peaks of temperature at t = 7725s and t = 11045s. These results are analysed in Table 7.5.

The response from the first interval is consistent with the prediction error characteristic curve shown in Ch. 5, Fig. 5.7. The second interval has distinctly increased errors, especially at higher prediction horizons, due to the change in expected current happening very close to the interval being examined. That said, the error of d = 100s suffices for safe load management, with the potential caveat that it might result to a conservative estimation of safe currents.

7.5 Transferability to Other Generators

Although ILM has been developed using an AC lab-based generator, the aim is for it to be transferable to on-board aircraft ones. Therefore, the purpose of this section is to give an example of the initial steps taken for such transfer. The aim is a demonstration of a proof of concept whilst providing the initial steps for the modelling side, as beyond that, the steps taken for the implementation of ILM are identical.

7.5.1 Setup

A decommissioned variable speed 28VDC generator was provided for modelling purposes from BAE Systems- Brough test facility (Fig. 7.22). New thermocouples were installed in the generator to monitor the temperature fluctuation. This placement of sensors had limited locations, due to not being able to get to the inner part of the generator. Five K-type thermocouples were installed: two on the end windings, one on the stator iron, one on the inlet duct and one on the frame just above the mid windings. It should be noted that the placement of the first five was done through the air inlet duct. The temperatures from these thermocouples, alongside the load current, were logged using a data logger. The field current was monitored using a current clamp meter during load changes, due to the data logger not interfacing with PWM signals. Cameras were used to monitor the health of the generator, as it was placed in a separate soundproofed room (Fig.7.23).

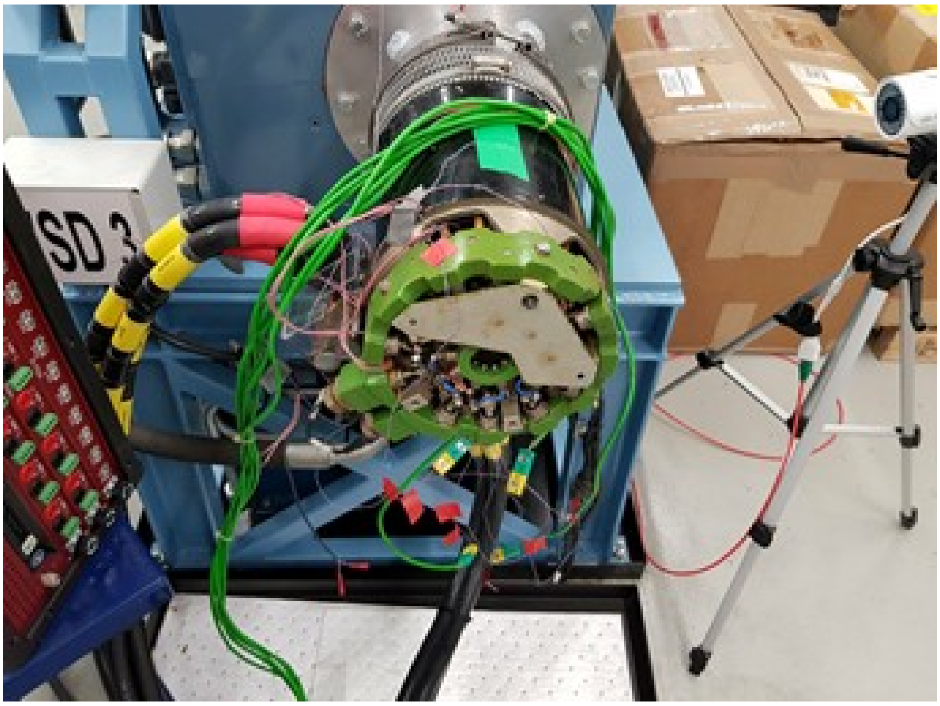

Fig. 7.22 DC aircraft generator from Brough test facility.

Fig. 7.23 Data logger (right) and cameras (left) used during testing.

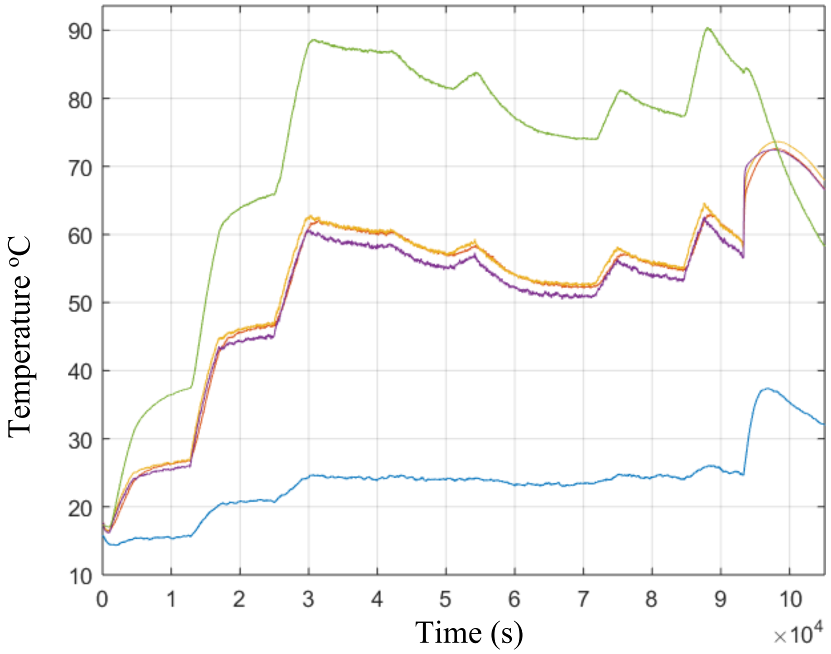

Fig. 7.24 Gathered temperatures from a variable load test.

7.5.2 Testing

Several tests were run in order to better understand the behaviour of the generator. These included steady state tests at set speeds (constant speed constant current), transient tests (constant speed variable current) and realistic mission test (variable speed variable current). The latter was done by matching the variable mission load profile to a speed profile for the corresponding phase of flight. These tests were repeated for a "faulty generator" where a 50% blockage in the air inlet was induced. Examples are provided in Figs. 7.24 and 7.25.

From a brief analysis of the currents and temperatures, it can be observed that whilst the generator is in operation $t \in [0, 9300]$ the measured temperatures by the sensors located on the windings, stator and air inlet, are very close. This is due to them being too close to the air inlet itself, hence being cooled throughout the experiment. The one located on the frame (just above the mid-windings) shows results have more pronounced transients and hence are easier to use. The observation of $t \in [9300, 11500]$ also supports this, as the remaining temperatures rapidly increase once the forced cooling stops. It should be noted that although the frame temperature is not directly indicative of the actual winding temperature, a direct relationship could be established.

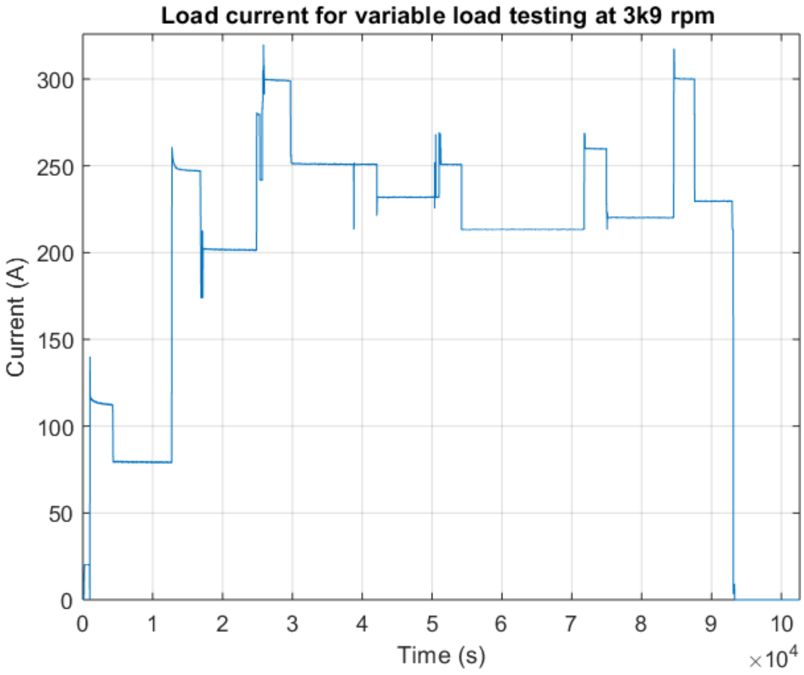

Fig. 7.25 Load current during the variable load test.

7.5.3 Creation of a black box model

In constant speed cases, a black box model can be created using the process outlined in Ch. 4 in an ARX form (7.3).

$$\boldsymbol{T}(t) = \boldsymbol{G}(\boldsymbol{\theta})\boldsymbol{I}(t) \tag{7.3}$$

where for a two-input system with $\boldsymbol{I}(t) = \left[I_{load}(t), I_{field}\right]^T$

$$\boldsymbol{G}(\boldsymbol{\theta}) = [G_1(\boldsymbol{\theta}), G_2(\boldsymbol{\theta})] \tag{7.4}$$

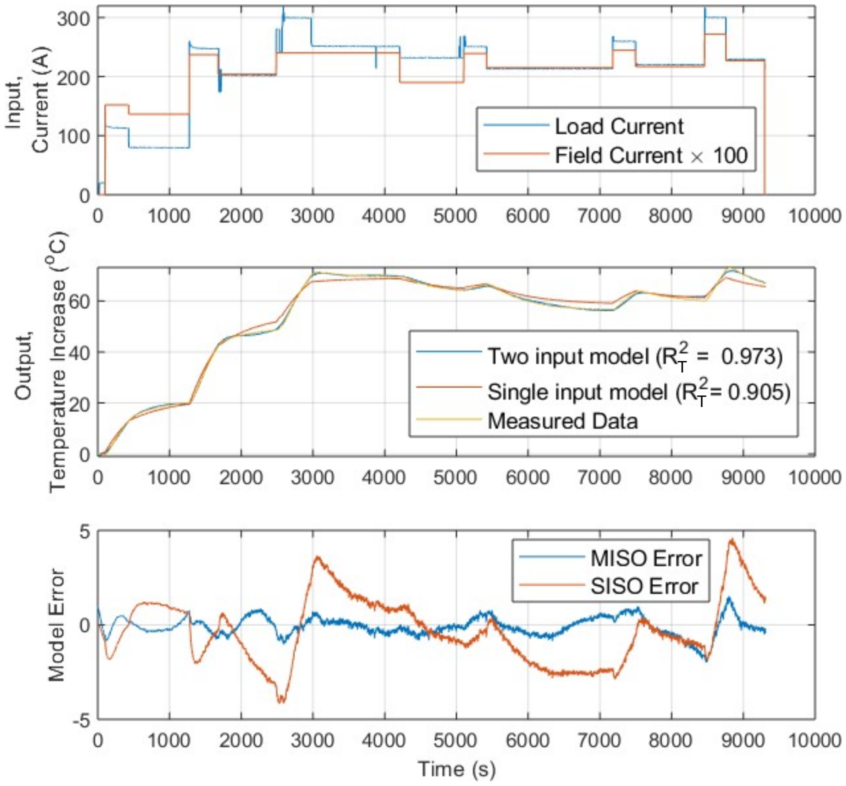

Fig. 7.26 Response of MISO and SISO black box ARX models for modelling the behaviour of the Brough Generator for a constant speed.

$$G_1(\theta) = \frac{10^{-3}(0.2562z^{-1} - 0.7635z^{-2} + 0.7585z^{-3} - 0.2511z^{-4})}{1 - 3992z^{-1} + 5.975z^{-2} - 3.975z^{-3} + 0.9916z^{-4}} \tag{7.5}$$

$$G_1(\theta) = \frac{10^{-3}(-7.484z^{-1} - 22.47z^{-2} - 22.48z^{-3} + 7.5z^{-4})}{1 - 3999z^{-1} + 5.996z^{-2} - 3.996z^{-3} + 0.9986z^{-4}} \tag{7.6}$$

or for a single input system with $I(t) = I_{laod}(t)$

$$G(\theta) = \frac{10^{-4}(1.149 + 3.002z^{-1})}{1 - 1.142z^{-1} + 0.2477z^{-2} - 0.1039z^{-3}} \tag{7.7}$$

The response of these systems can be observed in Fig. 7.26. The response of the two-input system is a lot more accurate and hence it should be preferred in offline cases.

It should be noted that this approach only works for constant speed, as a variable speed creates issues with variable cooling, which is not modelled. For the speed to be included in a single model, more accurate speed measurements are necessary.

7.5.4 Adaptive Modelling and ILM

The SISO system can be used as a basis for an online adaptive model by using the data vector from (7.7). The adaptive modelling has dual purpose in this case: firstly, it allows for accommodating for potential failures (similar to Ch. 5), but it also allows for another change of input output relationships, namely the change of speed.

3k9 rpm Dataset

The prediction capabilities are demonstrated at 3k9 rpm. There is no fault or otherwise change of conditions in this data set (Fig 7.27). The yellow line signifies when the data is actually available for further decision making, whereas the red one has been shifted in time to align with the measurements, which allows for a better visual comparison.

Concatenated data sets

For testing purposes, a larger data set being constructed by concatenating the data sets from the variable load tests of 6k rpm and 3k9 rpm, with the initial model being only trained with the 6k data set. This allows for testing with the speed being altered half way through the test, but the is current being repeated. This is shown in Fig. 7.28.

The behaviour of the prediction with regards to the prediction horizon is shown in Fig. 7.29. It shows the coefficient of determination as a function of prediction horizon, which deteriorates almost linearly (as expected) whilst the accuracy decreases.

Based on this graph, values of $d < 700s$ would be acceptable for prediction as they result to $R_T^2 > 0.9$. This is lower than the values discussed in Ch. 5. The main reason for this is the increased noise of the measurements of the system which add noise in the reduction. Although some filtering has occurred removing some noise, some issues remain.

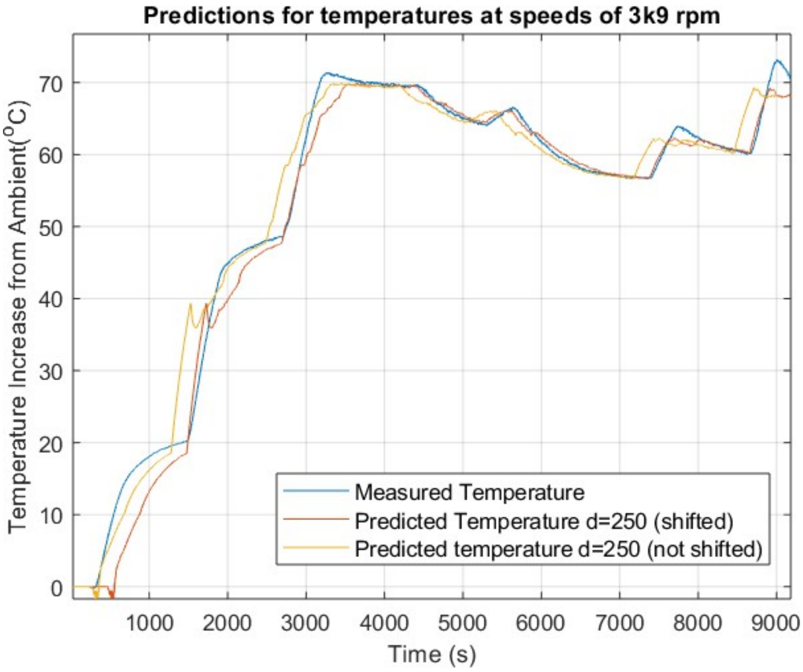

Fig. 7.27 Temperature prediction in the 3k9rpm experimental data.

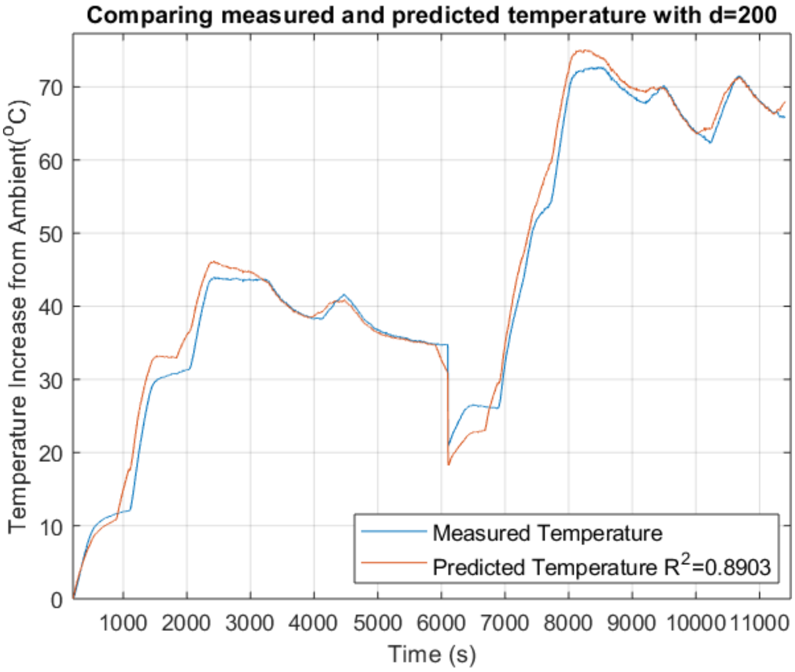

Fig. 7.28 Temperature prediction in the concatenated data scenario with prediction horizon d=200.

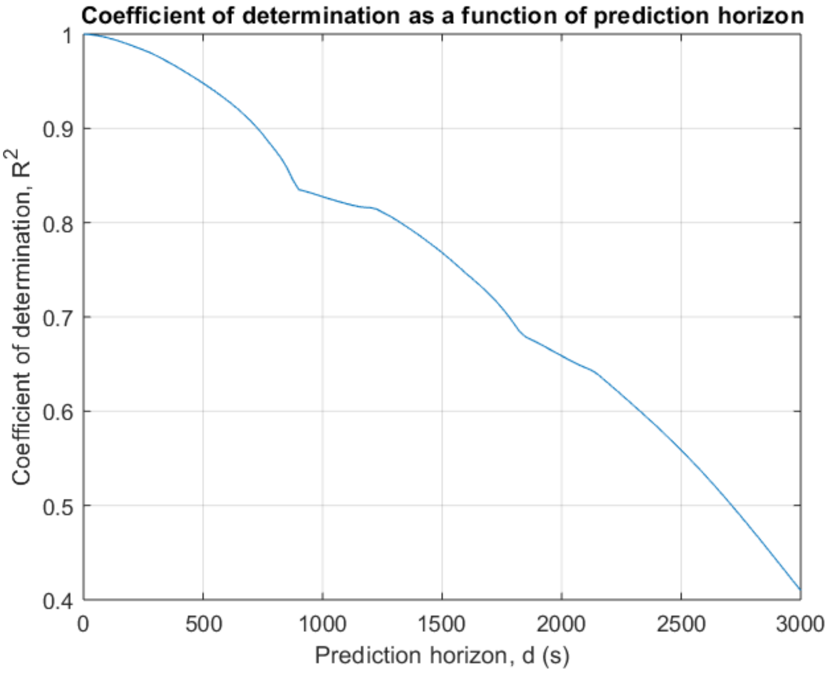

Fig. 7.29 Coefficient of determination as a function of the prediction horizon.

Using the information above, controller based ILM is employed on this data set by using threshold temperature of $T_{Thr} = 70^{o}C$. As it can be observed in Fig. 7.30, overheat is prevented in the interval of $t \in [8000, 12000]$ thanks to the inclusion of ILM.

Inclusion of a Fault

An example of a dataset with a fault induced during the flight is examined in this section. At 8k2 rpm, a fault is introduced half way through the test, with the air inlet aperture being covered by 50%. Figure 7.31 shows the prediction and ILM response of the generator after a fault occurs. The threshold temperature is set at $25^{o}C$ above the ambient ($33^{o}C$). The temperature of the ambient is this high as several tests were run that day, resulting to a large increase of the temperature of the room. This provides further supporting evidence regarding the transferability of ILM to generators of different types.

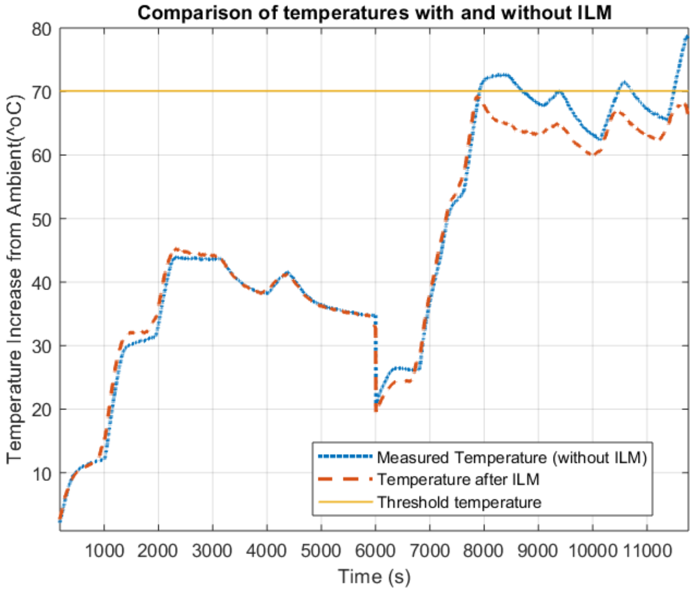

Fig. 7.30 Temperatures before and after ILM using concatenated data sets of 6k rpm and 3k9 rpm.

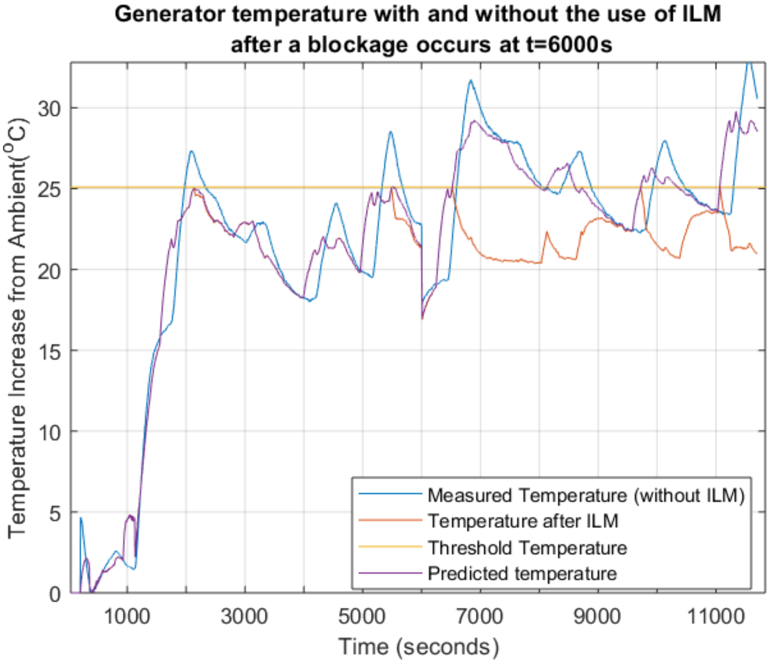

Fig. 7.31 Temperatures before and after ILM using data with a fault occurring.

7.6 Conclusions

In this chapter, ILM is implemented in a two-generator system for validation purposes. Initially, in a simulation environment it was shown how sequential load management occurs, i.e. the shed load of one generator is added on the desired load profile of the next. Two scenarios are examined, normal flight loading and aggressive transient loading: in both cases with and without failures occurring in the generators. This allowed for overheating to occur for different reasons at different parts of the flight and hence providing supporting evidence for ILM's operation. The improvement that the ILM provided to the system was also quantified. ILM is employed in a hardware in the loop system, where one generator is simulation based and the other is the generator rig discussed in Ch. 3, providing further supporting evidence. Lastly, ILM is developed and applied to a DC generator, further supporting the transferability of this method.

CHAPTER 8

CONCLUSION

8.1 Introduction

This chapter uses the objectives defined in Chapter 1 as a comparison to the results and methods presented. The achievement of said objectives is highlighted alongside the demonstration of the novelty contributions. Finally, recommendations are made for future paths that this work can be taken towards.

8.2 Assessment of Objectives

In Chapter 1, section 4 the objectives for this work are outlined. The intention is that by demonstrating the satisfaction of these objectives, the contributions of this body of work can be highlighted.

Objective 1: The design and validation of simulation models that are to be used for testing purposes instead of generators.

In Chapter 3, a nonlinear simulation model that takes into account both electrical and thermal aspects of the operation of the generator was created and validated against test data.

This provided a testing framework that allowed for easy implementation and assessment of different conditions. The two parts of this model (electrical and thermal) can be decoupled and acquired measured data can be used instead.

Objective 2: The design and validation of prognostic models that are able to predict the future temperatures of the system based on given inputs.

In Chapter 4, predictive models were created using linear models, with preference on Autoregressive Exogenous (ARX) modeling approaches, over physics based ones. These models were able to accurately predict the heat profile of the generators under normal operating conditions. Chapter 5 assesses the conditions where there are faults present. It was assumed that these faults would have gone undetected by the state of the art infrastructure. In order to tackle this, the faults were treated as being part of the plant/ system of interest and the predictive model changes to accommodate for them. To this end, adaptive ARX and adaptive neural networks were used. It was found to successfully predict the temperature of the system to 1000s with an error of $3^{o}C$ using ARX. The ANN models had an increased accuracy in prediction but suffered with robustness issues due to discontinuities and hence they would need more signal processing.

Objective 3: The design and validation of a load management algorithm that considers the present and future states of the generators and allocates the load to specific generators in order to ensure maximum functionality while not overheating.

In Chapter 6 different load management approaches were developed and validated.

They could connect directly to the system of interest and take the currents and temperatures as of different parts of the said system. They accurately predicted the future temperatures (as described in objective 2) and hence made decisions on the appropriate loading conditions of the generators while taking into account their health. The decision-making aspect was performed either using closed loop control systems paired with linear models or neural networks for more complicated systems. Neural networks were shown to be a viable alternative, but the increased complexity was not justifiable for constant speed generators.

Objective 4: To agree test plans and execute them together with BAE Systems for testing on aircraft generators, hence demonstrate the process on such generators.

This work was outlined in Chapter 7, where the modeling and first steps for implementation were done in collaboration with the engineering team in Brough. The use of the system on aircraft generators and its straightforward transferability was highlighted.

8.3 Assessment of Contributions

In Chapter 1 the contributions of this body of work were outlined in section 3. The main contribution has been the development of ILM, a load management system for aircraft generators that ensures that generators in a multi-generator system do not overheat and they remain functional both under normal and faulty conditions. This is most explicitly described in Chapter 7 where the ILM was tested in a Hardware in the Loop system. Subsequent contributions that have enabled ILM have been the simulation model framework from Chapter 3, focusing on decoupling electrical and thermal effects whilst ensuring easy implementation and communication to industry colleagues. ARX models have shown to be superior at predicting the temperature of generator components, whist being of lesser order. In ILM the adaptation and demand for accurate prediction has to occur in real time for a relatively short time-frame system. Previous attempts and iterations of load management have their decision making as a series of if statements. ILM provides a dynamic approach to this decision making by including control loops and machine learning to it and hence increasing its accuracy and decreasing the need for unnecessary load shedding. The last novelty outlined has been the demonstration of ILM on an aircraft generator; this was conducted with the collaboration of the Brough team. This not only did assist in validating the method but also provided information for a standard procedure for implementing ILM on both new and existing systems.

BAE Systems have been sufficiently contented with this approach, thus they have sought IP protection via patenting the ILM algorithm and methods (GB1810716.9-Load Controller).

8.4 Future Works

After demonstrating how a load management system would operate, there are three main avenues that need to be explored: optimisation, transferability, implementation/ integration.

8.4.1 Implementation

The question of implementation of this system is multi-faced. Firstly, the system needs to be integrated with existing systems. This raises the requirement for enhanced instrumentation in the generators; thermocouples should to be placed on the stator iron and windings whilst keeping clear from the main coolant path, as demonstrated in Chapter 7. Often this is not a simple task as the generators may be sealed, therefore research will need to be conducted about optimal sensor placement on the frame of the generator and using model-based approaches to estimate the temperature of the more vulnerable parts. Furthermore, the question of location of data analysis and signal routing needs to be answered, whether it occurs on a centralised system or locally close to the generators. Whether this system needs a designated processor for the model calculation or if this process can be run on existing equipment. Lastly, user interface and user involvement need to be assessed. Questions on system autonomy arise: what level of interaction should the user have? A higher user interaction with the system decreases the performance of the overall system but provides an easier path to system approval.

8.4.2 Temporal Load Management

Temporal load management refers to the idea of adding rest phases for the generators to cool down if necessary. The load needed to be driven during a rest phase should be minimal in order to reduce the heating effects. The purpose of this would be to allow an increased power demand for a prolonged period of time after a rest phase.

This is more applicable in a wider network where more generators (or other systems of interest) work in parallel. This allows for the rest phases to be independent for each generator, hence minimising the overall loss of functionality. In a system of two generators, under normal operation, each generator is running a minimum of 70% of its power capabilities, therefore a rest would result to a definite loss of functionality as not all subsystems can be driven.

This idea also allows for non-time critical operations to be rescheduled for a less power intensive part of the mission, instead of completely shedding them.

8.4.3 Extension to Different Types of Machines

The work conducted at Brough and using the data gathered demonstrated that the transfer of ILM from a constant speed machine to a variable speed one is non-trivial. This is mainly due to the increase of independent variables and how this can affect the temperature of the generators. Some research has been done in this body of work to accommodate for the increase of system complexity using neural networks, but this has not been validated due to the difficulty for real time data acquisition and analysis in these systems. With appropriate data acquisition hardware in place the neural network approaches for variable speed machines could be validated in a hardware in the loop test setup.

REFERENCES

[1] Abdel-Fadil, R., Eid, A., and Abdel-Salam, M. (2013). Electrical distribution power systems of modern civil aircrafts. In 2nd International Conference on Energy Systems and Technologies: 201–210.

[2] Abdel-hafez, A. (2009). Power Generation and Distribution System for a More Electric Aircraft - A Review.

[3] Akaike, H. (1987). Factor Analysis and AIC. PSYCHOMETRIKA, 52(3):317–332.

[4] Amarantidis, G., Dixon, R., Hubbard, P., and Harringtion, H. (2016). Integrated thermo- electric model for on-board aircraft generators, 7th IFAC Symposium on Mechatronic Systems MECHATRONICS 2016: 598-602

[5] Aminian, F., Suarez, E. D., Aminian, M., and Walz, D. T. (2006). Forecasting economic data with neural networks. Computational Economics, 28(1):71–88.

[6] Åström, K. J. and Eykhoff, P. (1971). System Identification - A Survay.

[7] Åström, K.-J. and Torsten, B. (1965). Numerical identification of linear dynamic systems from normal operating records. IFAC Proceedings Volumes, 2(2):96–111.

[8] Baillie, D. and Mathew, J. (1996). A comparison of autoregressive modeling techniques for fault diagnosis of rolling element bearings. Mechanical Systems and Signal Processing, 10(1):1–17.

[9] Barraza-Barraza, D. (2015). An Adaptive ARX model to Estimate an Asset Remaining Useful Life. PhD thesis, Texas Tech University.

[10] Barraza-Barraza, D., Tercero-Gómez, V. G., Beruvides, M. G., and Limón-Robles, J. (2017). An adaptive arx model to estimate the rul of aluminum plates based on its crack growth. Mechanical Systems and Signal Processing, 82:519–536.

[11] Barzegar, A., Su, R., Wen, C., Rajabpour, L., Zhang, Y., Gupta, A., Gajanayake, C., and Lee, M. Y. (2015). Intelligent power allocation and load management of more electric aircraft. In 2015 IEEE 11th International Conference on Power Electronics and Drive Systems: 533–538.

[12] Batzel, T. D. and Swanson, D. C. (2009). Prognostic health management of aircraft power generators. IEEE Transactions on Aerospace and Electronic Systems, 45(2):473– 482.

[13] Batzel, T. D., Swanson, D. C., and Defenbaugh, J. F. (2003). Predictive diagnostics for the main field winding and rotating rectifier assembly in the brushless synchronous generator. In 4th IEEE International Symposium on Diagnostics for Electric Machines, Power Electronics and Drives, 2003. SDEMPED 2003., pages 349–354

[14] Boglietti, A., Member, S., Cavagnino, A., Staton, D., Shanel, M., Mueller, M., and Mejuto, C. (2009). Evolution and Modern Approaches for Thermal Analysis of Electrical Machines. IEEE Transactions on Industrial Electronics: 871- 882

[15] Boice, W. and Levoy, L. (1944). Basic considerations in selection of electric systems for large aircraft. Electrical Engineering, 63(6):279–287.

[16] Borgnakke, C. and Sonntag, R. E. (2009). Fundamentals of thermodynamics: Part 2. John Wiley & Sons, Inc.

[17] Box, G. E. and Pierce, D. A. (1970). Distribution of residual autocorrelations in autoregressive-integrated moving average time series models. Journal of the American statistical Association, 65(332):1509–1526.

[18] Cai, Y. and de Lamare, Rodrigo, C. (2013). Low-complexity variable forgetting factor mechanism for recursive least-squares algorithms in interference suppression applications. IET Communications, 7(11):1070–1080.

[19] Cheng, S. and Pecht, M. (2007). Multivariate state estimation technique for remaining useful life prediction of electronic products.

[20] Chien, C.-J., Hsu, C.-T., and Yao, C.-Y. (2004). Fuzzy system-based adaptive iterative learning control for nonlinear plants with initial state errors. IEEE Transactions on Fuzzy Systems, 12(5):724–732.

[21] Chong, Y. C., Subiabre, E. J. P. E., Mueller, M. A., Chick, J., Staton, D. A., and Mcdonald, A. S. (2014). The Ventilation Effect on Stator Convective Heat Transfer of an Axial-Flux Permanent-Magnet Machine. IEEE Transactions on Industrial Electronics, 61(8):4392–4403.

[22] Cloyd, J. S. (1997). A status of the united states air force’s more electric aircraft initiative. In IECEC-97 Proceedings of the Thirty-Second Intersociety Energy Conversion Engineering Conference (Cat. No. 97CH6203), volume 1, pages 681–686.

[23] Cloyd, J. S. (1998). Status of the united states air force’s more electric aircraft initiative. IEEE Aerospace and Electronic Systems Magazine, 13(4):17–22.

[24] Cryer, J. and Chan, K. (2008). Time Series Analysis With Applications in R. Springer- Verlag New York, 2 edition.

[25] S. J. Cutts, "A collaborative approach to the More Electric Aircraft," 2002 International Conference on Power Electronics, Machines and Drives: 223-228

[26] Dajaku, G. and Gerling, D. (2006). An improved lumped parameter thermal model for electrical machines. 17th International Conference on Electrical Machines (ICEM2006), page 2006.

[27] de Schatz, C. H. V. (2015). Dynamic fuzzy-neural based tool for monitoring and predicting patients conditions using selected vital signs. Journal of Intelligent Fuzzy Systems, 28(6):2579–2591.

[28] Dishner, B. and Morris, A. (1989). A novel electromechanical approach to constant frequency power generation. In Aerospace and Electronics Conference, 1989. NAECON 1989., Proceedings of the IEEE 1989 National, pages 1765–1769.

[29] Dub, M. and Drlík, P. (2012). Modelling of Aircraft DC Generator Voltage Regulation, MECHATRONIKA, 2012 15th International Symposium: 209 – 214

[30] Eid, A., El-Kishky, H., Abdel-Salam, M., and El-Mohandes, M. T. (2010a). On power quality of variable-speed constant-frequency aircraft electric power systems. IEEE Transactions on Power Delivery, 25(1):55–65.

[31] Eid, A., El-Kishky, H., Abdel-Salam, M., and El-Mohandes, T. (2010b). Vscf aircraft electric power system performance with active power filters. In 2010 42nd Southeastern Symposium on System Theory (SSST), pages 182–187. IEEE.

[32] Elkobbah, K., Abdelhafez, A. A., and Forsyth, A. J. (2009). A Review of More-Electric Aircraft. In 13th International Conference on AEROSPACE SCIENCES & AVIATION TECHNOLOGY: 1–13.

[33] Emadi, K. and Ehsani, M. (2000). Aircraft power systems: technology, state of the art, and future trends. IEEE Aerospace and Electronic Systems Magazine, 15(1):28–32.

[34] Eykhoff, P. (1968). Process parameter and state estimation. Automatica, 4(4):205–233

[35] Garlick, W. G., Dixon, R., and Watson, S. J. (2009). A Model-based Approach to Wind Turbine Condition Monitoring using SCADA Data. In 20th International Conference on Systems Engineering, 8–10 September, Coventry University, Coventry, UK, volume 44.

[36] Gever, M. and Ljung, L. (1986). Optimal experiment designs with respect to the intended model application. Automatica, 22(5):543–554.

[37] Glahn, W., Dueser, G., Koenig, A., Finck, M., and Reitmann, J. (2006). Intelligent power distribution management for an on-board galley of a transport vehicle such as an aircraft. US Patent 7,098,555.

[38] Graham, J. (2015). Intelligent power management for unmanned air vehicles. PhD thesis, Loughborough University.

[39] He, X., Liu, S., and Asada, H. (1995). Modeling of vapor compression cycles for advanced controls in hvac systems. In Proceedings of 1995 American Control Conference - ACC'95, volume 5: 3664–3668 vol.5.

[40] Hess, A. and Fila, L. (2002). The joint strike fighter (jsf) phm concept: Potential impact on aging aircraft problems. In Proceedings, IEEE Aerospace Conference: 3021- 3026

[41] Hoffman, A. (1985). Advanced secondary power system for transport aircraft.

[42] Ishak, N., Julaihi, F., Yusof, N. M., Tajuddin, M., and Adnan, R. (2016). Load effect studies on ARX model parameters of vertical position Electro-Hydraulic Actuator. 2016 IEEE 12th International Colloquium on Signal Processing Its Applications (CSPA), pages 301–304.

[43] Iyer, N., Goebel, K., and Bonissone, P. (2006). Framework for post-prognostic decision support. In 2006 IEEE Aerospace Conference: 1-10

[44] Izquierdo, D., Azcona, R., Del Cerro, F. L., Fernandez, C., and Delicado, B. (2010). Electrical power distribution system (hv270dc), for application in more electric aircraft. In Applied Power Electronics Conference and Exposition (APEC), 2010 Twenty-Fifth Annual IEEE, pages 1300–1305.

[45] Jarvis, A., Leedal, D., Taylor, C. J., and Young, P. (2009). Stabilizing global mean sur- face temperature: A feedback control perspective. Environmental Modelling & Software, 24(5):665–674.

[46] Javaid, N., Ullah, I., Akbar, M., Iqbal, Z., Khan, F. A., Alrajeh, N., and Alabed, M. S. (2017). An intelligent load management system with renewable energy integration for smart homes, 5:13587–13600.

[47] Jia, Y. and Rajashekara, K. (2017). An induction generator-based ac/dc hybrid electric power generation system for more electric aircraft. IEEE Transactions on Industry Applications, 53(3):2485–2494.

[48] Jones, R. I. (2002). The more electric aircraft—assessing the benefits. Proceedings of the Institution of Mechanical Engineers, Part G: Journal of Aerospace Engineering, 216(5):259–269.

[49] Kalgren, P. W., Byington, C. S., Roemer, M. J., and Watson, M. J. (2006). Defining phm, a lexical evolution of maintenance and logistics. In 2006 IEEE autotestcon, pages 353–358. IEEE.

[50] Kan, M. S., Tan, A. C., and Mathew, J. (2015). A review on prognostic techniques for non-stationary and non-linear rotating systems. Mechanical Systems and Signal Processing, 62:1–20.

[51] Kennedy, J., Ciufo, P., and Agalgaonkar, A. (2012). Intelligent load management in microgrids. In 2012 IEEE Power and Energy Society General Meeting: 1–8.

[52] Krause, P. C., Wasynczuk, O., Sudhoff, S. D., and Pekarek, S. (2002). Analysis of Electric Machines and Drive Systems.

[53] Kurz-Kim, J.-R. (2009). A comparison of forecasting performance between ecm and the difference arx model. Applied Economics Letters, 16(2):121–125.

[54] Ljung, L. (1987). On the estimation of transfer functions. IFAC Proceedings, 20: 275- 286

[55] Ljung, L. (2002). System identification: theory for the user, volume 38. P T R Prentice Hall, New Jersey, 2 edition.

[56] Ljung, L. and Soderstrom, T. (1985). Theory and Practice of Recursive Identification The MIT Press, Cambridge Massachusetts, 2 edition.

[57] Lyman, R., Thaxton, L., Geyer, M., and Gordon, F. (1974). Electrical system with programmed computer control and manually initiated control means. US Patent 3,842,249.

[58] Mellor, P. H., Roberts, D., and Turner, D. R. (1991). Lumped parameter thermal model for electrical machines of TEFC design. IEEE Proceedings-B, 138(5):205–218.

[59] Mirabedini, H. and Gorji, A. (2001). The sort of fault diagnosis in large synchronous generators by analytic hierarchy process (ahp) method. In Canadian Conference on Electrical and Computer Engineering 2001. Conference Proceedings volume 2: 715–718.

[60] Moir, I. (1998). The all-electric aircraft-major challenges.

[61] Moir, I. and Seabridge, A. (2002). Electrical Systems. In Aircraft Systems: Mechanical, electrical, and avionics subsystem integration., chapter 5, pages 125–165. Professional Engineering Publishing.

[62] Moir, I. and Seabridge, A. (2008). Aircraft systems: Mechanical, electrical and avionics sub. Systems Integration, 2.

[63] Moir, I. and Seabridge, A. (2011). Aircraft Systems: Mechanical, electrical, and avionics subsystems integration, volume 52. John Wiley & Sons.

[64] Moir, I. and Seabridge, A. (2012). Design and development of aircraft systems, volume 67. John Wiley & Sons

[65] Mugglestone, J., Pickering, S., and Lampard, D. (1999). Effect of geometric changes on the flow and heat transfer in the end region of a tefc induction motor. In 1999. Ninth International Conference on Electrical Machines and Drives (Conf. Publ. No. 468): 40–44.

[66] Nair, V. and Hinton, G. E. (2010). Rectified linear units improve restricted boltzmann machines. In Proceedings of the 27th international conference on machine learning (ICML-10), pages 807–814.

[67] Natke, H. G. (2014). Application of system identification in engineering, volume 296. Springer

[68] Newill, J. F., Powell, J. D., and Zielinski, A. E. (2003). Coupled finite-element codes for armature design. IEEE transactions on magnetics, 39(1):148–152.

[69] Ng, B. C. (2014). Dynamic modelling of an automotive variable speed air conditioning system using nonlinear autoregressive exogenous neural networks. Applied Thermal Engineering, 73(1):1255–1270.

[70] Nikishkov, G. (2010). Finite Element Equations for Heat Transfer. In Programming Finite ELements in Java, pages 13–20.

[71] Noriega, J. R. and Wang, H. (1998). A Direct Adaptive Neural Network Control for Unknown Nonlinear Systems and its Application. IEEE TRANSACTIONS ON NEURAL NETWORKS, 9(1):27–34.

[72] Orsagh, R., Brown, D., Roemer, M., Dabnev, T., and Hess, A. (2005). Prognostic health management for avionics system power supplies. In 2005 IEEE Aerospace Conference, pages 3585–3591.

[73] Pearson, W. (1998a). The more electric/all electric aircraft-a military fast jet perspective.

[74] Pearson, W. (1998b). The more electric/all electric aircraft-a military fast jet perspective.

[75] Qi, R. and Brdys, M. (2008). Stable indirect adaptive control based on discrete-time t–s fuzzy model. Fuzzy Sets and Systems, 159:900–925.

[76] Qi, R. and Brdys, M. (2009). Indirect adaptive controller based on a self-structuring fuzzy system for nonlinear modeling and control. International Journal of Applied Mathematics and Computer Science, 19(4):619 – 630.

[77] Quigley, R. E. (1993). More electric aircraft. Applied Power Electronics Conference and Exposition, 1993. APEC ’93. Conference Proceedings 1993., Eighth Annual: 908–911.

[78] Raminosoa, T., Gerada, C., and Galea, M. (2010). Design considerations for a fault- tolerant flux-switching permanent-magnet machine. IEEE Transactions on Industrial Electronics, 58(7):2818–2825.

[79] Reynolds, R. (1991). Integrated Drive Generator System With Direct Motor Drive Prime Mover Starting.

[80] Rosero, J., Ortega, J., Aldabas, E., and Romeral, L. (2007a). Moving towards a more electric aircraft. IEEE Aerospace and Electronic Systems Magazine, 22(3):3–9.

[81] Rosero, J., Ortega, J., Aldabas, E., and Romeral, L. (2007b). Moving towards a more electric aircraft. IEEE Aerospace and Electronic Systems Magazine, 22(3):3–9.

[82] Santoso, G. B., Prahasto, T., and Widodo, A. (2013). Prognosis of bearing damage performance to industrial system using nonlinear autoregressive with exogenous (narx). In 2013 International Conference on QiR, pages 60–63.

[83] Sarlioglu, B. and Morris, C. T. (2015). More electric aircraft: Review, challenges, and opportunities for commercial transport aircraft. IEEE transactions on Transportation Electrification, 1(1):54–64.

[84] Schlabe, D. and Lienig, J. (2012). Energy Management of Aircraft Electrical Systems - State of the Art and Further Directions. In Electrical Systems for Aircraft, Railway and Ship Propulsion (ESARS), 2012, Bologna, number October, pages 1–6.

[85] Shanel, M., Pickering, S. J., and Lampard, D. (2003). Conjugate heat transfer analysis of a salient pole rotor in an air cooled synchronous generator. IEEE International Electric Machines and Drives Conference. IEMDC'03, 2:737–741 vol.2.

[86] Shokooh, F., Dai, J. J., Shokooh, S., Tastet, J., Castro, H., Khandelwal, T., and Donner, G. (2011). Intelligent load shedding. IEEE Industry Applications Magazine, 17(2):44–53.

[87] Si, X.-S. (2015). An adaptive prognostic approach via nonlinear degradation modeling: Application to battery data. IEEE Transactions on Industrial Electronics, 62(8):5082– 5096.

[88] Smeulers, J., Zeelen, R., and Bos, A. (2002). Promis-a generic phm methodology applied to aircraft subsystems. In Proceedings, IEEE Aerospace Conference, volume 6: 6–6..

[89] Sodoski, A. F., Hamilton, B. S., and Bradford, M. P. (2003). Power management under limited power conditions. US Patent 6,633,802.

[90] Staton, D. (2001). Thermal computer aided design-advancing the revolution in compact motors. In IEMDC 2001. IEEE International Electric Machines and Drives Conference (Cat. No. 01EX485): 858–863.

[91] Steger, C., Ulrich, M., and Wiedemann, C. (2018). Machine vision algorithms and applications. John Wiley & Sons.

[92] Stjsao, C. (2009). Induction Motors Thermal Analysis. Strojarstvo : Journal for the theory and application in mechanical engineering, 51(6):623–631.

[93] Sun, B., Zeng, S., Kang, R., and Pecht, M. G. (2012). Benefits and challenges of system prognostics. IEEE Transactions on reliability, 61(2):323–335.

[94] Tajjudin, M., Ishak, N., Ismail, H., Rahiman, M. H. F., and Adnan, R. (2011). Optimized pid control using nelder-mead method for electro-hydraulic actuator systems. In 2011 IEEE Control and System Graduate Research Colloquium: 90–93.

[95] Taylor, C. J., Pedregal, D. J., Young, P. C., and Tych, W. (2007). Environmental time series analysis and forecasting with the captain toolbox. Environmental Modelling & Software, 22(6): 797–814.

[96] Taylor, C. J. and Young, P. C. (2010). Captain toolbox analysis of the hyperfast switching peltier cooling system benchmark.

[97] Taylor, C James, e. a. (2017). The captain toolbox for system identification, time series analysis, forecasting and control getting started guide.

[98] The MathWorks (2018). Simulink.

[99] Triven, M. B. and Ratnakumari, U. V. (2016). Comparative study of neoteric adaptive model predictive controller with model predictive control for temperature regulation of cstr. In 2016 International Conference on Signal Processing, Communication, Power and Embedded System (SCOPES): 2120–2024.

[100] Tsatsanis, M. K. and Giannakis, G. B. (1993). Time-Varying System Identification and Model Validation Using Wavelets. In IEEE TRANSACTIONS ON SIGNAL PROCESSING, 41: 3512–3523.

[101] Vrancik, J. E. (1968). PREDICTION OF WINDAGE POWER LOSS IN ALTERNA TORS.

[102] Weckesser G, T., Jóhannsson, H., and Østergaard, J. (2013). Impact of Model Detail of Synchronous Machines on Real-time Transient Stability Assessment Impact of Model Detail of Synchronous Machines on Real-time Transient Stability Assessment. IREP Symposium- Bulk Power System Dynamics and Control -IX.

[103] Weimer, J. A. (1993). Electrical power technology for the more electric aircraft. In [1993 Proceedings] AIAA/IEEE Digital Avionics Systems Conference, pages 445–450.

[104] Weimer, J. A. (2003). The role of electric machines and drives in the more electric air- craft. In IEEE International Electric Machines and Drives Conference, 2003. IEMDC'03., volume 1, pages 11–15

[105] Wheeler, P. (2009). The More Electric Aircraft Why Aerospace Needs Power Electronics.

[106] Wheeler, P., Clare, J., Trentin, A., and Bozhko, S. (2013). An overview of the more electrical aircraft. Proceedings Of the Institution Of Mechanical Engineers Part G-Journal Of Aerospace Engineering, 227(G4):578–585.

[107] Xia, X. (2011). Dynamic power distribution management for all electric aircraft.

[108] Young, P. C., Taylor, C. J., Tych, W., Pedregal, D., and McKenna, P. G. (2010). The captain toolbox.

[109] Zadeh, L. A. (1962). From circuit theory to system theory. Proceedings of the IRE, 50(5), 856-865.

APPENDIX 1

USE OF ARMAX FOR TEMPERATURE PREDICTION

Alongside the methods outlined in Ch. 4, autoregressive moving average exogenous models were considered ARMAX defined in (A.1), but they did not outperform ARX.

$$\begin{aligned} y(t) + a_1 y(t-1) + \cdots + a_m y(t-n_a) \\ = b_1 u(t-n_k) + \cdots + b_l u(t-n_k-n_b+1) \\ + c_1 e(t-1) + \cdots + c_p e(t-n_c) + e(t) \end{aligned} \tag{A.1}$$

where $y(t)$ is the output at time t, n_a is the number of poles, n_b is the number of zeros plus one, n_c is the number of c coefficients, n_k is the number of input samples that can occur before the input can affect the output; subscripts $m, l\,, p \in \mathbb{Z}$.

The performance of the models is assessed in tabular form ordered in descending order of R_T^2.

For this exploration, the number of n_a and n_c is kept constant for modelling the temperatures when using the field excitation current or the armature current.

Table A.1 ARMAX coefficients being ranked in descending order of R_T^2 for predicting stator iron temperature T_{si}.

n_a	$n_{b_{If}}$	$n_{b_{Ia}}$	n_c	$n_{k_{If}}$	$n_{k_{If}}$	R_T^2	$\bar{R}_T^2$	$nAIC$
2	4	3	2	1	1	0.9986	0.9623	-4.278
1	3	4	1	0	1	0.9983	0.9584	-4.183
2	4	4	2	0	1	0.9983	0.9583	-4.243
…	…	…	…	…	…	…	…	…
1	1	1	1	0	0	0.9981	0.9559	-4.180
1	1	1	1	0	1	0.9980	0.9555	-4.179
2	3	2	3	0	1	0.9974	0.9489	-4.456
…	…	…	…	…	…	…	…	…
2	4	4	4	0	0	0.9970	0.9456	-4.483

Table A.2 ARMAX coefficients being ranked in descending order of R_T^2 for predicting the winding temperature T_{sw}.

n_a	$n_{b_{If}}$	$n_{b_{Ia}}$	n_c	$n_{k_{If}}$	$n_{k_{If}}$	R_T^2	$\bar{R}_T^2$	$nAIC$
3	4	3	4	1	0	0.9809	0.8617	-6.246
2	3	2	4	1	1	0.9382	0.7514	-6.181
1	1	1	4	0	1	0.9365	0.7481	-6.030
1	1	2	4	0	1	0.9363	0.7475	-6.030
…	…	…	…	…	…	…	…	…
1	1	2	4	1	1	0.9308	0.7370	-6.032
1	2	1	3	1	1	0.9305	0.7365	-5.880
1	1	1	1	0	0	0.9277	0.7312	-5.655
…	…	…	…	…	…	…	…	…
2	2	3	4	1	0	0.8993	0.6826	-6.2707